Petter Lervik

Effect of Natural Ageing Temperature and Time on Precipitation in 6xxx Aluminium Alloys

Graduate thesis in Physics
Supervisor: Randi Holmestad
Co-supervisor: Christoph Hell

June 2022

Graduate thesis

NTNU
Norwegian University of Science and Technology
Faculty of Natural Sciences
Department of Physics

NTNU
Norwegian University of
Science and Technology

Petter Lervik

Effect of Natural Ageing Temperature and Time on Precipitation in 6xxx Aluminium Alloys

Graduate thesis in Physics
Supervisor: Randi Holmestad
Co-supervisor: Christoph Hell
June 2022

Norwegian University of Science and Technology
Faculty of Natural Sciences
Department of Physics

NTNU

Norwegian University of
Science and Technology

Abstract

The main goal of this MSc project is to investigate the influence of temperature during natural ageing (NA) on the 6xxx aluminum (Al) class. The 6xxx Al family shows a peak hardness behavior which is heavily dependent on the natural ageing time and alloy composition. Research shows evidence that different clusters form during natural ageing. Some of those clusters are of beneficial and others of detrimental nature for achieving peak hardness condition. An earlier study carried out by Hydro in Sunndalsøra in 2006 suggests that, besides the alloy composition and the natural ageing duration, the natural ageing temperature might have a severe impact on the formation of clusters. It was hypothesized that the exceeding of a solvus temperature during natural ageing might trigger the growth of beneficial clusters. This hypothetical solvus temperature would be highly dependent on the alloy composition, mainly, the magnesium (Mg), silicon (Si) and copper (Cu) content. Here, four types of Mg-Si aluminium alloys are naturally aged at various temperatures and over several time-periods. Hardness and electrical conductivity measurements are taken of the samples after ageing. Transmission electron microscopy images are taken from aged and measured samples. Precipitate statistics such as precipitate length, cross-section and precipitates density are derived from TEM images. Hardness and electrical conductivity values are compared to the precipitate statistics. Natural ageing are found to be beneficial for hardening of the 6005 and 6060 alloys, with both higher storage temperature and prolonged natural ageing showing better results. At temperatures below $40°C$, natural ageing are found to be detrimental for hardening of the 6060 and 6110 alloys. NA temperatures of $80-100°C$ show an increase in hardness. Precipitates formed in stronger naturally aged conditions are found to be smaller, but be more densely packed and occupy more of the total volume, than precipitates formed in naturally aged conditions with lower strength.

Abstrakt

Hovedformålet med dette MSc prosjektet er å undersøke påvirkningen av temperatur i mellomlagrings-leddet på 6xxx aluminium (Al) serien. Familien av 6xxx Al legeringer er vist å nå et platå i hardhet som er avhengig av mellomlagrings-tid og legeringssammensetning. Undersøkelser viser at forskjellige typer legerings-klynger dannes under mellomlagring. Noen av disse legeringsklyngene har en positiv effekt, mens andre har en negativ effekt på oppnåelse av høyere hardhet. En tidligere studie gjennomført av Hydro Sunndalsøra i 2006 foreslår at i tillegg til legeringssammensetning og mellomlagrings-tid, så vil mellomlagrings-temperatur også muligens ha en merkbar effekt på dannelse av legeringsklynger. En hypotese ble formulert om å overstige en fase-overgangstemperatur under mellomlagring vil muligens sette i gang dannelse av positive legeringsklynger. Den hypotetiske overgangstemperaturen vil være avhengig av legeringssammensetningen, da hovedsaklig magnesium (Mg), silisium (Si) og kobber (Cu). Fire typer Mg-Si aluminiumslegeringer er varmebehandlet med forskjellig mellomlagrings-temperaturer og tidsperioder. Hardhet og elektrisk ledningsevne er målt fra prøvene etter varmebehandling. Transmisjons elektronmikroskop er brukt til å ta bilder av ferdig varmebehandlet og målte prøver. Presipitatstatistikk, som presipitatlengde, tverrsnitt og tetthet, er hentet fra mikroskop-bildene. Hardhets og ledningsevne-verdier blir sammenlignet med presipitatstatistikken. Mellomlagring vises å være gunstig for herding av legeringer 6005 og 6060. Både høyere lagringstemperatur og tid gir bedre resultat. Mellomlagringstemperaturer under $40°C$ vises å være skadelig for herding av legeringer 6082 og 6110, mens temperaturer $80-100°C$ viser en økning i styrke. Presipitater i prøver med høyere målt hardhet viser seg å være mindre, men opptrer med høyere tetthet og okkuperer mer av det totale volum, enn presipitater i prøver med lavere hardhet. Høyere mellomlagrings-temperaturer og tid gir dannelse av mindre og flere presipitater som vises å være gunstig for økning av hardhet.

Preface

This thesis is the conclusion of a 5 year study of physics, 3 years in Tromsø at UiT and 2 years in Trondheim at NTNU. The thesis work is done in the TEM Geminicentre group at the department of physics, NTNU. The work is connected to the SumAl project, and the problem is formulated by Hydro.

Thanks to my supervisor Randi Holmestad for the opportunity to conduct this work and for her guidance throughout. Thanks to Bjørn Gunnar Solem and Emil Frang Christiansen for the initial training on the TEM. Thanks to Christoph Hell and Calin D. Marioara for more specialized training on the TEM related to imaging of aluminium alloys and precipitate statistics. Also a special thanks to Christoph Hell for his guidance and patience through all aspects of the experiment. Lastly, thanks to my family for their support during this work.

Contents

1   Introduction

Aluminium has become an integral part of modern society and is found anywhere from aviation to the food industry due to its properties. The SumAl project, hosting partners from NTNU, SINTEF, Hydro and Benteler, is investigating the behaviour of clustering in aluminium alloys during production and its effect on material properties. As part of the SumAl project, this thesis is investigating a certain set of aluminium alloys from the 6xxx series consisting mainly of Al-Mg-Si but also Cu. Composition and thermomechanical treatment decide the properties of age hardenable aluminium alloys. 'Alloy design' is to combine these to match desired properties. The experiment outlined in this text is building upon an experiment by Røyset *et al.* [1] from Hydro. The Hydro experiment looked at the effect of intermediate storage between solution heat treatment and artificial ageing on the age hardening response of three alloys, the 6005, 6060 and 6082, containing different amounts of Mg-Si. A solvus line was hypothesized marking which Mg-Si content and intermediate storage combination are beneficial or detrimental to precipitation hardening, see figure 1(a). Figure 1(b) presents the equivalent figure for this experiment, without a solvus line. Several natural ageing temperatures are added, mainly above room temperature, as well as an additional alloy, the 6110. Hardness are measured to give insights into mechanical properties, and electrical conductivity measurements can potentially give insights into clustering and its use in electronics. Transmission electron miscoscopy (TEM) imaging is used to investigate precipitates in the aluminium matrix.

(a)	(b)
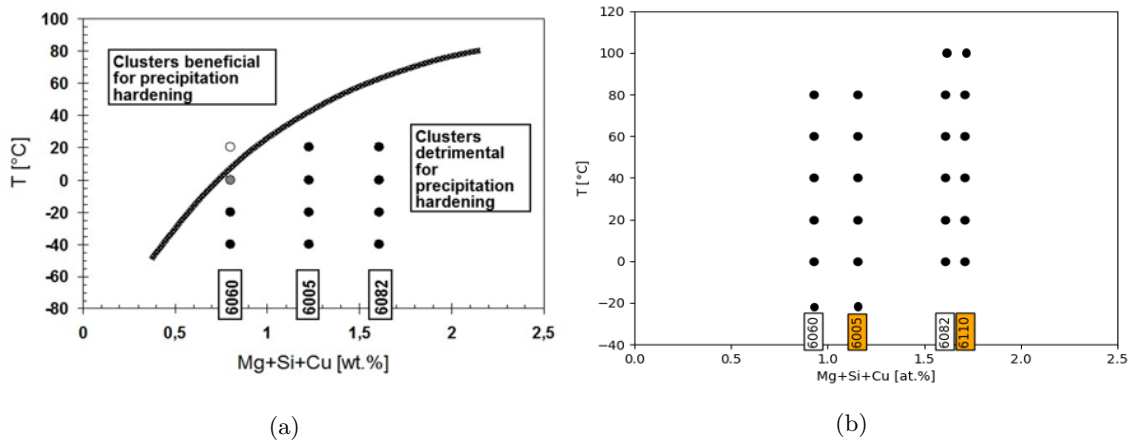
Figure 1: (a) Results from the Hydro Sunndalsøra 2006 experiment with the hypothetical solvus line. Aluminium alloys with larger contents of its constituents Mg-Si are expected to form detrimental clusters during heat treatment. (b) Equivalent figure for this experiment with added natural ageing temperatures and an additional alloy, 6110. The alloys 6005 and 6110 do contain Cu and are marked in orange.

This thesis will first present the theoretical background in chapter 2. The methods used in this experiment are presented in chapter 3, while results and discussion are given in chapter 4 followed by a conclusion in chapter 5. Extended data from the experiment are presented in the appendix. Appendix A presents the hardness data, appendix B presents the electrical conductivity data and appendix C presents detailed precipitate statistics as well as some TEM images taken.

2 Theoretical Background

2.1 Aluminium

Aluminium is the name of element 13 with symbol Al in the periodic table and was discovered in the 19th century. At room temperature aluminium has the face-centered cubic crystal structure with lattice constant $a = 4.05$ Å [2]. Different elements are added to aluminium to enhance its properties through alloying. Several aluminium alloys are used today, named as eg. 1xxx, 2xxx,... etc. The first number reveals which element(s) are the main alloying component(s) [3]. The main constituents of aluminium alloys of the 6xxx series are magnesium (Mg) and silicon (Si). These elements provides the aluminium alloy its ability to become solution heat treated for improved strength. Heat treatment allows these elements to form clusters in the aluminium matrix which leads to reinforcement of the material [4].

2.2 Nucleation

During the phase transformation from liquid form to a solid, the atoms recrystallize in a lattice. Primary 'static' recrystallization is the reconstruction of the grain structure during annealing of deformed materials [5]. If recrystallization occurs during heat treatment of a deformed material, small new grains grow at the expense of the deformed microstructure until they completely replace the deformed microstructure. This is known as nucleation and nucleus growth [5]. If the heat treatment is continued after complete primary recrystallization the grain size usually increases [5]. In order to generate a recrystallization nucleus successfully from the deformed microstructure, three criteria have to be met, which are also referred to as the three instability criteria [5]: *i*) Thermodynamic instability. Nucleation during solid state phase transformations has to exceed a critical nucleus size for stable growth. *ii*) Mechanical instability. The grain boundary of the nucleus has to move in a defined direction, which requires a local imbalance of the driving forces. *iii*) Kinematic instability. The surface of a nucleus, the grain boundary, must be mobile to make the nucleus grow. The constraint to comply with all three instability criteria favors nucleation in specific regions of the deformed microstructure. All these processes require a local rearrangement of the deformed dislocation structure, i.e., nucleation is always connected to recovery processes [5]. The kinetics of primary recrystallization are determined by thermal activation of its mechanisms, nucleation and nucleus growth, all of which control the progress of recrystallization with annealing time [5].

2.3 Precipitates

Precipitates are needle-shaped structures in the aluminium matrix growing along the $< 100 >$Al directions [6]. Precipitates are formed during ageing. Different ageing temperatures influence the rate of precipitate formation as well as its size in length and cross-section, which in turn have an effect on the hardness of the material. Precipitation usually proceeds by nucleation and growth of individual nuclei [5]. In the course of annealing the nuclei of a precipitating phase grow until equilibrium is attained, i.e. when both phases have achieved their equilibrium concentration [5]. The growth kinetics are diffusion controlled [5]. In the course of annealing small precipitates dissolve, while large precipitates continue to grow. This is referred to as Ostwald ripening [5].

2.4 Strengthening

There are several mechanisms for strengthening of a crystalline material. Some of these include: *i*) Precipitation hardening. Precipitates which form during cooling of a homogeneous solid solution into the two-phase regime contribute to the strength of a material [5]. They share a phase boundary with the matrix. Three types of phase boundaries exist, coherent, partially coherent and incoherent [5]. *ii*) Dispersion hardening. If a material contains nonmetallic particles strengthening

can be obtained. The reason for this dispersion hardening is particle-dislocation interaction. The dislocations cannot cut or penetrate a hard particle so they have to circumvent the particle by bowing out between the particles [5]. *iii*) Solid solution hardening. If the alloy is a solid solution, the strength differential between the solid solution and the pure metal are known as solid solution hardening [5]. Solid solution hardening is caused by the interaction of an alloying element with the dislocations, which results in an increased glide resistance. There are three ways solute atoms can interact with dislocations [5]: (a) Parelastic interaction (lattice parameter effect). Solute atoms have an atomic size different from the matrix. Their incorporation into the crystal lattice causes compressive or tensile stress depending on if the solute atom is larger or smaller than the matrix atom [5]. (b) Dielastic interaction (shear modulus effect). The dielastic interaction is caused by the fact the density of a dislocation is proportional to the shear modulus [5]. If the solute atom has a different shear modulus, the volume of the solute atom contributes to the total energy of the dislocation differently from atoms of the pure solvent crystal [5]. (c) Chemical interaction (Suzuki effect). This effect is caused by the dependence of the stacking fault energy on chemical composition in such a way that the stacking fault energy decreases with increasing solute concentration [5]. A decreasing stacking fault energy leads to an increase of the dissociation width of dislocations, which reduce the total dislocation energy [5]. Solute atoms segregate to the dislocations to decrease the stacking fault energy. If the dislocation moves, it has to leave the segregated solute atoms behind, which changes the composition of the dislocation and increases the energy of the dislocation. This makes itself felt as a back stress on the dislocation [5]. *iv*) Age hardening. Age hardening is the strengthening by precipitates of a second phase during annealing of a supersaturated solid solution. If the homogeneous alloy is quenched to room temperature, a supersaturated solid solution is obtained [5]. Heating to slightly higher temperatures see an increase in strength. If age hardening remains confined to only this first hardening stage because of low temperature, this is referred to as room temperature age hardening [5]. The second hardening stage is obtained at higher annealing temperatures. This is called artificial ageing [5]. It is the aim of age hardening to attain maximum strengthening. At long annealing times a decrease of strength can be seen which is known as overaging [5]. Age hardening becomes optimal if the precipitate spacing is small, that is, if the precipitates are homogeneously distributed within the crystal [5].

2.5   Heat Treatment

Heat treatment in aluminum production is a complicated process but can be divided into several stages, solution heat treatment (SHT), natural ageing (NA) and artificial ageing (AA). The goal of heat treatment is to optimize an alloys' properties for its dedicated application. This could be making it stronger, more ductile or more conductive.

2.5.1   Solution Heat Treatment

Solution Heat Treatment (SHT) is a way to increase the amount of solute in the aluminium matrix, effectively resetting the sample atomic matrix from previous configurations. The temperature needed for SHT is above the solvus line of the phases that might have already formed and holding it there for enough time such that diffusion can dissolve them into a solid solution, then rapidly cooled to preserve the properties of the solution and to freeze in the equilibrium vacancy concentration of the high SHT temperature. The higher the temperature the higher the equilibrium vacancy concentration. This creates a precipitate free supersaturated solid solution [7]. The exercised SHT temperature here are $550°C$ for 30min followed by room-tempered water quench.

2.5.2   Natural Ageing

The intermediate storage near room temperature after quench and before artificial ageing is called natural ageing (NA). This storage increases hardness over time which is caused by clustering of solute atoms [4]. Several NA temperatures are investigated here mainly above room temperature, over several time periods, in an attempt to observe its effect on hardness and precipitation.

2.5.3 Artificial Ageing

Artificial ageing (AA) is heat treatment at elevated temperatures following NA. Typical temperatures of AA is 150-250°C [7]. This is to accelerate precipitate formation [6]. Here, AA is done at 185°C for 5hr.

2.6 Transmission Electron Microscopy

The transmission electron microscope (TEM) is a powerful tool allowing us to observe structure through the use of electrons instead of photons in ordinary light-microscopes. Electrons have a much shorter wavelength than photons and can be diffracted through regions in a crystal on the nanometer scale. The TEM sends a beam of electrons through a column of magnetic lenses that allows the beam to be focused. The beam is sent through the specimen which has to be very thin, less than 1200 nm, sitting lower in the column, and the electrons scatter, creating an image on a screen sitting at the bottom. This is where "transmission" comes from in the name, the electrons of interest are those transmitted and scattered through the crystal. A schematic of the column of the TEM used here, the "JEOL JEM-2100", are shown in figure 2 [8].
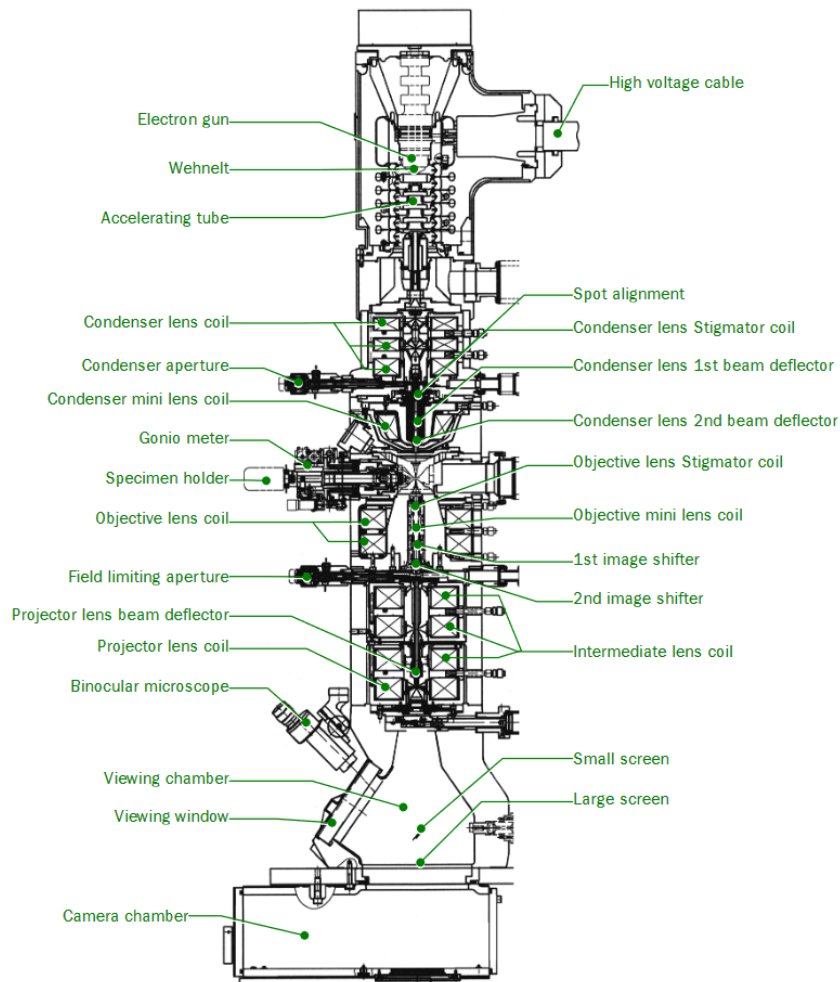
Figure 2: Schematic of the JEOL JEM-2100 electron microscope used for this experiment, image taken from the JEM-2100 manual [8]. The beam originates from the electron gun at the top of the microscope and travel downwards through a series of lenses and apertures allowing for manipulation of the beam. The specimen holder is situated in the middle of the column such that the transmitted beam may also be manipulated. The viewing screen are at the bottom of the column together with a camera.

2.6.1 Diffraction

In a diffraction experiment, electrons are directed into a material and a detector is recording the direction and intensity of the outgoing diffracted electrons. Constructive or destructive interference occurs along different directions as scattered electrons are emitted by the material. The electrons that interfere constructively gives the diffraction pattern. There is a geometrical relationship between the diffraction pattern and the crystal structure of a material [9]. The diffraction pattern is a spectrum of real space periodicities in a material [9]. A crystal lattice periodicity with long repeat distance cause diffraction at small angles, while short repeat distances cause diffraction at large angles [9]. "Precisely and concisely, the diffraction pattern measures the Fourier transform of an autocorrelation function of the scattering factor distribution" -Fultz & Howe [9]. Bragg's law, $2d \sin \theta = n\lambda$, shows that constructive interference occurs when the difference in path length for the incoming electrons is equal to an integer of the wavelength $n\lambda$ where $n = 1, 2...$, d is distance between parallel lattice planes and θ is the angle of incoming electrons. Therefore a diffraction pattern shows sharp peaks of intensity where the electrons constructively interfere and little to no intensity where the electrons destructively interfere.

2.6.2 Imaging Modes

The transmitted and scattered electrons leaving the specimen combine to form an image on the screen at the bottom of the microscope. However, this image have little contrast and features on the image are hardly distinguishable. By inserting an objective aperture in the back focal plane of the objective lens, contrast can be observed and features of the specimen becomes far more visible [9]. Bright field (BF) imaging is achieved when the objective aperture is placed such that only the transmitted (un-diffracted) electrons are allowed to pass. Similarly, dark field (DF) imaging is achieved when the objective aperture is placed such that only some diffracted electrons are allowed to pass [9]. These two imaging modes, BF and DF, highlights different features of the specimen. When looking at an aluminium alloy specimen containing precipitates, precipitates along the $< 001 >$ direction in the imaging area generates a diffracted beam that pass through the objective aperture during DF imaging and are highlighted. A selected area diffraction (SAD) pattern is obtained by inserting a selected area aperture in the image plane of the objective lens and entering diffraction mode on the microscope with a spread beam [9]. If instead the beam is converged to a spot and diffraction mode is entered without inserting the selected area aperture, the converged-beam electron diffraction (CBED) mode is obtained. In this mode, Kikuchi-bands appear which can be used as a "roadmap" to see in what crystallographic direction the material is viewed in. If an aluminium sample is viewed in the $< 100 >$ zone-axis a four-fold symmetry is seen, and if the sample is tilted off-axis, the "roads" leading the way to the zone-axis is seen. Obtaining high resolution images (HRTEM) is a complicated concept [9], but in practice it is similar to that of BF and DF imaging. The objective aperture, in this case, is placed such that the transmitted electron beam, along with some diffracted electron beams, is allowed to pass. This means that a larger objective aperture is used for HRTEM than in BF imaging, but their placement is the same. This allows for higher resolution imaging than BF and with higher magnification to reveal smaller-scale structure in a smaller area of the sample.

3 Methodology

3.1 Material

Four samples of different Mg-Si contents are investigated. These are all part of the 6xxx aluminium alloy series. The full name of the alloys are 6005 AC, 6060.35, 6082.27 and 6110.21. The 6005 AC and 6060.35 samples was produced by Hydro and the 6082.27 and 6110.21 samples was produced by Benteler. A full overview of their composition, both in atom% and weight%, including trace elements is presented in table 1.

For easier reading these alloys will be referred to as the 6005, 6060, 6082 and 6110. Naturally,

Table 1: Alloy composition in atom% and weight%.

	Fe	Si	Mg	Mn	Cr	Cu	Zn	Ti	Zr	V	B	Al
6005 AC												
at%	0.096	0.596	0.493	0.091	0.002	0.065	0.008	0.006	0.000	0.000	0.000	98.642
wt%	0.198	0.619	0.443	0.185	0.003	0.153	0.020	0.011	0.000	0.000	0.000	98.368
6060.35												
at%	0.093	0.406	0.520	0.007	0.000	0.001	0.002	0.005	0.000	0.000	0.000	98.966
wt%	0.193	0.422	0.468	0.015	0.000	0.002	0.005	0.008	0.010	0.000	0.000	98.887
6082.27												
at%	0.102	0.878	0.725	0.257	0.083	0.004	0.025	0.011	0.000	0.011	0.010	97.894
wt%	0.210	0.910	0.650	0.520	0.160	0.010	0.060	0.020	0.000	0.020	0.004	97.436
6110.21												
at%	0.083	0.734	0.882	0.282	0.084	0.094	0.025	0.011	0.003	0.011	0.008	97.784
wt%	0.170	0.760	0.790	0.570	0.160	0.220	0.060	0.020	0.010	0.020	0.003	97.217

as Mg has the atomic number 12 and Si has the atomic number 14 while Al sit in between with atomic number 13, the at% of Si is slightly lower than the wt% of Si, and similarly the at% of Mg is slightly higher than the wt% of Mg. Interestingly we can see that the wt% of Al is slightly lower than the at% of Al for all samples. This is largely due to the presence of heavier trace elements Fe, Mn, Cr, Cu and Zn with atomic numbers 26, 25, 24, 29 and 30 respectively. A simplified table in at% with round-off values for the main components Si and Mg, along with the presence of Cu, is presented in table 2.

Table 2: Simplified composition with Si, Mg and Cu in **at%**.

	Si	Mg	Cu	Mg/Si
6005	0.6	0.5	0.07	1.2
6060	0.4	0.5	-	0.8
6082	0.9	0.7	-	1.3
6110	0.7	0.9	0.09	0.8

Here it is clear we have two "lean" alloys, 6005 and 6060, containing a smaller amount of Si and Mg. The Mg contents of these two alloys are similar while the Si content varies from higher in 6005 to lower in 6060. The two remaining alloys, 6082 and 6110, referred to as "rich" alloys, contains a higher amount of both Si and Mg. For the two rich alloys the at% of Mg and Si are swapped. Additionally there are two alloys with Cu contents, the lean 6005 and the rich 6110.

3.1.1   Sample Preparation

The lean 6005 and 6060 samples are cut by handsaw from larger sheets of extruded alloy table-like plates. Once sufficiently small these samples are cut by machine of type Struers Accutom-50 into a 35mm x 20mm rectangular shape with a thickness of 3mm. The thickness of 3mm is the original thickness of the larger sheets of material and is not cut in any way. The rich 6082 and 6110 are delivered by Benteler in extruded sheets, but came pre-cut into the same 35mm x 20mm rectangular shapes, however with a thickness of 6mm. A sketch of the samples are shown in figure 3.
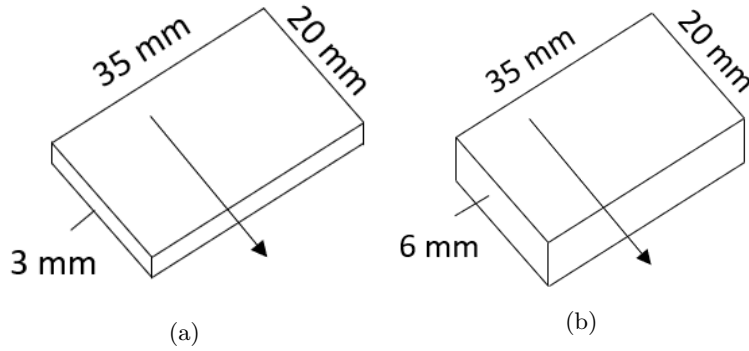
Figure 3: Sketch of sample shape. The arrows indicate the extrusion direction. (a) The lean 6005 and 6060 from Hydro with a thickness of 3mm. (b) The rich 6082 and 6110 from Benteler with a thickness of 6mm.

At this point the 35mm x 20mm surface is rough and therefore not ideal for hardness measurements. The surface is ground down using a Struers LaboPol-60 polishing machine with fine sandpaper, running water and neutral soap in three stages. The sandpaper grit used for each stage respectively is p1200, p2400 and p4000, leaving a smooth reflective mirror-like surface better suited for hardness measurements. This process is repeated for both 35mm x 20mm surfaces on each sample. With the fine sandpaper in use the grinding process will not reduce the sample thickness in any meaningful way for this experiment. The samples are rinsed in cold water to remove traces of soap, dried and are now ready for heat treatment.

3.2   Heat Treatment

Solution heat treatment (SHT) is the first stage of heat treatment. This is carried out in an air oven of type "Nabertherm N17/HR Muffle Furnace" pre-heated to 550 °C. The samples are placed directly from room temperature into the pre-heated oven at 550 °C and stay there for 30 minutes. At the 30 minute mark the samples are directly quenched in room tempered water for 10-20 seconds. This SHT process is identical for every sample treated.

The second phase of heat treatment is natural ageing (NA), however part of this experiment is to look at the effect of directly aged samples, meaning one of each sample alloy, four in total, are taken directly from water quench to artificial ageing (AA) in a pre-heated oilbath at 185 °C. The oilbath is of type "Memmert Oilbath" filled with silicone oil. Since both air oven and oilbath are located in the same room, the time from a sample is quenched to placed in the pre-heated oilbath is estimated to be about 1 minute. That is, the directly aged samples, after SHT, is exposed to approximately 1 minute of room temperature before AA at 185 °C for 5 hours in the oilbath. The full heat treatment process for directly aged samples are:

SHT (550 °C : 30 min) → quench (21 °C : ∼10 sec) → NA (21 °C : <1 min) → AA (185 °C : 5 h).

The time spent taking the sample from quenching to the next ageing process, be it NA or AA, can probably be seen as part of the quenching process itself, seeing as they both are at room temperature. It is important to note however that while the sample is quenched it is submerged in room tempered water, and while transported it is in air. For a clearer picture the process becomes SHT→quench→AA:

SHT (550 °C : 30 min) → quench (21 °C : 1 min) → AA (185 °C : 5 h).

It should also be noted that after every AA process, the samples are quenched in room tempered water again, marking the end of heat treatment. For the main bulk of samples there are four designated NA storage areas depending on NA temperature. The idea is to store the samples in temperatures incremented by 20 °C from 0 °C to 80 °C. That is 0, 20, 40, 60 and 80 °C, in total

five NA storage temperatures. The same type of "Memmert Oilbath" used in AA is used for NA storage for the three storage temperatures 40-80 °C, all pre-heated before use. The 0 °C samples are stored in a fridgeroom, and the 20 °C samples are stored at the TEM prep-lab. The fridgeroom and TEM prep-lab are busy areas and temperatures may vary over the course of a week. This fluctuation, together with the mean temperature, were measured prior to storage using a K-type thermocouple connected to a multimeter device. The result from these measurements are presented in figure 4.

(a)   (b)
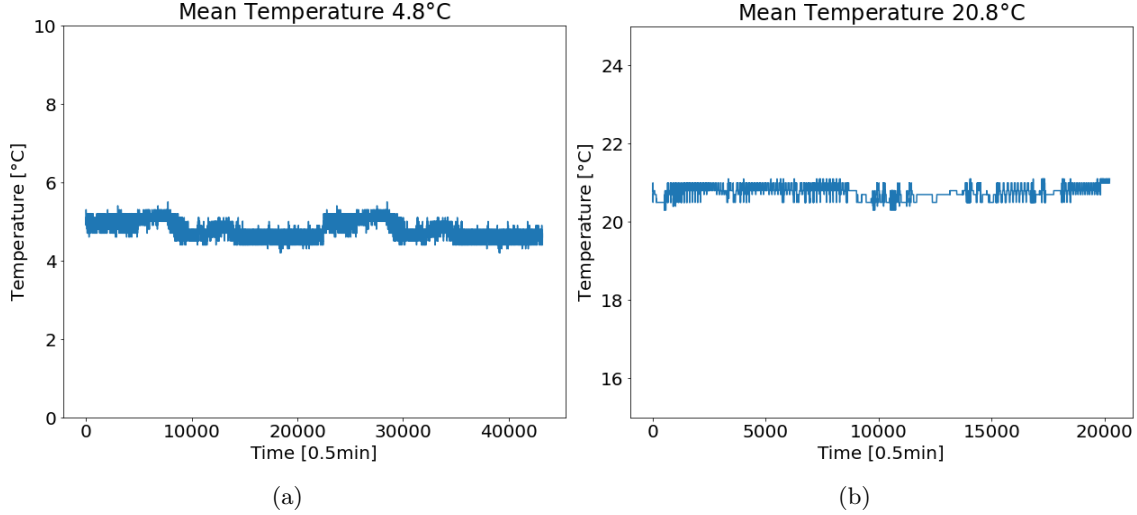
Figure 4: Thermocouple temperature measurements of NA storage areas (a) fridgeroom with one measurement every 30 sec over a period of two weeks with a mean temperature of 4.8 °C. (b) TEM prep-lab with one measurement every 30 sec over a period of one week with a mean temperature of 20.8 °C.

The measured mean temperature in the fridgeroom and TEM prep-lab are taken to be 5 °C and 21 °C, respectively. In reality the five NA storage temperatures is then 5, 21, 40, 60 and 80 °C. After SHT and water quench these samples are directly taken to their designated NA storage. For the three NA storage temperatures 40, 60 and 80 °C the time from SHT+quench to storage in oilbath is similar to that of the directly aged, ∼1 min. However, the fridgeroom and TEM prep-lab is in another building on campus but close to each other, so the time from SHT+quench to these storage facilities is estimated to be ∼5 min. These samples are transported in liquid nitrogen to avoid temperature contamination in the NA process.

In addition there are three NA storage times; 24 h, 7 days and 28 days. An individual sample is created for each NA temperature and time combination for each alloy. This means there are $5 \times 3 = 15$ (temperature × time) samples created per alloy, not including the directly aged samples.

The last step of heat treatment is artificial ageing. This is done in a pre-heated Memmert Oilbath at 185 °C for 5 h, the same for every sample treated. When a sample is finished with NA it is taken directly from its designated NA storage to hardness and electrical conductivity measurements for its "before AA measurement", more on this in section 3.3. Samples in oilbath are also dipped in ethanol and dried with paper to remove excess oil before measurement. This measurement process is estimated to take ∼20 min, including travel time back and forth. This means that every sample, except the directly aged, will be exposed to about 20 min of room temperature before artificial ageing. The full heat treatment process for NA at 40, 60 and 80°C are:

SHT (550 °C : 30 min) → quench (21 °C : 1 min) → NA (40,60,80 °C :1,7,28 days) → NA (21 °C : 20 min) → AA (185 °C : 5 h).

And for 5 and 21°C:

SHT (550 °C : 30 min) → quench (21 °C : 10 sec) → transport (−196 °C : 5 min) → NA (5,21 °C :1,7,28 days) → NA (21 °C : 5 + 20 min) → AA (185 °C : 5 h).

A simplified illustration of the NA heat treatment process in the form of SHT→quench→NA→AA is shown in figure 5.
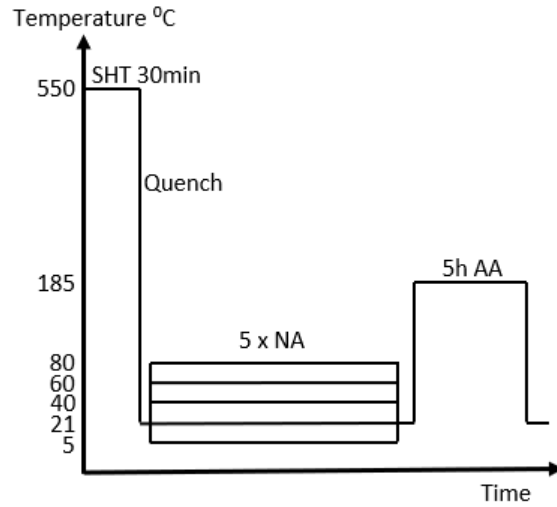
Figure 5: Illustration of the NA heat treatment process as SHT→quench→NA→AA. Samples going through NA hotter than room temperature are quenched before AA, and all samples are quenched after AA.

In addition to the five NA storage temperatures, two more NA temperature samples are added, $-20\,°C$ for the lean alloys 6005 and 6060, and $100\,°C$ for the rich alloys 6082 and 6110. The $100\,°C$ NA are done in oilbath as with 40, 60 and $80\,°C$, while the $-20\,°C$ NA are done in a freezer in the TEM prep-lab. Each of these follow the same procedure as the rest, depending on oilbath storage or prep-lab storage. A thermocouple measurement were also done for the freezer prior to heat treatment, the result presented in figure 6.
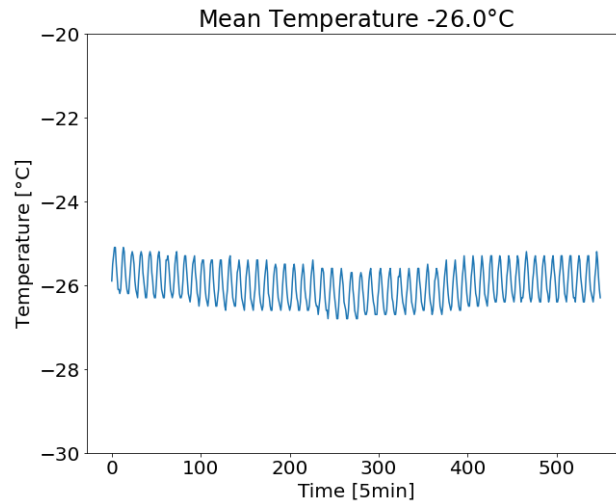
Figure 6: Thermocouple temperature measurement of NA storage freezer with one measurement every 5min over a period of 48 hours with a mean temperature of $-26\,°C$. The sinusoidal pattern is assumed to be normal temperature fluctuations in a standard freezer.

The mean temperature of the freezer is taken to be $-26\,°C$. In total there are seven NA storage temperatures; -26, 5, 21, 40, 60, 80 and $100\,°C$, along with three NA storage times; 1, 7 and 28 days. Since NA at $-26\,°C$ and $100\,°C$ is only done for two alloys each, the total amount of treated samples per alloy are $6 \times 3 + 2 = 20$, including directly aged before and after AA measured samples, more on this in chapter 3.3. This concludes the method of heat treatment on the effect of NA time and temperature.

The final batch of samples going through heat treatment is to do an investigation into the peak AA hardness value for a set of NA samples. This is an entirely new batch of samples different from those discussed previously. These samples include, for all four alloys; the direct aged, the 5, 21, 60 and 80 °C naturally aged for 24 h as well as the 60 and 80 °C naturally aged for 28 days, for a total of seven samples per alloy. These samples are subsequently artificially aged for a total of 1, 2, 5, 10 and 24 h at 185 °C. The heat treatment process for these samples are similar to the previous batch, the difference being in the AA time as well as interrupted AA for measurements at the mentioned AA times. The previously discussed samples are all artificially aged at 185 °C for 5 h without interruption, assuming 5 h AA to generally represent peak hardness across all samples. The investigation into the effect of NA temperature and time with SHT at 550 °C for 30 min and AA at 185 °C for 5 h were completed before investigating peak AA hardness.

3.3   Hardness and Conductivity Measurements

In the early stages of measurements the samples were given a quick grinding with sandpaper grit p4000 along with running water and soap before measurements. This to remove oil residue from heat treatment, however due to concerns of work hardening effects on the surface where hardness measurements are taken, this practice was abandoned. All samples are drenched in ethanol and dried off with paper before measurements to remove oil with minimal effects on the surface of the sample. Hardness and electrical conductivity measurements are always done in tandem as these instruments are close by. There are two sets of hardness and conductivity measurements per sample, one set of measurements taken before the sample is artificially aged, and one set of measurements after the sample is artificially aged, as shown in figure 7(a). The only exception to this is the direct aged samples which require an independent set of samples for the "before AA" measurements and another for the "after AA" measurements. The measurements taken after artificial ageing represent the saved conditions that is studied in the TEM. Figure 7(b) shows the heat treatment process along with the measurements for the peak AA investigation.
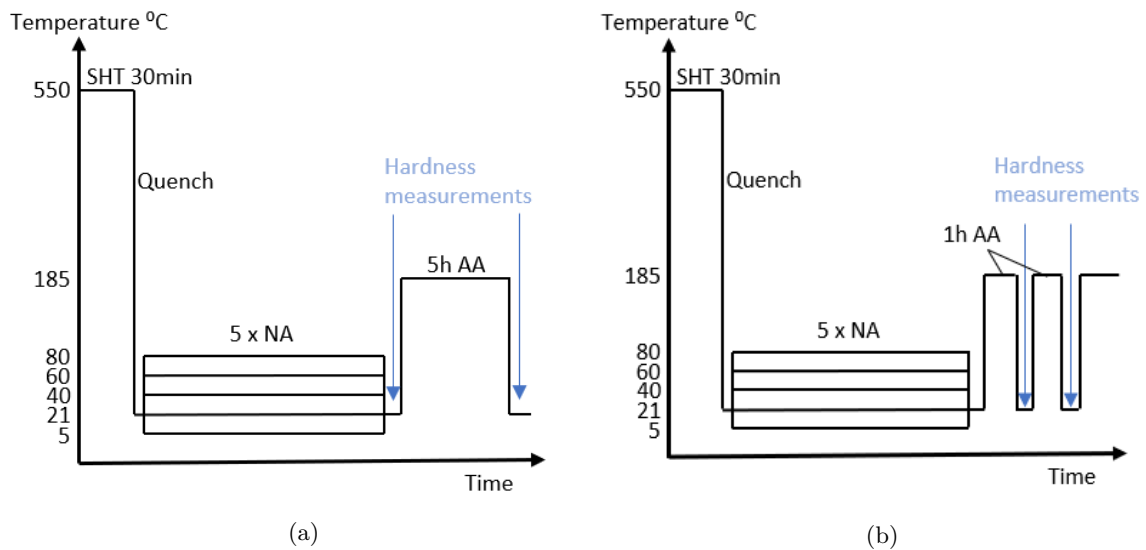
Figure 7: (a) Illustration of NA heat treatment process as SHT→quench→NA→AA. When measurements are taken are shown in blue. The samples are quenched both for the "before AA" and "after AA" measurements. (b) Illustration of the process of investigating peak AA hardness with subsequent AA for a total of 1, 2, 5, 10 and 24 h.

3.3.1   Vicker's Hardness

The instrument used for hardness testing are Innovatest - Vicker's hardness testing machine. Here the sample are placed on a platform with a microscope above. The machine produces a diamond

shaped indentation of which two diameters are measured by hand. The diameters measured are the length across the indentation from corner to corner, as shown in figure 8.
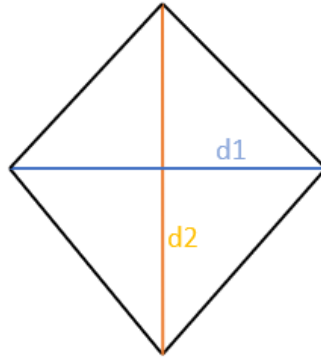
Figure 8: Illustration of the diamond shaped indentation made by the vicker's hardness machine. The lengths measured are in blue d_1 and in red d_2.

As a sample is measured the testing machine gives the hardness value. The load used for all measurements are 1 kg for 10 sec, and the vicker's hardness value is presented as HV1. Of each sample there are taken 5-10 hardness measurements, with sufficient space both between each measurement and the edge of the sample. Of these 5-10 measurements the mean value is calculated along with the standard deviation. The calibration of the measuring apparatus along with the measurements themselves are always done in a consistent manner. However, since the measurements are done by hand the recorded values are prone to error. The results should be viewed more of in relation to eachother rather than as exactness in relation to other work.

3.3.2 Electrical Conductivity

Electrical Conductivity measurements are conducted with a Sigmatest 2.069 device. A sensor is pressed on the sample and the device reads the conductivity value. In total 10 readings are done on separate parts of the sample, of which the mean value is calculated along with the standard deviation. The highest frequency option of 960 kHz is used for all measurements. The units of measurement are in mega siemens per meter $\mathrm{MS\,m^{-1}}$ ([10]).

3.4 TEM Sample Preparation

The set of samples to be viewed in the TEM are of the saved "after AA" condition. Seven samples are chosen for TEM study, these conditions are from the lean 6060 and the rich 6082 alloys. These conditions include the direct age and the 5, 21 and 80 °C aged for one month from 6060, as well as the direct age and the 5 and 21 °C aged for one month from 6082. The samples are cut by machine along the 35mm length such that the large surface of the new rectangle are 35mm×3mm for 6005 and 6060, and 35mm×6mm for 6082 and 6110, as shown in figure 9. These cut samples are ground down to between 150-50 µm in thickness, from either side such that the remaining piece is the center piece of the original. This happens in three stages with sandpaper grit p800, p1200 and p2400, running water and soap, see figure 10. To achieve this kind of thin sample-thickness the samples are mounted on a device that can be screwed such that a thinner and thinner sample can be made through the grinding process.

Once the sample reach the desired thickness of 150-50 µm, circular discs with a diameter of approximately ∼3 mm are punched out from the sample. A special purpose device is used for punching. The material that form these holes are ready for electropolishing, see figure 11.
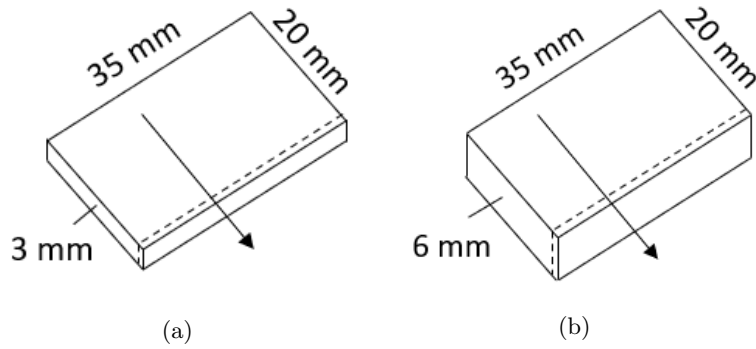
Figure 9: Sketch of samples with a dotted line. The dotted line represents where the samples are cut to produce TEM samples. The arrows indicate the extrusion direction. (a) 6005 and 6060. (b) 6082 and 6110.
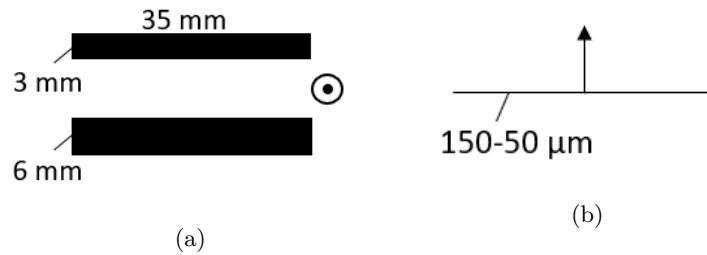
Figure 10: (a) View from above, looking down on the cut sample. The circle with a dot represents the extrusion direction. (b) Side-view of the cut and ground-down sample. The thickness are between 150-50 μm. The arrow represents the extrusion direction.
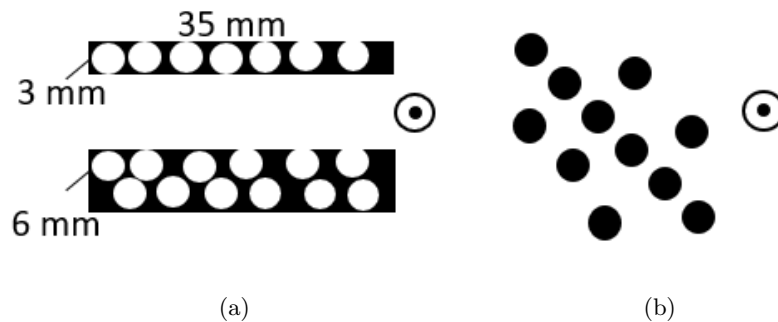
Figure 11: (a) Example of a sample thats been punched out. The circle with a dot represents the extrusion direction. (b) A typical batch of electropolish-ready samples. The diameter of these circular discs are ∼3 mm. The thickness are between 150-50 μm. The circle with a dot represents the extrusion direction.

3.4.1 Electropolishing

The device used for electropolishing are Struers - Tenupol - Electropolishing Unit. The electropolish-ready circular disc samples are placed in a holder that clamp the edges of the sample such that the center part is exposed from both sides. A container is filled with a 1 L mixture of methanol and nitric acid, acting as the electrolyte. The electrolyte are hosed in tiny beams from both sides into the center of the sample, etching away at the sample. In addition there is a sensor mounted on one side of the sample, along with a beam of light shot at the sample from the other side. As soon as the electrolyte has etched its way through the center of the sample, the sensor catches a beam of light and the process is ended. The sensitivity to light setting of the sensor is set to very low such that only a very small intensity of light is adequate to end the process. This produces a very small hole in the center of the sample, sometimes barely visible to the naked eye. On the very edge of

this hole the sample thickness in a good sample is between 50-150 nm. In a bad sample, the edge of this hole is seen as smooth, and is thus thicker and usually not suited for TEM-imaging. In a good sample, the edge of the hole is rugged like the coastline of Norway on a map, producing the thickness suitable for TEM-imaging, see figure 12.

(a)   (b)
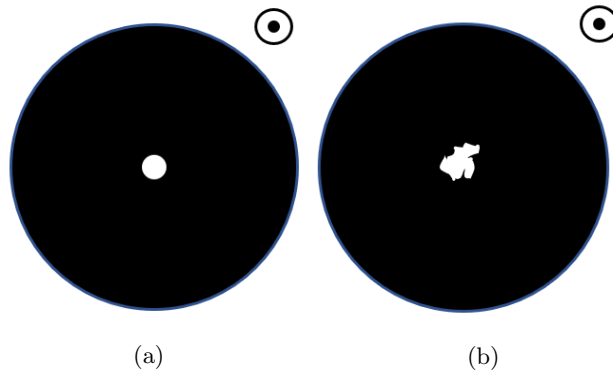
Figure 12: (a) Example of an electropolished sample with a smooth hole usually not fit for TEM-imaging. The circle with a dot represents the extrusion direction. (b) Example of an electropolished sample with a rugged hole better suited for TEM-imaging. The circle with a dot represents the extrusion direction.

A larger hole may sometimes be preferred as it will increase the amount of edge with potentially good imaging opportunities.

3.5   Transmission Electron Microscopy

A Transmission Electron Microscope (TEM) of type JEOL JEM-2100 are used throughout this experiment for imaging. A double-tilt holder is used to contain the sample in the microscope, allowing for tilting of the sample in both x and y direction. The acceleration voltage are set to 200 kV for all operation on the microscope. Three apertures are available on the microscope, the condenser aperture, the objective aperture and the selected area (SA) aperture, each with several sizes. The largest condenser aperture will be inserted through all imaging. The first step in imaging is to find a suitable area. This area needs to be close to the $< 100 >$ zone-axis to avoid excessive tilting of the sample. The samples are prepared relative to the extrusion direction because this increases the chance of the general grain to be viewed in the $< 100 >$ direction. Once a suitable area on a grain viewed close to the $< 100 >$ direction are found, the sample are tilted to view as directly as possible into the $< 100 >$ direction. This is done both through viewing the diffraction pattern of the area and the kikuchi-lines. The diffraction pattern is produced by inserting a SA aperture, spreading the electron beam to maximum size, and entering diffraction mode on the microscope. An example of a diffraction pattern viewed very close to the $< 100 >$ direction, if not spot on, can be seen in figure 13. If the viewing angle is slightly off, the intensity of the diffraction pattern will be skewed to one side. Tilting the sample such that the intensity of beams are strongest for the center beam and dissipate evenly in all directions, as seen in figure 13(b), will ensure a very close to spot on viewing angle.

(a) (b)
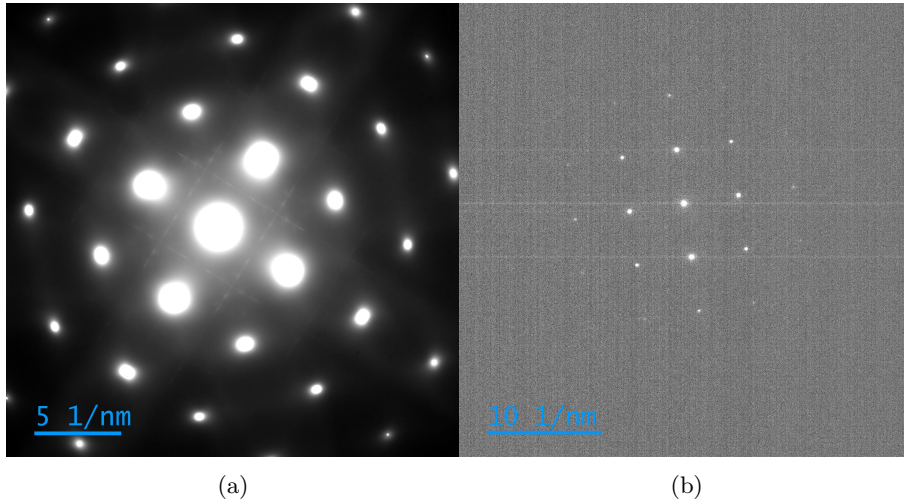
Figure 13: (a) Example of a diffraction pattern produced by viewing close to, or directly at the $< 100 >$ zone-axis. (b) $< 100 >$ zone-axis diffraction pattern with clear dissipating intensity of beams further from the center in all directions.

To obtain the kikuchi-bands the electron beam is converged to a spot and diffraction mode is entered on the microscope. The only aperture inserted now are the condenser aperture. If the $< 100 >$ zone-axis is close a 4-fold symmetrical crossroad will appear with 8 roads leading to it, see figure 14(a). These roads are known as the kikuchi-bands. Tilting the sample such as to view directly into this crossroad is to be in the $< 100 >$ zone-axis. A view of the converged beam directly placed in the $< 100 >$ zone-axis can be seen in figure 14(b).

(a) (b)
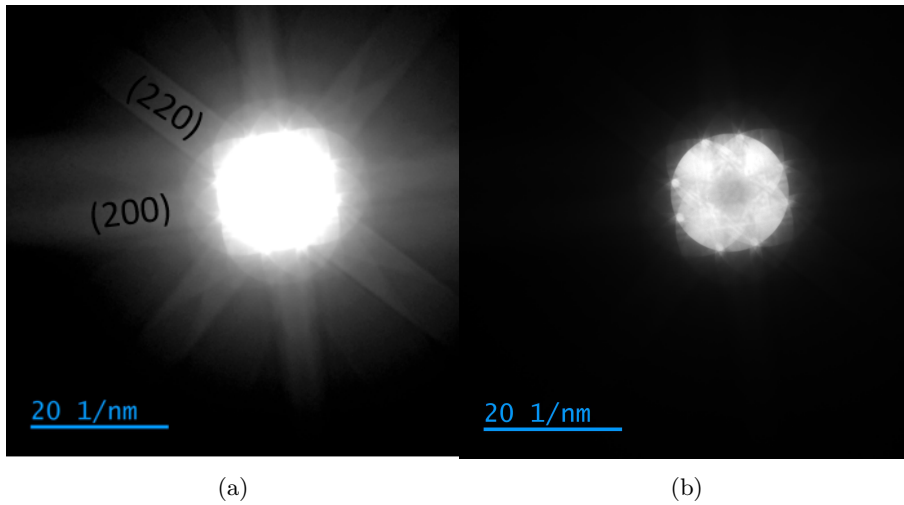
Figure 14: (a) A view directly into the 4-fold symmetrical crossroad with 8 roads (kikuchi-bands) leading to it. This is the $< 100 >$ zone-axis. There are two types of bands, one wide (220) and one thinner (200). The bands are barely visible due to the converged beam sitting in zone-axis, however they are much more clear when seen on the microscope screen. (b) A view of the converged beam directly placed in the $< 100 >$ zone-axis as seen in the microscope.

When the viewing-angle is directly in the $< 100 >$ zone-axis of a suitable sample area, the imaging can start.

3.5.1 Bright-Field Imaging

To achieve a Bright-Field (BF) image the first thing to do is reveal the diffraction pattern of the chosen area, as described above. Once the diffraction pattern is clearly seen an objective aperture are inserted around the center beam of the diffraction pattern. The objective aperture must be of such size that only the intensity of the center beam goes through, see figure 15(a). All other beams are masked out. When the objective aperture is in place the SA aperture is removed and imaging mode is entered on the microscope. To take an image the attached camera is inserted with usually 1 sec exposure time to start viewing on the computer screen. The beam is converged such that a clear image appears, but not so much as to burn the sample or more importantly the camera. For the Mg-Si samples in question needle-like structures, the precipitates, will appear. A suitable magnification is chosen based on the length of these precipitates, in this case 120k to 250k is used. The precipitates grow perpendicular to one another in the xyz directions. When BF images are taken only the length of precipitates growing in two directions are revealed, the third set of precipitates grow into the sample such that only their cross-section is seen. An example of a BF image is shown in figure 15(b). The length of the precipitates are measured using ImageJ software by drawing a line along the precipitates, see example in figure 16. All precipitates, except those extending outside the image, are measured to avoid bias towards certain precipitate lengths.

(a)   (b)
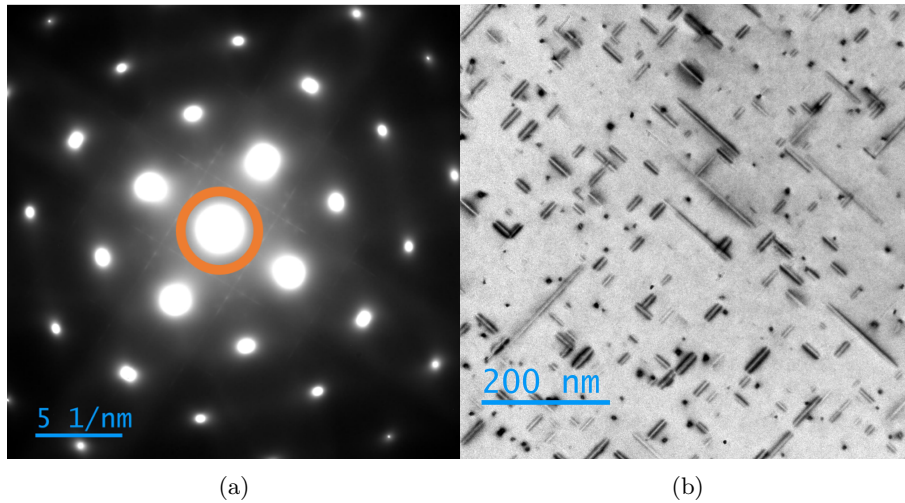
Figure 15: (a) Illustration of objective aperture placement for BF-imaging marked as orange circle. Only the intensity from the center beam are let through as all others are masked out. (b) Example of a BF image taken at 120k magnification. Precipitates can be seen extending in two directions perpendicular to each other. The third set of precipitates growing into the sample can be seen as black dots on the image.

(a)   (b)
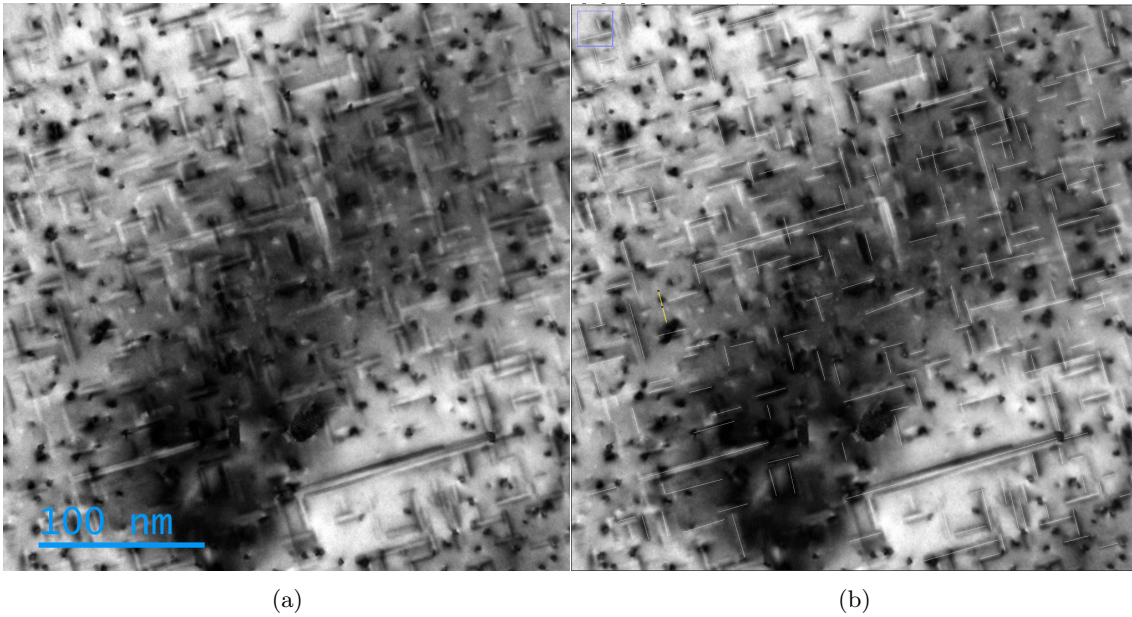
Figure 16: (a) BF image of 6082 direct age taken at 250k magnification with an X-tilt of $-0.5°$ and a Y-tilt of $-9.5°$. (b) The same BF image with length of precipitates measured by drawing lines along precipitates. Here the average precipitate length are measured to be $< l >= 17.66\,\mathrm{nm}$ with a standard deviation of $\sigma = 12.65\,\mathrm{nm}$.

3.5.2   Dark-Field Imaging

The method of Dark-Field (DF) imaging is similar to that of BF imaging, the difference being the placement of the objective aperture. Every other step of the process is identical to BF imaging. The placement of the objective aperture is showcased in figure 17(a). Unlike a BF image, the DF image have a dark background with white dots spread across it, see figure 17(b). These white dots are the precipitates facing into the sample. These dots are counted by a marking function in the ImageJ software, and the area of the image is fetched from the image metadata. An example of a DF image, as well as the counted image, is shown in figure 18.

(a)   (b)
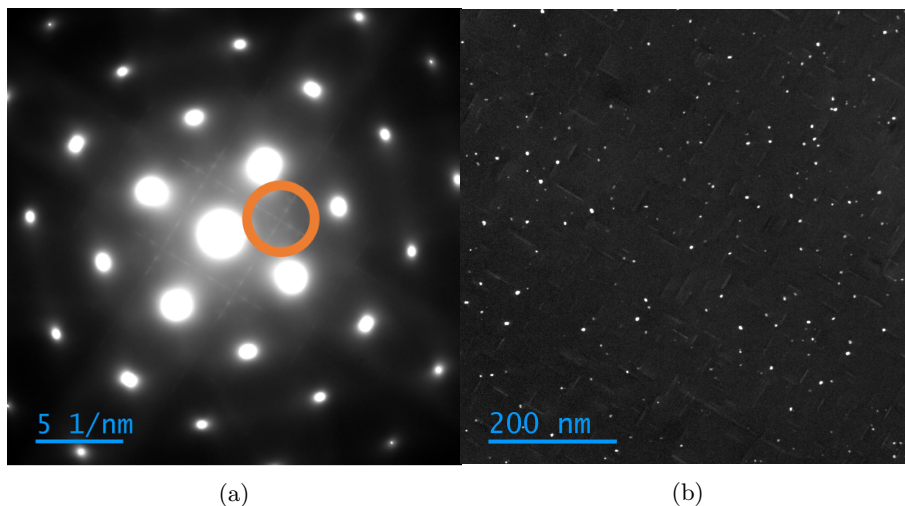
Figure 17: (a) Example of placement of objective aperture for DF imaging marked as orange circle. Any of the four cross-marked areas may be chosen with the same result. (b) Example of DF image with white dots across a dark background.

16
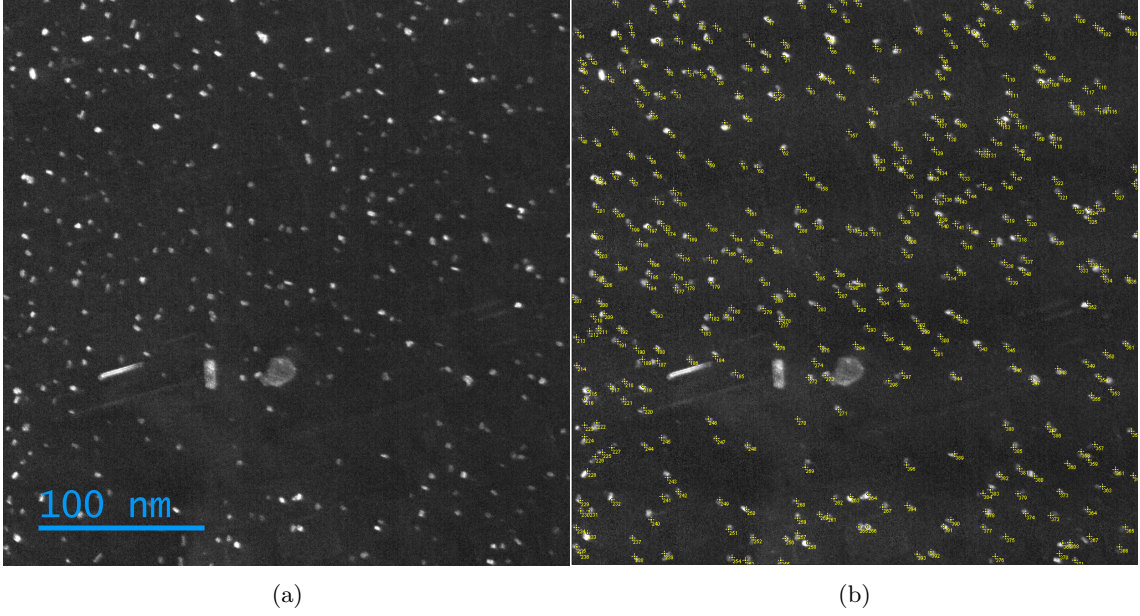
Figure 18: (a) DF image of 6082 direct age taken at 250k magnification. The white dots are precipitates facing into the sample, resembling the night sky. (b) The fully counted DF image, each precipitate is marked during counting. The total number N of precipitates counted here are $N = 395$ and the area of the image is $341.7 \, \text{nm} \times 341.7 \, \text{nm}$.

3.5.3 Converged-Beam Electron Diffraction

Converged-Beam Electron Diffraction (CBED) are used to measure sample area thickness in this experiment. A comparison between CBED and EELS (Electron Energy Loss Spectroscopy) thickness determination were made together with prof. Calin D. Marioara (SINTEF). The CBED and EELS data were taken from the same area of the same sample, across five different areas. The results are showcased in table 3. The CBED method gives consistent lower thickness data in comparison with EELS.

Table 3: Comparison of thickness determination with CBED and EELS. CBED gives lower values for thickness-data than EELS for all areas that is found to be between 60% and 90% of the EELS value.

	CBED	EELS	CBED/EELS$\sim$
Area 1	45.60 nm	59.19 nm	0.77
Area 2	69.72 nm	78.47 nm	0.89
Area 3	42.48 nm	68.92 nm	0.62
Area 4	61.27 nm	87.01 nm	0.70
Area 5	84.65 nm	101.98 nm	0.83

To obtain a CBED thickness measurement the kikuchi-lines must first be revealed, as mentioned in chapter 3.5. It is important that this is done together with DF imaging, as the area from the DF image together with the thickness from CBED gives the volume of the sample area. This also makes the process straight forward since for DF imaging the microscope is already in the (100) zone-axis. Once the kikuchi-bands are revealed, the sample is tilted along a (220) band. Care must be taken during tilting to make sure the CBED image is not taken at a different area of the sample than the DF image. When enough tilting is done such that the viewing angle is on top of the (220) band, a slight tilting is done away from the band. This causes a two-beam condition, revealing a second dark disc next to the beam. In the beam a dark line can now be seen, and in the dark disc there are one bright line along with several dark fringes, see figure 19(a). The distance between the dark line in the beam-disc to the brightest line in the dark disc are measured, as well as the distance between the brightest line in the dark disc to its three nearest dark fringes.

In total four measurements to determine thickness. These measurements are done using Gatan Digital Micrograph software, by drawing an intensity plot from the dark line in the beam to past the third fringe in the dark disc, see figure 19(b). When these four measurements are taken, they are entered into a python script written by Christoph Hell ([11]) that calculates the thickness based on distance between fringes, see figure 20(a). Shorter distance between fringes means more fringes and a thicker sample, and vice versa. The program presents three plots representing three iterations of the thickness calculation, see figure 20(b). The first iteration $n_k = 1$ are chosen for all CBED images.
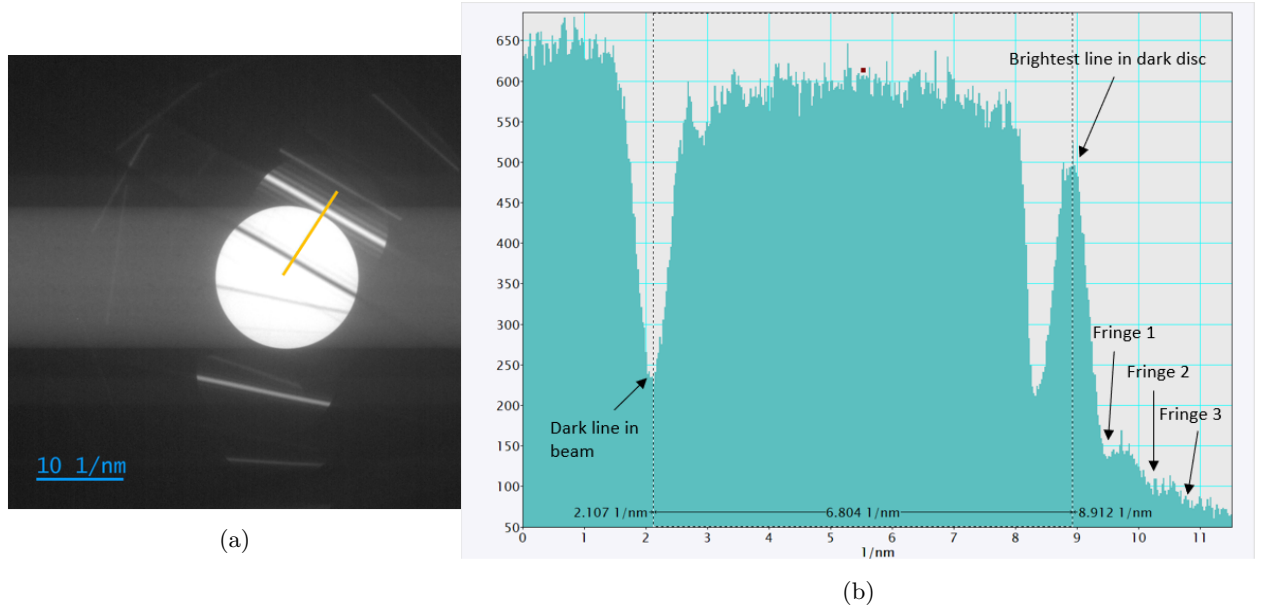
Figure 19: (a) CBED two-beam image used for thickness determination of a 6082 direct age sample area. An orange line is drawn starting from center of beam and ending past the third fringe in the dark disc. (b) Resulting intensity plot from line drawn in CBED two-beam image. The dip in intensity at $2\,\text{nm}^{-1}$ is from the dark line in the beam and the peak in intensity at $9\,\text{nm}^{-1}$ is the very bright line in the dark disc. The minor dips in intensity starting past $9\,\text{nm}^{-1}$ are from the three fringes.
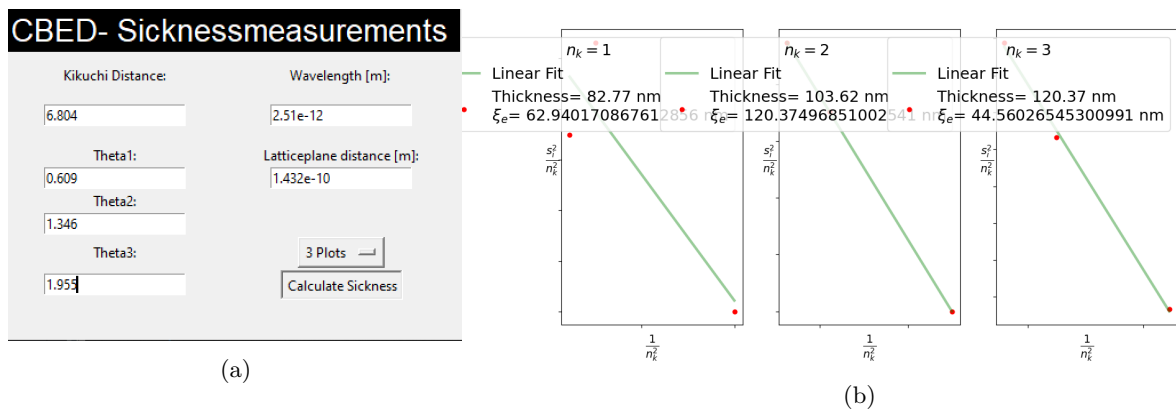
Figure 20: (a) User interface of thickness determination program. Kikuchi distance and the three fringe distances θ_1, θ_2, θ_3 are entered. Wavelength $\lambda = 2.51\,\text{pm}$ and latticeplane distance $d = 1.432\,\text{Å}$ are constant throughout the experiment. (b) Three iterations of thickness determination. $n_k = 1$ are chosen for all CBED measurements. Here the thickness are found to be $82.77\,\text{nm}$. ξ_e are the extinction distance.

18

3.5.4 High-Resolution TEM-Imaging

The High-Resolution TEM-imaging (HRTEM) process are similar to that of the BF and DF process, with a different placement of the objective aperture as shown in figure 21(a). The aperture are placed in the center of the diffraction pattern including the center beam and the four beams closest to it. This means a larger aperture are used for HRTEM in comparison to BF and DF. HRTEM-imaging are used to measure the cross-section (CS) area of precipitates, the same as can be seen as white dots in a DF image. To achieve this a higher magnification has to be used, usually 500k-1200k magnification will be sufficient depending on the sample. To ensure a clear view of the CS of the precipitates, the height of the specimen holder is carefully adjusted as well as the spread of the beam. Every other step of the process are the same as for BF and DF imaging. An example of a HRTEM image is shown in figure 21(b). The precipitate CS are seen to have structure in the HRTEM images. The CS are measured by free-hand drawing using the ImageJ software. A line is drawn around the circumference of the precipitate CS and the ImageJ software calculates the area. An example of a HRTEM image with measured cross-sections are shown in figure 22.

(a)   (b)
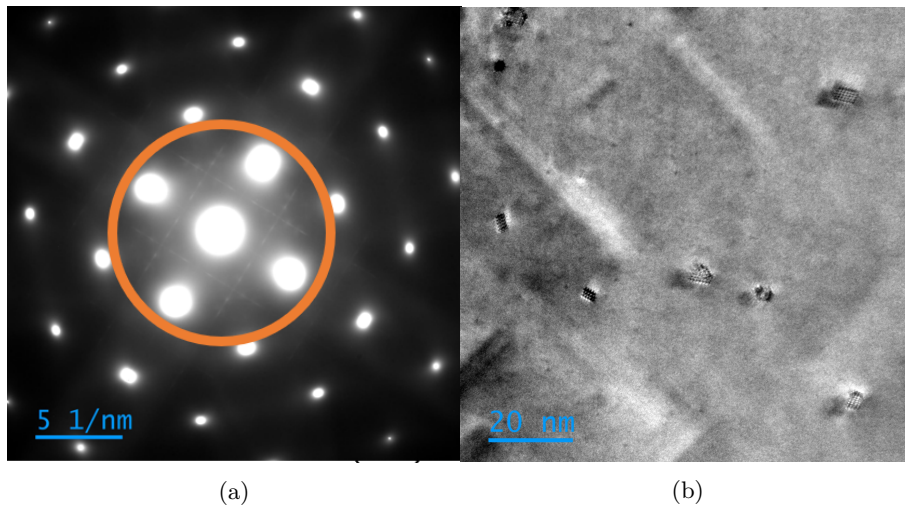
Figure 21: (a) Example of placement of objective aperture for HRTEM imaging marked as orange circle. The aperture are large enough to include the center beam and its four closest neighbours. (b) Example of HRTEM image taken at 800k magnification. Precipitate cross-sections can be seen containing structure. Precipitate needle-lengths can also be seen, most of which stretch outside the image.

(a)	(b)
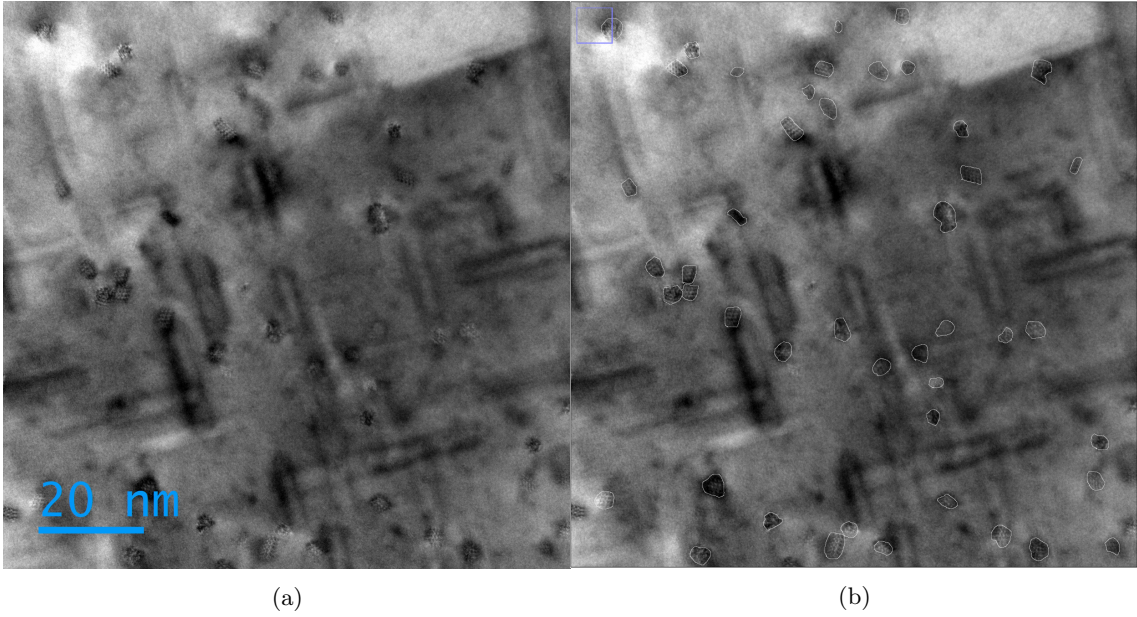
Figure 22: (a) HRTEM-image of 6082 direct aged taken at 800k magnification. In this sample a higher magnification than 800k is useful due to the high amount of small precipitate cross-sections per image. (b) Fully measured HRTEM image of 6082 direct aged. Measurement are done by drawing around the circumference of the cross-section of the precipitates. Here the average CS area are found to be $<CS>= 9.96\,\text{nm}^2$ with a standard error of $\pm 0.33\,\text{nm}^2$.

3.6 Precipitate Statistics

Figure 23 shows the defined [100], [010] and [001] directions.
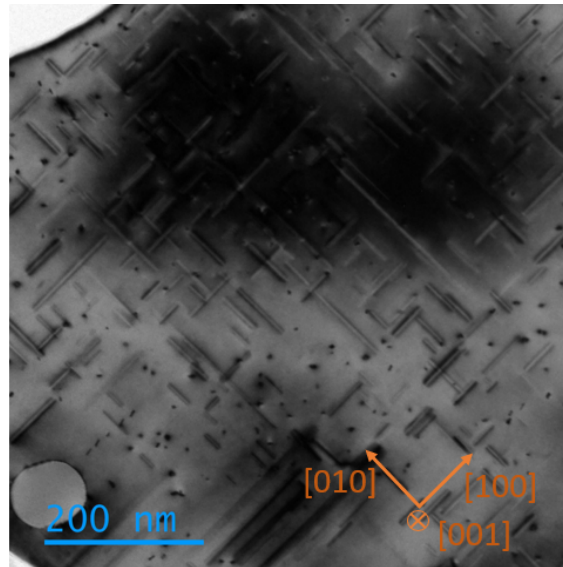
Figure 23: BF image with defined directions [100], [010] and [001].

Since the number of precipitates N facing in the [001] direction are taken from a DF image along with the specimen area A, together with the CBED specimen thickness measurement t, the volume $V = At$ can be calculated as well the precipitate number density $\rho = \frac{3N}{At} = \frac{3N}{V}$. N is multiplied by 3 to account for precipitates in the [100] and [010] directions, and therefore we have a value for the number of precipitates per volume of sample. However, a volume-correction is made to account for the relative size of the specimen thickness and the average precipitate length $\frac{<l>}{t}$, with

the average precipitate length $< l >$ measured from BF images. The expression for the volume corrected volume becomes $V' = V(1 + \frac{<l>}{t})$ [12]. If the average precipitate length is much smaller than the specimen thickness the volume correction is small. The volume-corrected equation for precipitate number density becomes

$$\rho = \frac{3N}{V(1 + \frac{<l>}{t})} = \frac{3N}{At(1 + \frac{<l>}{t})}. \tag{1}$$

Equation 1 are used to calculate precipitate number density ρ for all sample conditions investigated by TEM imaging. Some precipitate needles along the [100] and [010] directions may have their length cut due to the electropolishing process. The measured value of $< l >$ is therefore assumed to always be smaller than its real value. The relative error in average precipitate length is calculated as

$$\frac{\Delta < l >}{< l >} = \frac{<l>_m}{t} \cos\theta \tan\phi \tag{2}$$

where $< l >_m$ are the measured average precipitate length across all BF images of the same specimen. It is assumed that needles in both [100] and [010] direction are cut in a similar manner in all images, therefore θ is taken to be $\theta = 45°$ in all calculations. ϕ is a function of the misorientation of the sample, and is taken as $\phi = \arccos(\cos(X)\cos(Y))$ where X and Y is the tilt of the sample holder in respect to its orginial position. This tilt is noted for every image taken and is usually between 0-10° in either direction. The relative error of the precipitate number density is found from

$$\frac{\Delta\rho}{\rho} = \sqrt{(\frac{\Delta V}{N})^2 + (\frac{\Delta V'}{V'})^2} \approx \frac{\Delta V'}{V'} = \sqrt{(\frac{\Delta V}{V})^2 + \frac{(\frac{\Delta<l>}{<l>})^2 + (\frac{\Delta t}{t})^2}{(1 + \frac{t}{<l>})^2}}$$

where

$$\frac{\Delta V}{V} = \sqrt{(\frac{\Delta A}{A})^2 + (\frac{\Delta t}{t})^2}.$$

The relative error of the area A is estimated to be zero since this is taken directly from the image metadata, while the relative error of the specimen thickness are assumed to be 10%. Therefore $\frac{\Delta V}{V} = 0.1$ and the relative error of the precipitate number density becomes

$$\frac{\Delta\rho}{\rho} = \sqrt{(0.1)^2 + \frac{(\frac{\Delta<l>}{<l>})^2 + (\frac{\Delta t}{t})^2}{(1 + \frac{t}{<l>})^2}}. \tag{3}$$

Equation 1, 2 and 3 together with the volume fraction of precipitate needles VF

$$VF = \rho < CS >< l >_m \tag{4}$$

completes precipitate statistics for one set of images. Several sets of images are taken per sample and the average values across these sets of images are presented in section 4. As an example one set of measured images from the 6082 direct aged condition are presented in previous sections 3.5.1 to 3.5.4 in figures 16, 18, 19 and 22. The average precipitate length are found to be $< l >= 17.66$ nm in figure 16 together with tilt $(X, Y) = (-0.5°, -9.5°)$, the total number of precipitates counted in figure 18 are $N = 395$ together with an area of $A = 341.7$ nm $\times 341.7$ nm $= 116\,758.89$ nm^2. The measured thickness of this area are determined to be $t = 82.77$ nm in figure 20 and the average precipitate cross-section are measured as $< CS >= 9.96$ nm^2 from figure 22 together with several other HRTEM images of the area. These values are inserted into equations 1, 2, 3 and 4, and a table is made. The result are presented in table 4.

Table 4: Precipitate statistics for one set of images taken from the 6082 direct aged sample. The imaging area are $A = 116\,758.89\,\text{nm}^2$ and the tilt of the images are $(X, Y) = (-0.5°, -9.5°)$. The precipitate number density ρ are calculated from eq.1, the relative error of the precipitate length and precipitate number density are calculated from eq.2 and eq.3 respectively. The volume fraction of precipitates are calculated from eq.4 and are found to be 1.78%. Additional sets of images are used to complete the precipitate statistics for the 6082 direct aged condition.

N	t [nm]	$<l>$ [nm]	$\frac{\Delta <l>}{<l>}$	ρ [nm^{-3}]	$\frac{\Delta \rho}{\rho}$	$<CS>$ [nm^2]	VF
395	82.77	17.66	0.025	0.0001	0.101	9.96 $\pm$0.33	0.0178

4 Results and discussion

The results presented in this section are measured after artificial ageing as these are stabilized conditions of the samples after heat treatment and are used for TEM investigation. For measurements taken before AA see appendix. In table 5 are presented again an overview of the sample composition.

Table 5: Simplified composition with Si, Mg and Cu in **at%**.

	Si	**Mg**	**Cu**	**Mg/Si**
6005	0.6	0.5	0.07	1.2
6060	0.4	0.5	-	0.8
6082	0.9	0.7	-	1.3
6110	0.7	0.9	0.09	0.8

The measured peak AA values for each sample is first presented in chapter 4.1. Hardness values from the main experiment are presented in chapter 4.2, followed by electrical conductivity values in chapter 4.3. Precipitate statistics from TEM imaging are presented in chapter 4.4.

4.1 Artificial Ageing Peak-Age values

Results from the AA peak-age condition investigation are shown in figure 24, 25, 26 and 27. These measurements include all four alloys, but only a selection of NA conditions. These conditions include the direct aged, the 5, 21, 60 and 80°C aged for 24hr, and the 60 and 80°C aged for 1 month. Subsequent measurements are taken after a total of 1, 2, 5, 10 and 24hr AA at 185°C of the same sample.

AA for 5-10hr at 185°C are found to reach peak AA hardness for most alloy/conditions. An increase in hardness are seen from 1-5hr AA and a decline in hardness from 10-24hr AA. The chosen 5hr AA used throughout this experiment seem to be a good middle ground for most conditions, however adding extra AA time up to 10hr does not seem to reduce the measured HV1 value for most conditions and would see an increase for some.
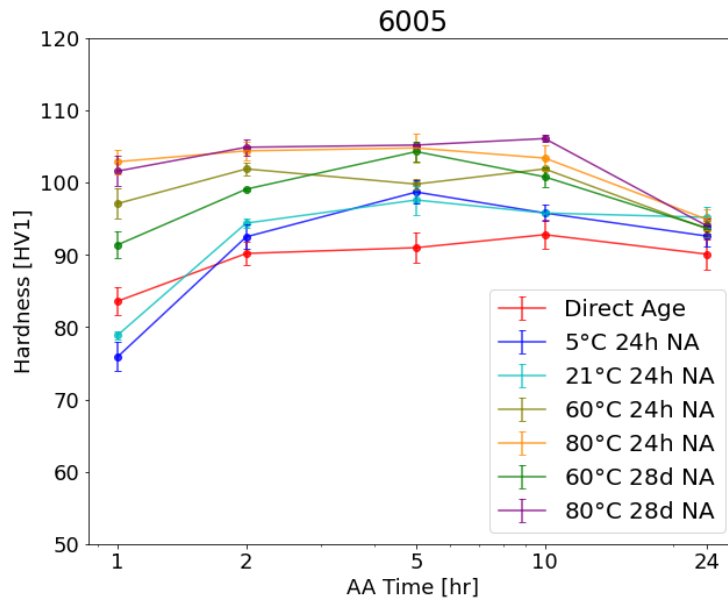
Figure 24: 6005 peak AA hardness measurements. Cu containing alloy. The maximum change in hardness across different AA times are 10-20HV1. All conditions reach peak AA somehwere between 2-10hr of AA.
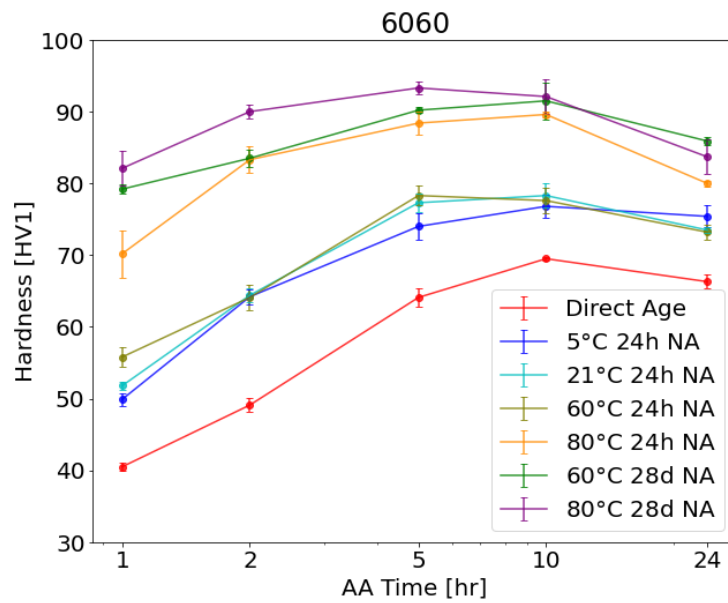
Figure 25: 6060 peak AA hardness measurements. Cu free alloy. A steady increase in HV1 can be seen for all conditions from 1-5hr of AA. The peak AA hardness are between 5-10hr of AA for most conditions.
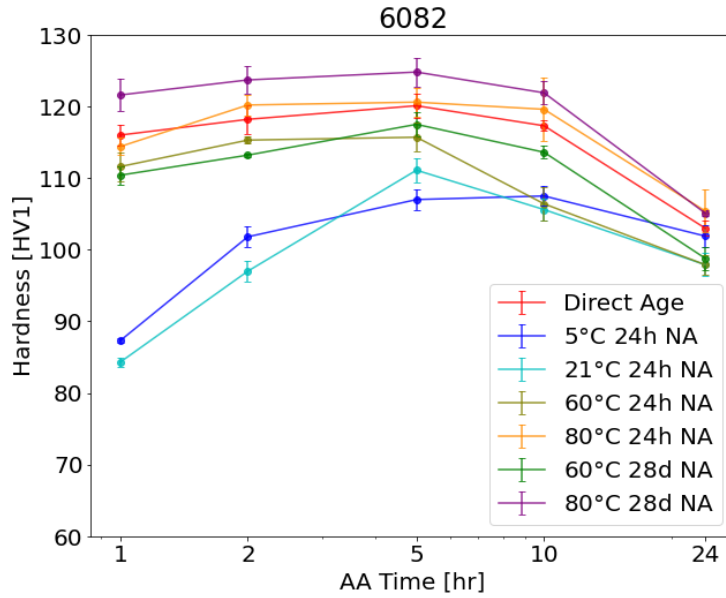
Figure 26: 6082 peak AA hardness measurements. Cu free alloy. Peak AA hardness are found between 2-10hr of AA.
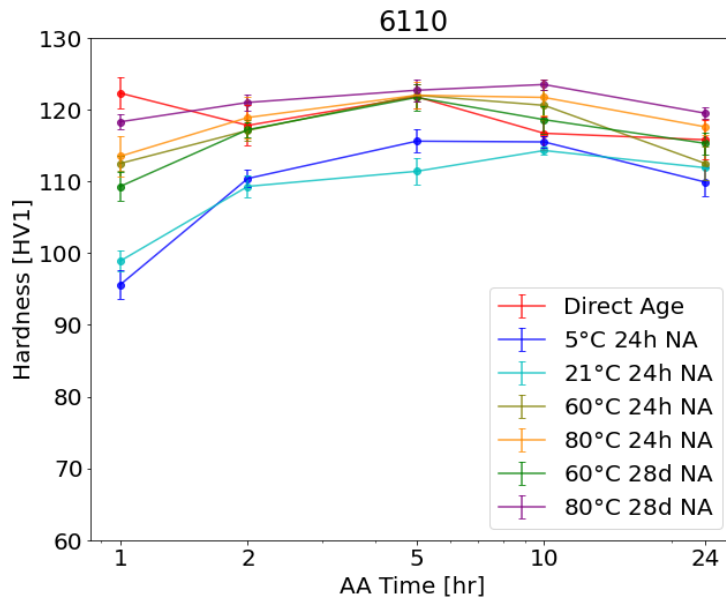
Figure 27: 6110 peak AA hardness measurements. Cu containing alloy. Peak AA hardness found between 5-10hr for most conditions.

4.2 Hardness values after AA

All hardness mesurements are done by method presented in section 3.3 with SHT at 550°C for 30 min and AA at 185°C for 5 h as constants in the heat treatment process for all samples. NA temperatures range from −26°C to 100°C and NA times include 1 day, 1 week, 1 month as well as the direct aged. The values presented are measured after artificial ageing, see figure 7(a) in section 3.3. The hardness values measured after AA for the two lean alloys 6005 and 6060 are presented in figure 28 and 29, and for the two rich alloys 6082 and 6110 in figure 30 and 31. The measured values are presented in table-format in the appendix.
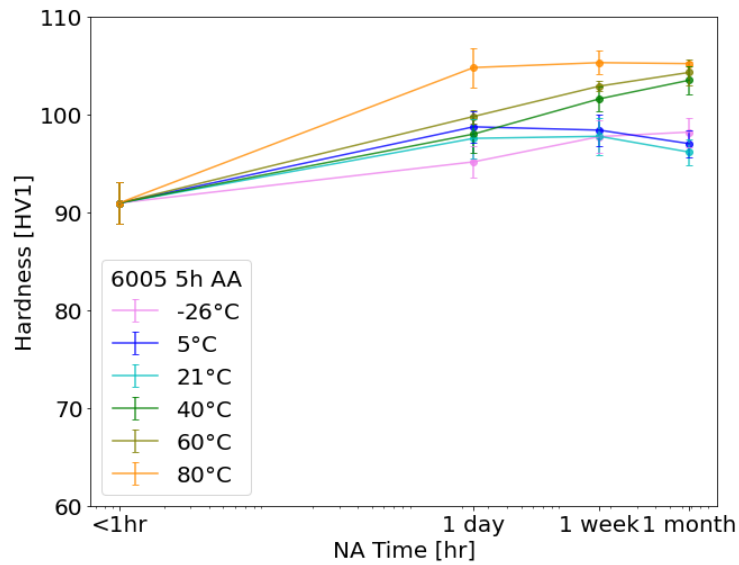
Figure 28: Alloy 6005 hardness values taken after AA. Relative to the direct aged condition a clear increase in hardness are seen across all NA temperatures and times. A separation of the values taken after 1 month of ageing can be seen in two groups, one lower and one harder. For NA temperatures -26, 5 and 21°C the hardness measurements are slightly below 100HV1 and for NA temperatures 40, 60 and 80°C the hardness measurements are slightly above 100HV1. The 80°C NA condition are clearly giving higher hardness values across all NA times, however the curve flatten out after only 1 day of NA. The 5 and 21°C reach their hardest measured values after 1 day of NA and their value decreases with more NA. However -26°C, together with 40 and 60°C, have an increasing tendency in hardness for more NA. The -26°C measurements were added after the rest to see if the hardness values would decrease below the direct aged.
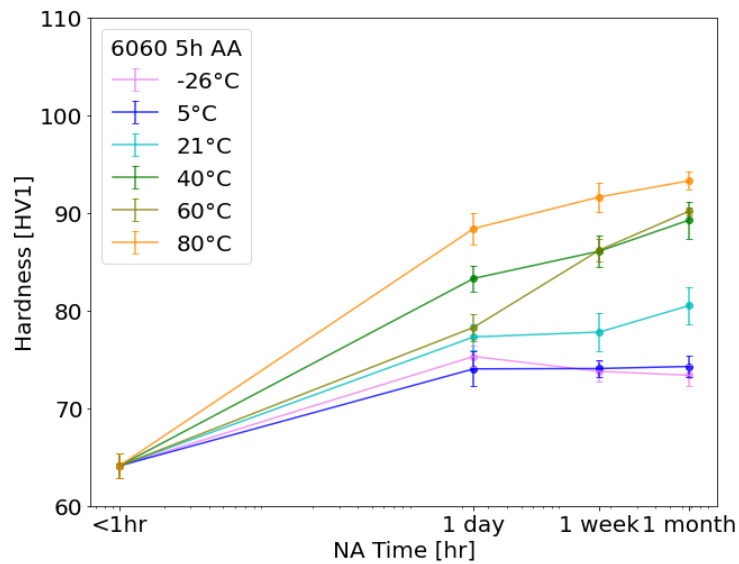
Figure 29: Alloy 6060 hardness values taken after AA. Relative to the direct aged condition a clear increase in hardness are seen across all NA temperatures and times. A similar behaviour can be seen here as for 6005, a separation of hardness values in two groups after 1 month of NA with temperatures -26, 5 and 21°C are measured to be 70-80HV1 and NA temperatures 40, 60 and 80°C are measured to be approximately 90HV1. NA temperatures of 21°C and higher have an increasing tendency in hardness for more NA time. -26 and 5°C reach maximum hardness after 1 day of NA and flattens out/decrease slowly with more NA. The -26°C measurements were added after the rest to see if the hardness values would decrease below the direct aged.
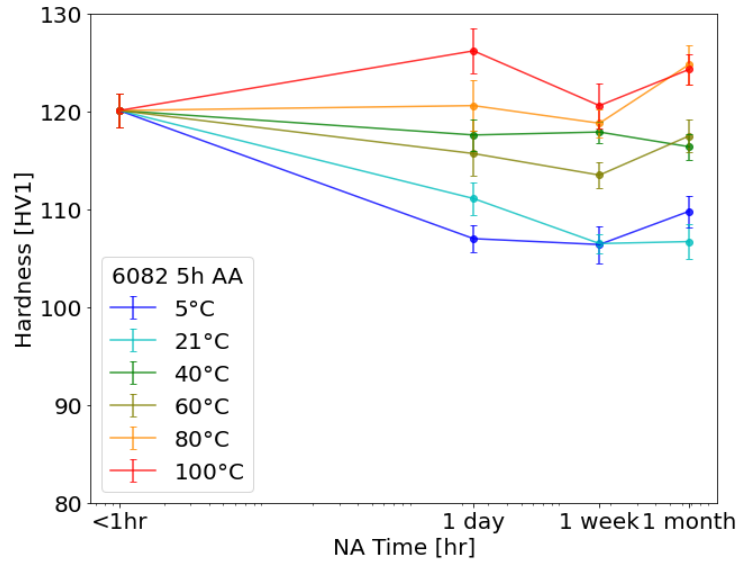
Figure 30: Alloy 6082 hardness values taken after AA. The direct aged sample start out hard at 120HV1, and most of the NA time and temperatures have a detrimental effect on hardening. After 1 month NA the values can be separated in three groups. The 5 and 21°C samples decrease steadily in hardness with NA and end with the lowest hardness values after 1 month. The 40 and 60°C have a very slight decrease in hardness with respect to the direct aged sample. The 80 and 100°C samples have a slight increase in hardness after 1 month NA. The behaviour of 60, 80 and 100°C samples are similar with a high hardness value after 1 day, a decline in hardness after 1 week, and increasing after 1 month. The 100°C measurements were added after the rest to see if the hardness values would increase above the direct aged.
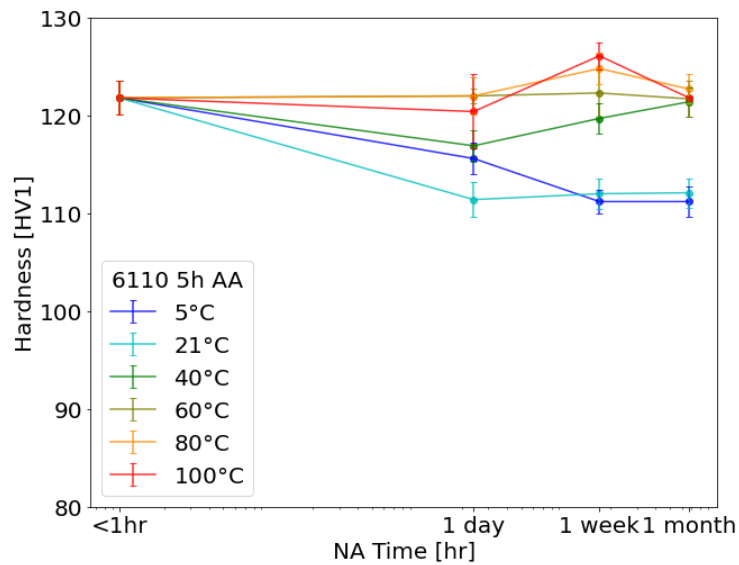
Figure 31: Alloy 6110 hardness values taken after AA. The hardness value of the direct aged sample are high being slightly above 120HV1. After 1 month NA the samples can be separated in two groups, the 5 and 21°C conditions measured at close to 110HV1, and the 40, 60, 80 and 100°C conditions measured to be close to the direct aged at 120HV1. The 5 and 21°C have a decreasing tendency across all NA times, however 21°C decrease fast after 1 day NA and the curve is more or less flat with additional NA. The 40°C condition decrease after 1 day NA and increase in hardness with subsequent NA, reaching direct aged hardness value after 1 month NA. The 60, 80 and 100°C conditions stay close to the direct aged condition, however the 80 and 100°C conditions see an increase in hardness after 1 week NA, but decline with more NA. The 100°C measurements were added after the rest to see if the hardness values would increase above the direct aged.

In both lean alloys 6005 and 6060 a NA temperature ranging from -26°C to 80°C increases the hardness value for all NA times relative to the direct aged condition. Alloy 6005 contain a higher at% of Si and Cu than the 6060 alloy and show higher values of hardness measurements across all NA conditions. However for both these alloys NA are found to be beneficial across the board. For the rich 6082 and 6110 most NA are either detrimental or equivalent to direct aged. However higher NA temperatures like 80°C and 100°C show signs of a possible increase in hardness with additional NA. These results compared to the Hydro Sunndalsøra 2007 experiment are presented in figure 32 with an approximate solvus line for this experiment.
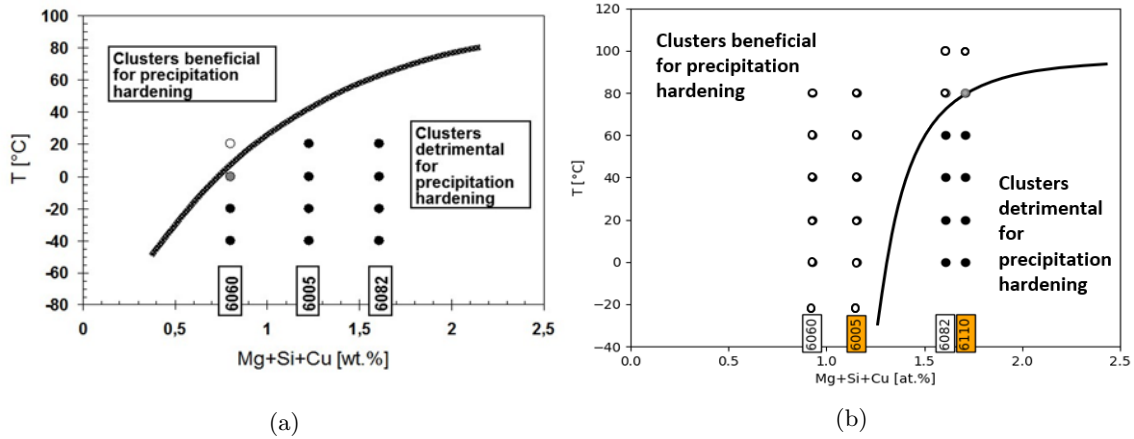
Figure 32: (a) Hypothetical solvus line from Hydro Sunndalsøra 2006. (b) Results from this experiment with the approximate solvus line for the results after 1 month NA. Beneficial and detrimental clusters are determined relative to the direct aged condition.

4.3 Electrical Conductivity values after AA

Electrical conductivity measurements are taken from the same samples as the hardness measurements. The measurements presented here are the after AA measurements, as in hardness in section 4.1. The before AA measurements are presented in the appendix, together with the values used for the following figures, in table-format. The lean 6005 and 6060 alloys are shown in figure 33 and 34, and the rich 6082 and 6110 alloys are presented in figure 35 and 36. All measurements are presented in mega siemens per meter $MS\,m^{-1}$.

Higher NA temperatures lead to a decrease in conductivity with subsequent NA time in all alloys. This is shown for the 40, 60, 80 and 100°C NA conditions. The 21°C condition seem to be most stable relative to its direct age sample for all alloys, however the -26°C condition in the two lean alloys 6005 and 6060 also show similar results relative to the direct aged condition. The 5°C condition lead to a decrease in conductivity for all alloys.
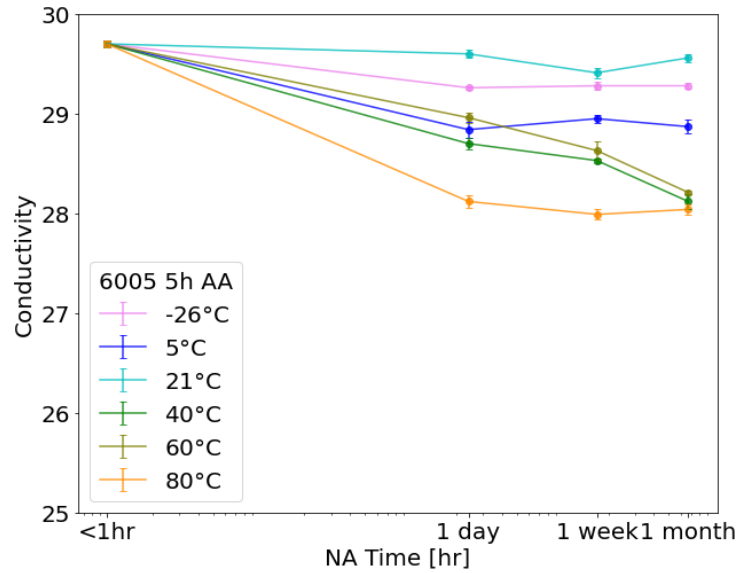
Figure 33: Electrical conductivity measurements of the 6005 alloy taken after AA heat treatment. All measurements decrease with both NA time and temperature relative to the direct aged. Lower NA temperature gives results more similar to the direct aged, with the 21°C sample as most similar across all NA times. The higher NA temperature samples all decrease steadily, except the 100°C condition which decrease rapidly and stabilize. The 40, 60 and 80°C conditions seem to converge to a value close to $28\,\mathrm{MS\,m^{-1}}$.
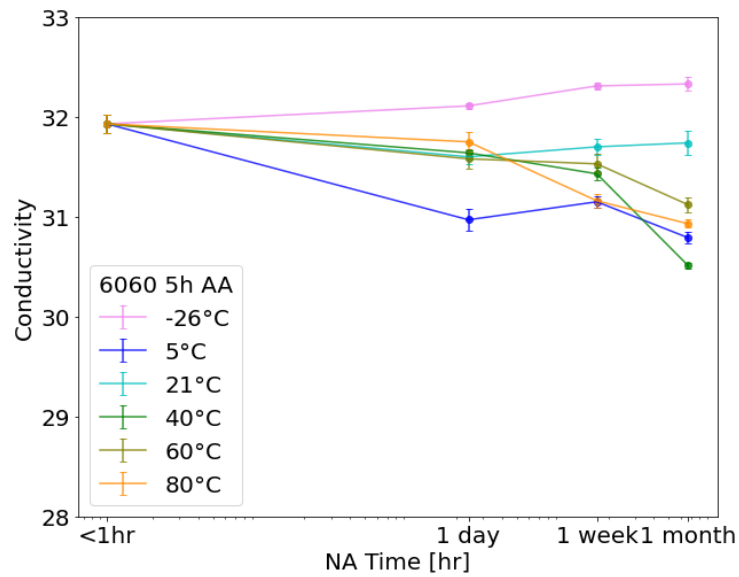
Figure 34: Electrical conductivity measurements of the 6060 alloy taken after AA heat treatment. Most conditions with NA temperature above 5°C see a decrease in conductivity, except the 21°C condition which is most stable relative to the direct aged. The -26°C NA however see a steady increase in conductivity with additional NA time.
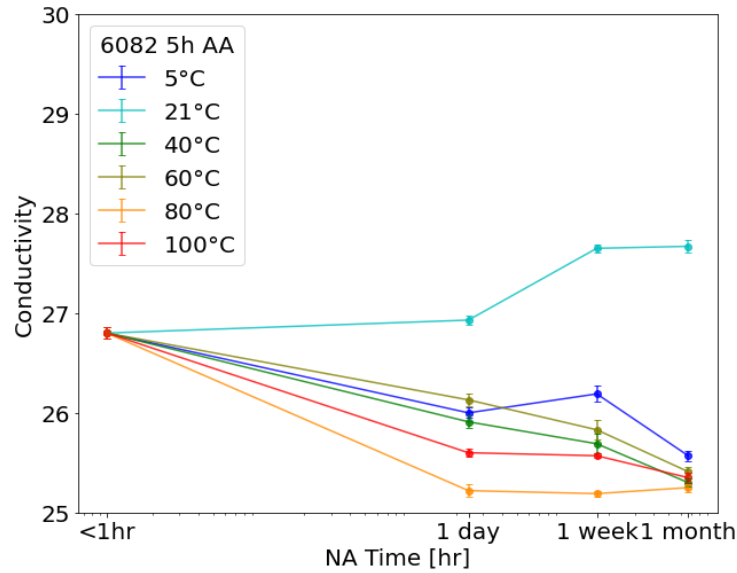
Figure 35: Electrical conductivity measurements of the 6082 alloy taken after AA heat treatment. The 21°C NA condition increase in conductivity between 1day and 1week of NA, and seem to stabilize. All other NA temperature conditions decrease with NA time, including the 5°C condition, and seem to converge to a value between 25-26 $\mathrm{MS\,m^{-1}}$.
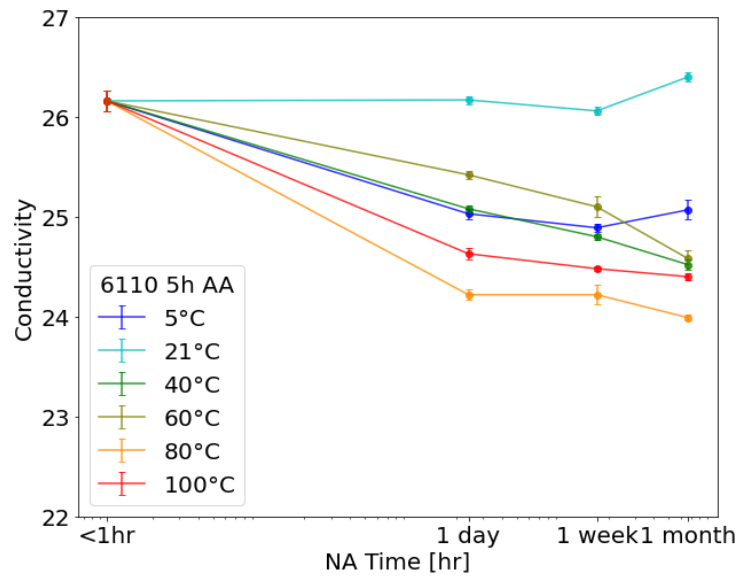
Figure 36: Electrical conductivity measurements of the 6110 alloy taken after AA heat treatment. The 21°C NA conditions are most stable relative to the direct aged. All other NA temperature conditions decrease with subsequent NA time. The 5°C condition show an increase in conductivity after 1week NA.

4.4   Precipitate Statistics Results

The conditions investigated with TEM imaging and precipitate statistics are from the lean 6060 alloy and the rich 6082 alloy, neither containing Cu. The summarized results from precipitate statistics, as well as the measured hardness and conductivity of the given condition, are presented in table 6. The investigated conditions from 6060 and 6082 alloys include the direct aged, the 5 and 21 °C conditions, as well as the 80 °C condition from the 6060 alloy, see figure 37. The 80 °C condition from 6082 were also supposed to be included, however producing suitable TEM samples

proved difficult.

Table 6: Precipitate statistics of the investigated conditions. Only the 6060 and 6082 alloys are included in the investigation. The very left column shows the NA temperature of the given condition. All conditions are aged for one month at NA, except the direct aged. HV1 results are shown as well as the conductivity. All presented results from TEM imaging are the calculated average across several sets of images per NA condition. This table includes the average precipitate length $< l >$ and the precipitate number density ρ, along with their relative error. The average cross-section $< CS >$ and the volume fraction of precipitates VF are also included.

NA	HV1	EC [$\mathrm{MS\,m^{-1}}$]	$< l >$ [nm]	$\frac{\Delta <l>}{<l>}$	ρ [$\mathrm{nm^{-3}}$]	$\frac{\Delta\rho}{\rho}$	$< CS >$ [$\mathrm{nm^2}$]	VF [%]
6060								
DA.	61.1	31.93	35.69	0.044	$7.87 \cdot 10^{-6}$	0.108	24.31	0.68
5°C	74.3	30.79	30.07	0.037	$6.63 \cdot 10^{-6}$	0.112	17.62	0.35
21°C	80.5	31.74	26.38	0.029	$2.25 \cdot 10^{-5}$	0.108	14.66	0.86
80°C	93.3	30.93	13.25	0.008	$7.40 \cdot 10^{-5}$	0.104	7.11	0.69
6082								
DA.	120.1	26.80	17.01	0.025	$1.04 \cdot 10^{-4}$	0.104	9.96	1.76
5°C	109.8	25.57	48.09	0.045	$1.32 \cdot 10^{-5}$	0.117	23.08	1.46
21°C	106.7	27.67	39.97	0.032	$3.25 \cdot 10^{-5}$	0.113	13.96	1.77
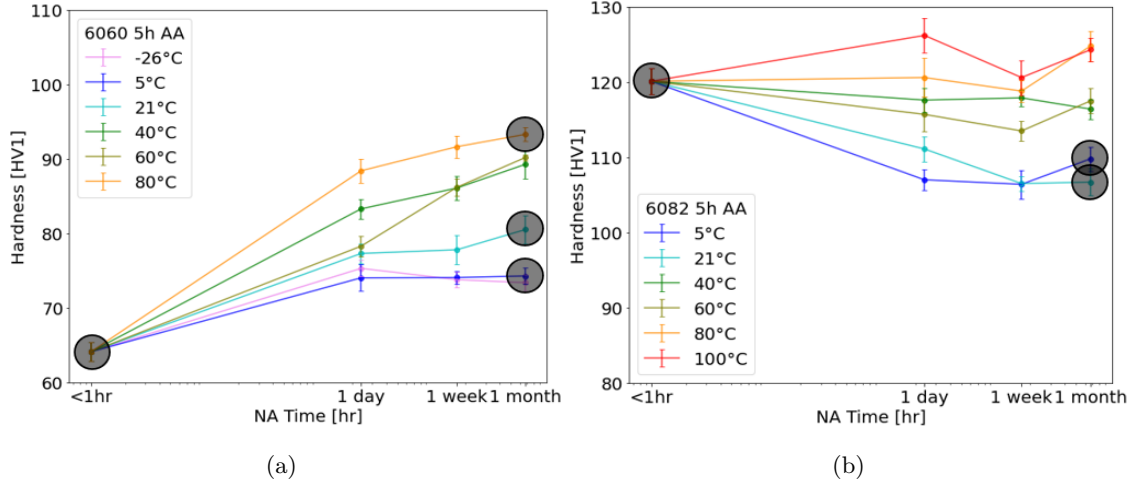
Figure 37: Illustration of which NA conditions are included in the TEM investigation. Only alloys 6060 and 6082 are investigated. The included conditions are marked with a dark circle. These conditions include the direct aged, the 5°C and 21°C from both alloys, as well as the 80°C from 6060. The 80°C from 6082 were supposed to be included however producing suitable TEM-samples proved difficult.

Looking at the 6060 alloy TEM-results a trend appears. Lower HV1 value samples have measured longer precipitates as well as precipitates with a larger cross-section. This means a lower HV1 value seem to correspond in general to larger precipitates. However the number density of precipitates seem to increase with higher HV1 values, such that the higher HV1 conditions have more precipitates per volume, although the precipitates are smaller, both in length and cross-section, than the lower HV1 conditions. There are deviations to this however, the 5°C condition have a higher HV1 value than the direct age, but the direct age have larger ρ and VF. This may be caused by the presence of dislocations in the TEM images. These dislocations form precipitate-free zones which cause the precipitate number density to be lower than its actual value. An example of such a zone are shown in figure 38.

In the 6082 alloy however the 5°C condition have a higher HV1 value than the 21°C along with longer precipitates and a larger cross-section. The lower HV1 21°C condition have formed more
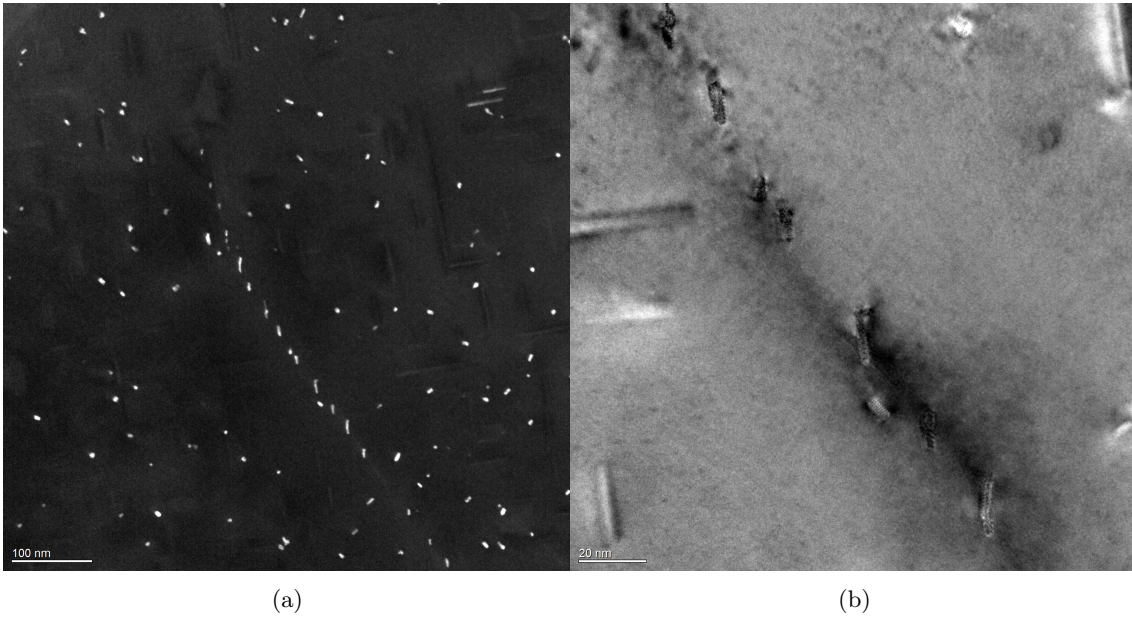
Figure 38: (a) DF image with precipitate-free zone around dislocations. The dislocations are seen as a line of dots in the middle of the image. (b) HRTEM-image of the same dislocations as shown in (a). There are very few precipitates in the vicinity of the dislocations.

precipitates with a higher ρ and VF, such as would be expected with a higher HV1 value, but this is not the case here.

5   Conclusion

For the lean alloys 6005 and 6060, a clear benefit in hardness is seen with the addition of intermediate NA storage before AA. Lower NA temperatures, up to room temperature, reach maximum strength already after 24h NA and stabilize or slowly decrease in strength with prolonged NA. The 6005 shows, similar to lower NA temp., a rapid increase in strength at 80°C NA, reaching peak strength already after 24hr, and the hardness is stable with prolonged NA. In the 6060 alloy, hardness is seen to increase both with higher NA temperatures and prolonged NA. Higher NA temperatures is shown to produce smaller precipitates with higher density, leading to an increase in hardness. This is opposite to Ostwald ripening, where smaller precipitates dissolve, allowing larger precipitates to grow. Higher NA temperatures favours smaller precipitates which have a positive effect on hardening. For the rich 6082 and 6110, NA is found to detrimental for hardening at lower NA temperatures, up to one month NA. This means the clusters forming are bad for hardening, and in the 6082 these precipitates are found to be much larger than the direct aged. NA at 60°C and above is shown to have a similar, or better, strength than the direct aged. Therefore, it can be concluded that increasing NA temperature, as well as prolonging NA, will lead to formation of good clusters for hardening of the alloy. NA are found to lead to a decrease in electrical conductivity, except for the odd room temperature NA. This behaviour is seen in all alloys.

A Appendix Hardness Data

Hardness data taken after artificial ageing at 185°C for 30 min are presented in table 7, 8, 9 and 10. Hardness data taken before AA are presented in table 11, 12, 13 and 14.

A.1 Hardness Data after AA

A.1.1 6005

Table 7: 6005 after AA hardness data. The mean values are presented and the values in () are the standard deviation. 5-10 measurements are taken per condition. All values are in HV1. The direct age condition are presented in the top right corner.

After AA	Direct age: 91.0(2.1)		
NA temp.	1 day	1 week	1 month
-26°C	95.2(1.6)	97.7(1.7)	98.2(1.5)
5°C	98.7(1.6)	98.4(1.6)	97.0(1.4)
21°C	97.6(2.0)	97.8(1.9)	96.2(1.3)
40°C	98.0(1.9)	101.6(1.3)	103.5(1.4)
60°C	99.8(0.7)	102.9(0.5)	104.3(1.3)
80°C	104.8(2.0)	105.3(1.2)	105.2(0.2)
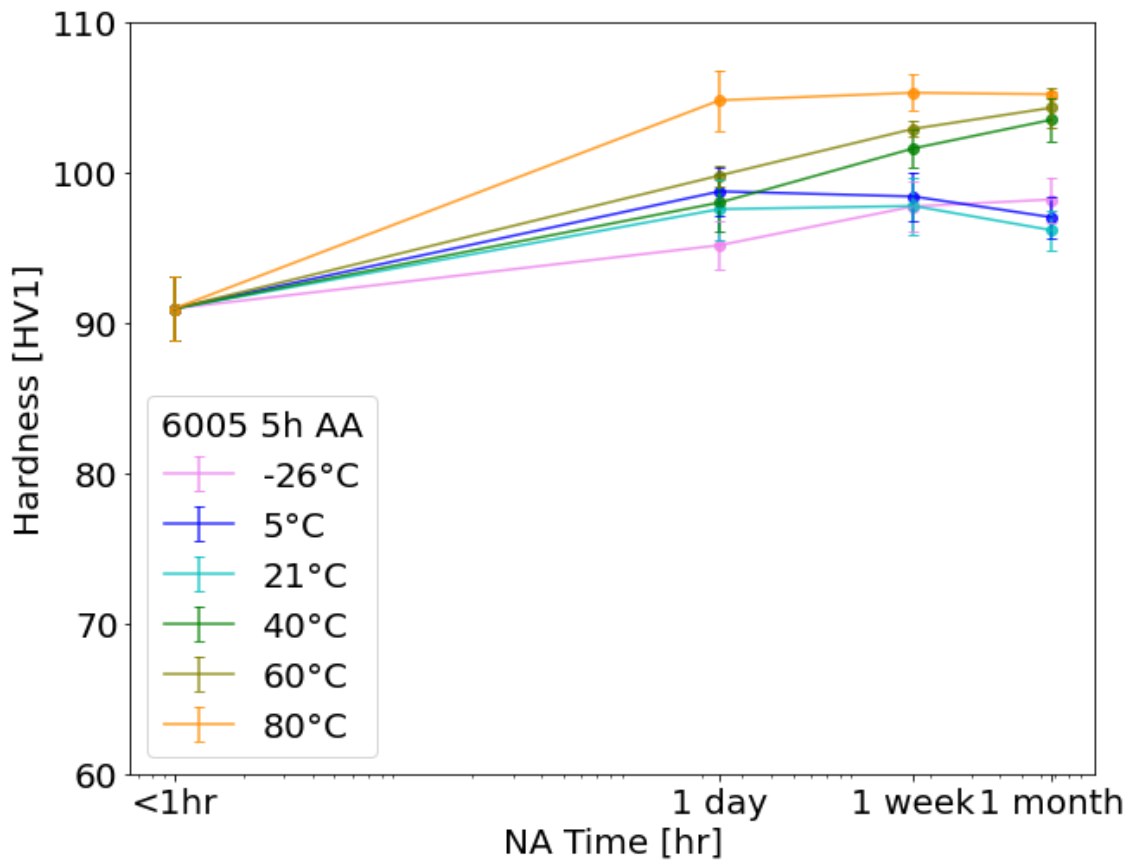
Figure 39: 6005 after AA hardness curve.

A.1.2 6060

Table 8: 6060 after AA hardness data. The mean values are presented and the values in () are the standard deviation. 5-10 measurements are taken per condition. All values are in HV1. The direct age condition are presented in the top right corner.

After AA	Direct age: 64.1(1.3)		
NA temp.	1 day	1 week	1 month
-26°C	75.3(1.1)	73.8(1.0)	73.4(1.1)
5°C	74.0(1.8)	74.1(0.9)	74.3(1.1)
21°C	77.3(1.3)	77.8(2.0)	80.5(1.9)
40°C	83.3(1.3)	86.1(1.6)	89.3(1.9)
60°C	78.3(1.4)	86.2(1.2)	90.2(0.4)
80°C	88.4(1.6)	91.6(1.5)	93.3(0.9)
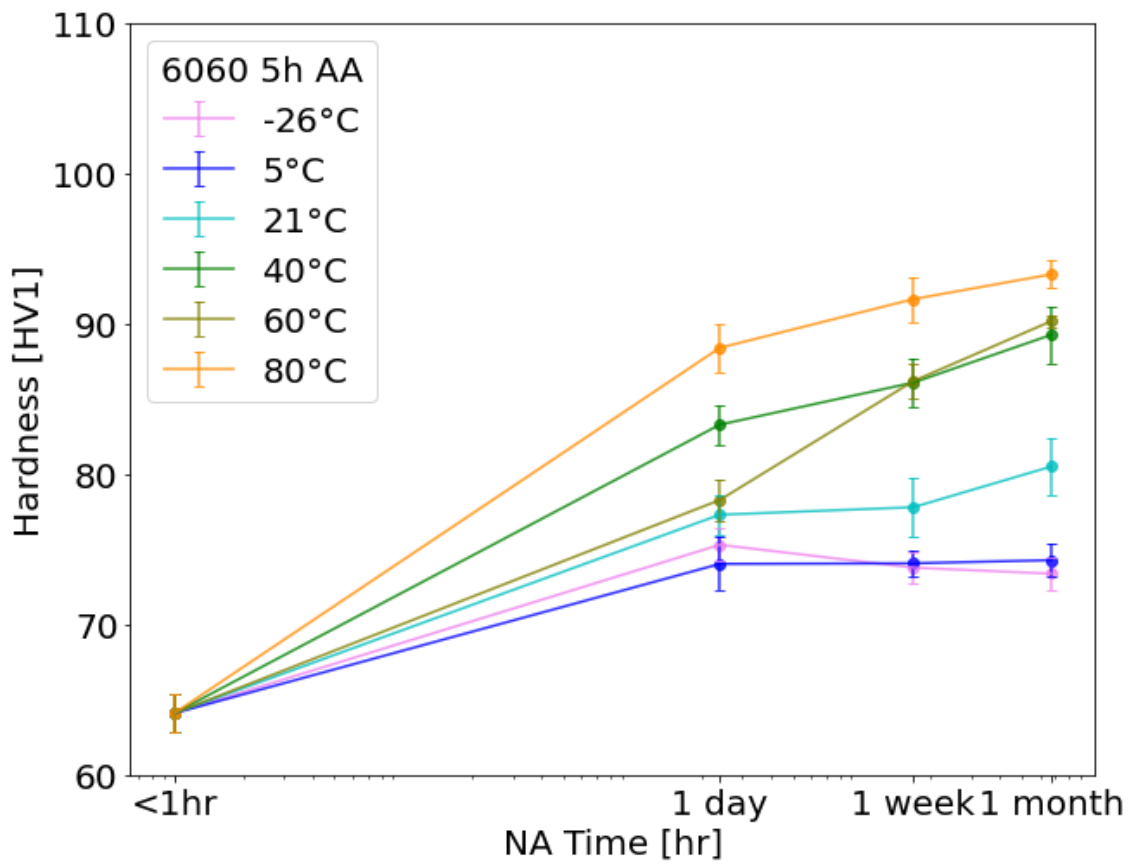
Figure 40: 6060 after AA hardness curve.

A.1.3   6082

Table 9: 6082 after AA hardness data. The mean values are presented and the values in () are the standard deviation. 5-10 measurements are taken per condition. All values are in HV1. The direct age condition are presented in the top right corner.

After AA	Direct age: 120.1(1.7)		
NA temp.	1 day	1 week	1 month
5°C	107.0(1.4)	106.4(1.9)	109.8(1.6)
21°C	111.1(1.7)	106.5(1.0)	106.7(1.8)
40°C	117.6(1.6)	117.9(1.1)	116.4(1.3)
60°C	115.7(2.0)	113.5(1.3)	117.5(1.7)
80°C	120.6(2.6)	118.8(1.4)	124.8(2.0)
100°C	126.2(2.3)	120.6(2.3)	124.3(1.5)
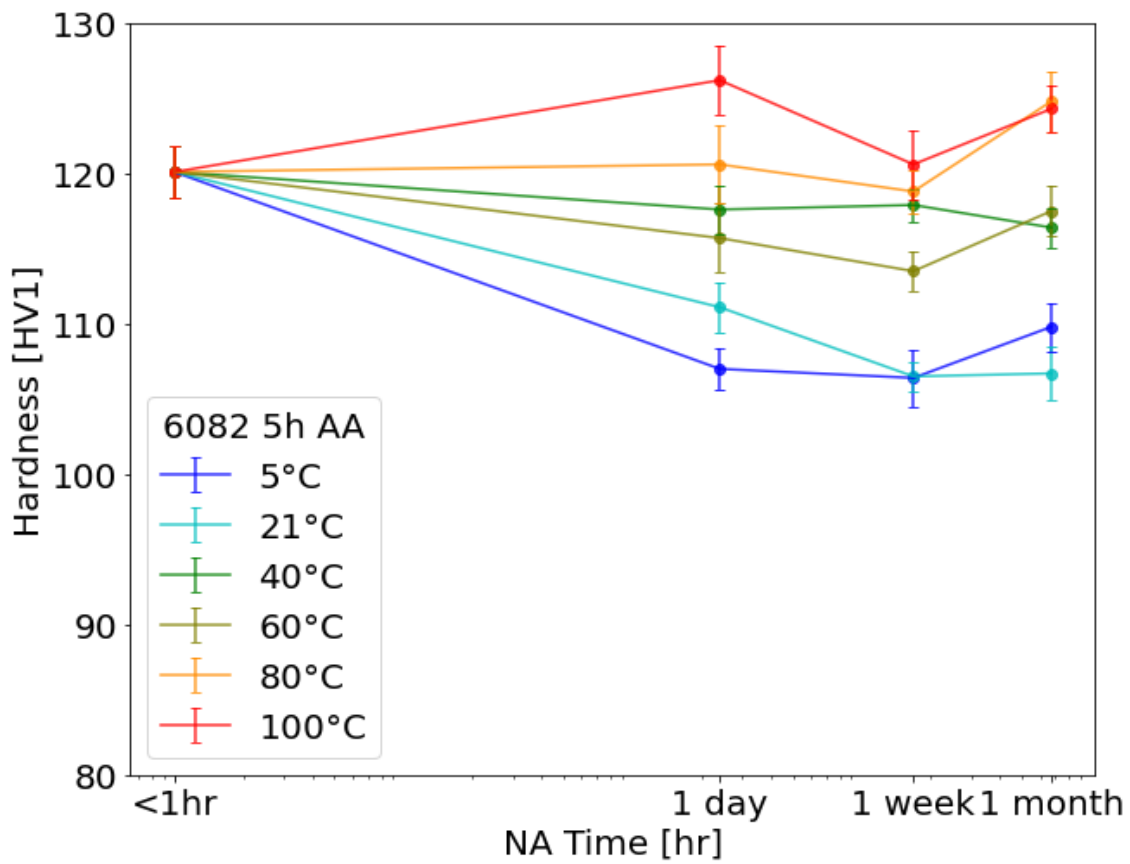
Figure 41: 6082 after AA hardness curve.

A.1.4 6110

Table 10: 6110 after AA hardness data. The mean values are presented and the values in () are the standard deviation. 5-10 measurements are taken per condition. All values are in HV1. The direct age condition are presented in the top right corner.

After AA	Direct age: 121.8(1.7)		
NA temp.	1 day	1 week	1 month
5°C	115.6(1.6)	111.2(1.2)	111.2(1.6)
21°C	111.4(1.8)	112.0(1.6)	112.1(1.5)
40°C	116.9(1.6)	119.7(1.6)	121.4(1.5)
60°C	122.0(0.8)	122.3(2.4)	121.7(1.8)
80°C	122.0(1.9)	124.8(1.6)	122.7(1.5)
100°C	120.4(3.8)	126.1(1.4)	121.8(0.2)
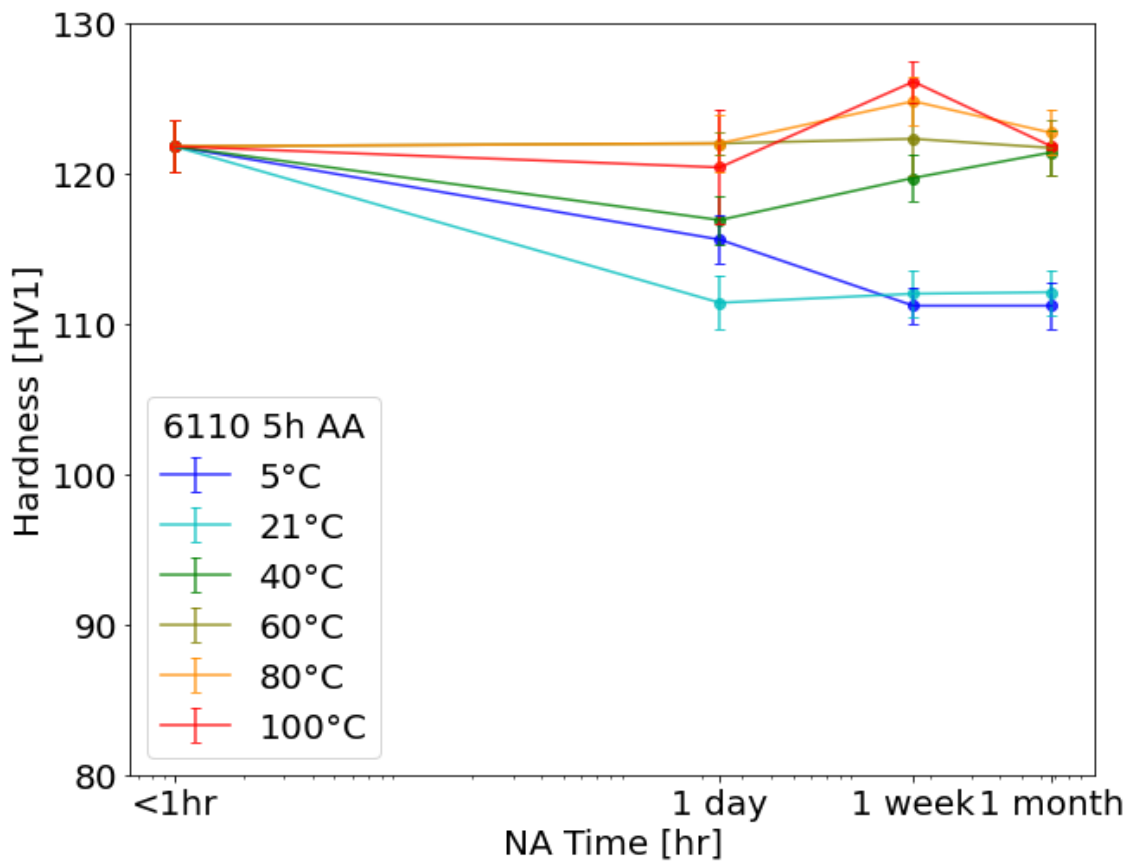
Figure 42: 6110 after AA hardness curve.

A.2 Hardness Data before AA

A.2.1 6005

Table 11: 6005 before AA hardness data. The mean values are presented and the values in () are the standard deviation. 5-10 measurements are taken per condition. All values are in HV1. The direct measurement are presented in the top right corner. The direct measurement are here directly measured after SHT+quench.

Before AA	**Direct:** 41.8(1.2)		
NA temp.	1 day	1 week	1 month
-26°C	39.5(0.7)	41.1(0.7)	44.3(0.5)
5°C	52.6(0.8)	60.2(1.3)	65.2(1.0)
21°C	55.2(0.8)	58.9(1.8)	61.5(1.3)
40°C	53.9(1.2)	59.1(1.1)	61.5(1.6)
60°C	48.2(1.3)	57.8(1.2)	72.6(0.8)
80°C	55.5(1.5)	76.0(0.7)	96.2(2.0)
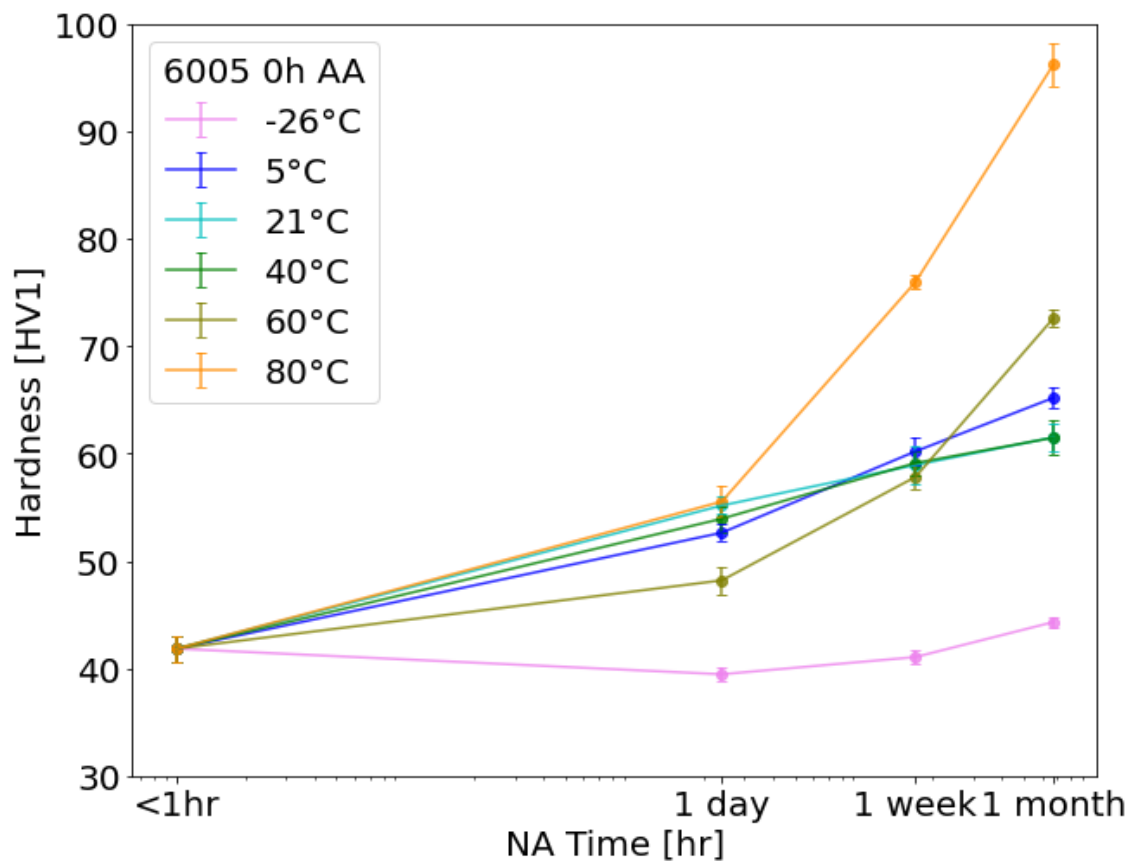
Figure 43: 6005 before AA hardness curve.

A.2.2 6060

Table 12: 6060 before AA hardness data. The mean values are presented and the values in () are the standard deviation. 5-10 measurements are taken per condition. All values are in HV1. The direct measurement are presented in the top right corner. The direct measurement are here directly measured after SHT+quench.

Before AA	Direct: 34.1(0.9)		
NA temp.	1 day	1 week	1 month
-26°C	32.3(0.4)	33.1(0.6)	36.6(0.6)
5°C	42.5(0.7)	47.9(0.9)	53.1(0.9)
21°C	42.5(0.9)	47.1(1.3)	47.8(0.8)
40°C	40.0(0.8)	43.5(0.6)	47.6(0.8)
60°C	36.8(0.5)	39.9(1.0)	57.3(1.4)
80°C	37.0(1.5)	56.0(1.0)	75.9(1.0)
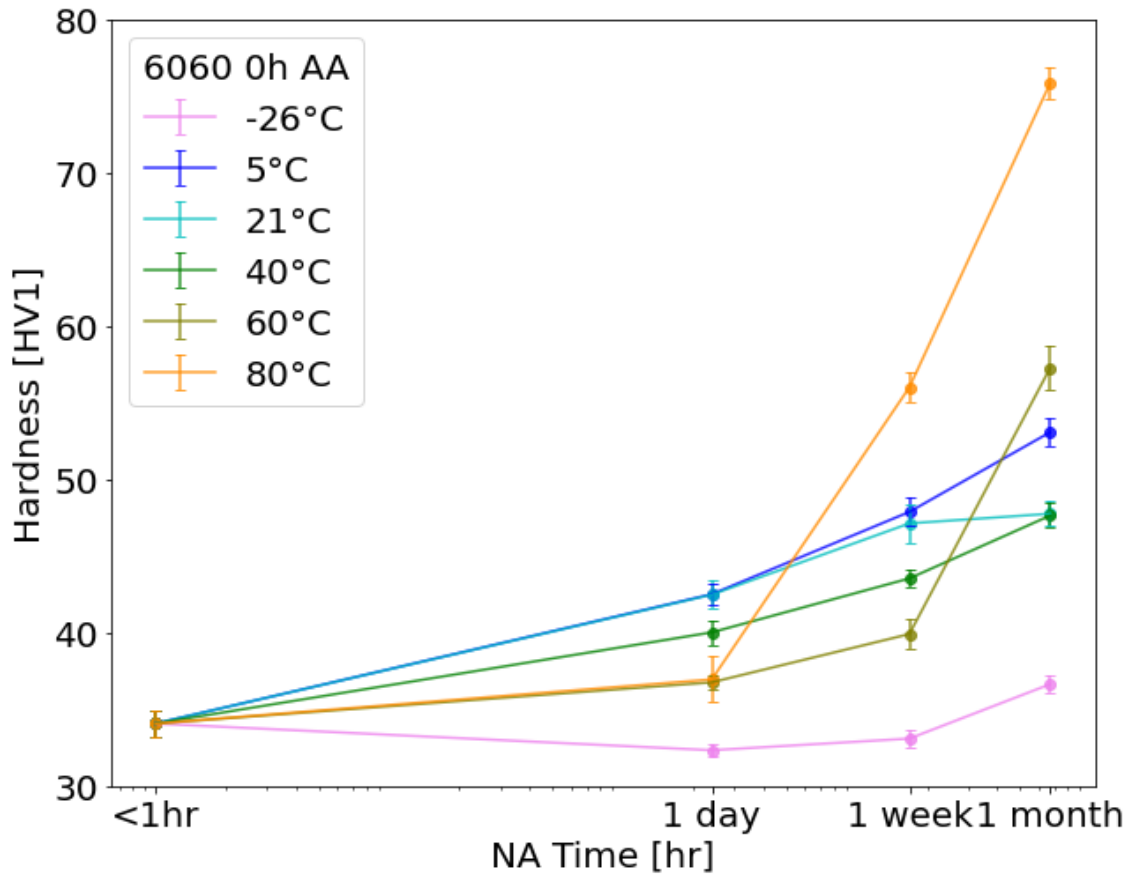
Figure 44: 6060 before AA hardness curve.

Table 13: 6082 before AA hardness data. The mean values are presented and the values in () are the standard deviation. 5-10 measurements are taken per condition. All values are in HV1. The direct measurement are presented in the top right corner. The direct measurement are here directly measured after SHT+quench.

Before AA		Direct: 55.1(1.1)	
NA temp.	1 day	1 week	1 month
5°C	77.5(1.0)	80.3(1.1)	84.9(1.9)
21°C	77.1(0.9)	80.4(0.8)	84.8(1.2)
40°C	76.4(1.4)	80.7(1.6)	81.6(1.1)
60°C	73.4(1.8)	84.5(1.4)	93.6(0.6)
80°C	79.4(1.9)	99.6(1.7)	112.8(1.5)
100°C	95.3(1.1)	128.2(1.3)	126.3(1.3)
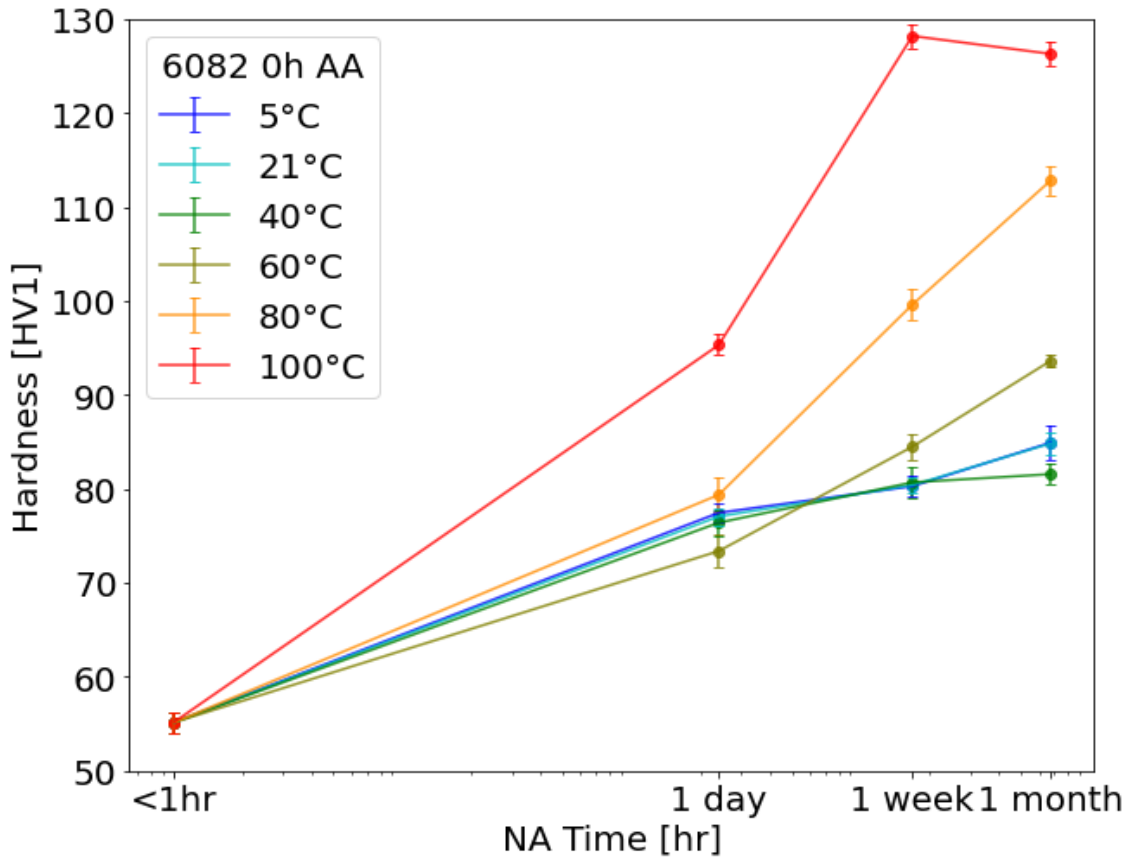
Figure 45: 6082 before AA hardness curve.

A.2.4   6110

Table 14: 6110 before AA hardness data. The mean values are presented and the values in () are the standard deviation. 5-10 measurements are taken per condition. All values are in HV1. The direct measurement are presented in the top right corner. The direct measurement are here directly measured after SHT+quench.

Before AA		Direct: 55.9(0.8)	
NA temp.	1 day	1 week	1 month
5°C	68.8(1.1)	77.3(1.4)	85.6(1.2)
21°C	73.9(1.2)	81.0(1.8)	83.2(1.0)
40°C	78.3(1.5)	85.9(1.2)	87.7(1.6)
60°C	75.2(1.0)	82.5(1.7)	91.5(1.5)
80°C	80.9(1.7)	99.4(1.9)	114.4(1.0)
100°C	99.0(1.9)	121.5(1.2)	124.1(1.4)
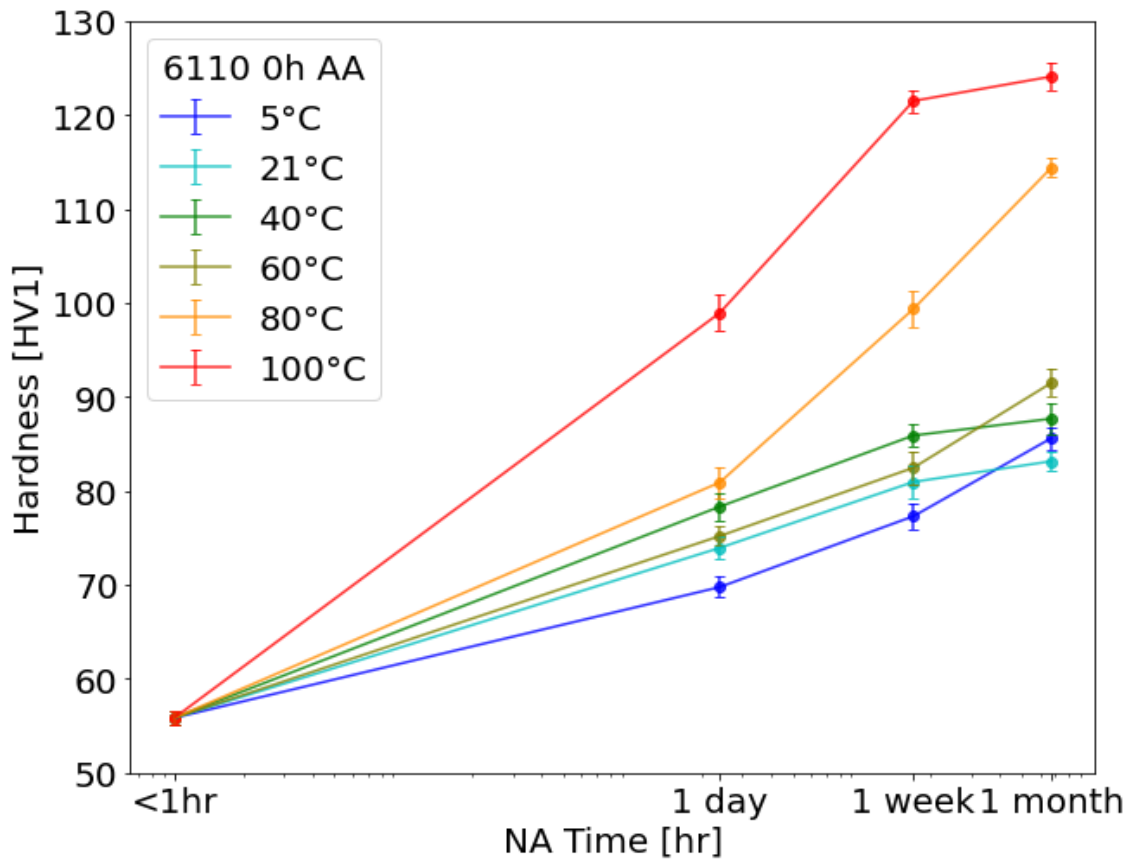
Figure 46: 6110 before AA hardness curve.

B   Appendix Electrical Conductivity Data

Electrical Conductivity data taken after artificial ageing at 185°C for 30 min are presented in table 15, 16, 17 and 18. Conductivity data taken before AA are presented in table 19, 20, 21 and 22.

B.1   Electrical Conductivity Data after AA

B.1.1   6005

Table 15: 6005 after AA conductivity. The mean values are presented and the values in () are the standard deviation. 10 measurements are taken per condition. All values are in $\mathrm{MS\,m^{-1}}$. The direct age condition are presented in the top right corner.

After AA	Direct age: 29.70(0.03)		
NA temp.	1 day	1 week	1 month
-26°C	29.26(0.02)	29.28(0.04)	29.28(0.03)
5°C	28.84(0.08)	28.95(0.04)	28.87(0.07)
21°C	29.60(0.04)	29.41(0.05)	29.56(0.04)
40°C	28.70(0.06)	28.53(0.02)	28.12(0.07)
60°C	28.96(0.05)	28.63(0.09)	28.21(0.02)
80°C	28.12(0.06)	27.99(0.05)	28.04(0.05)
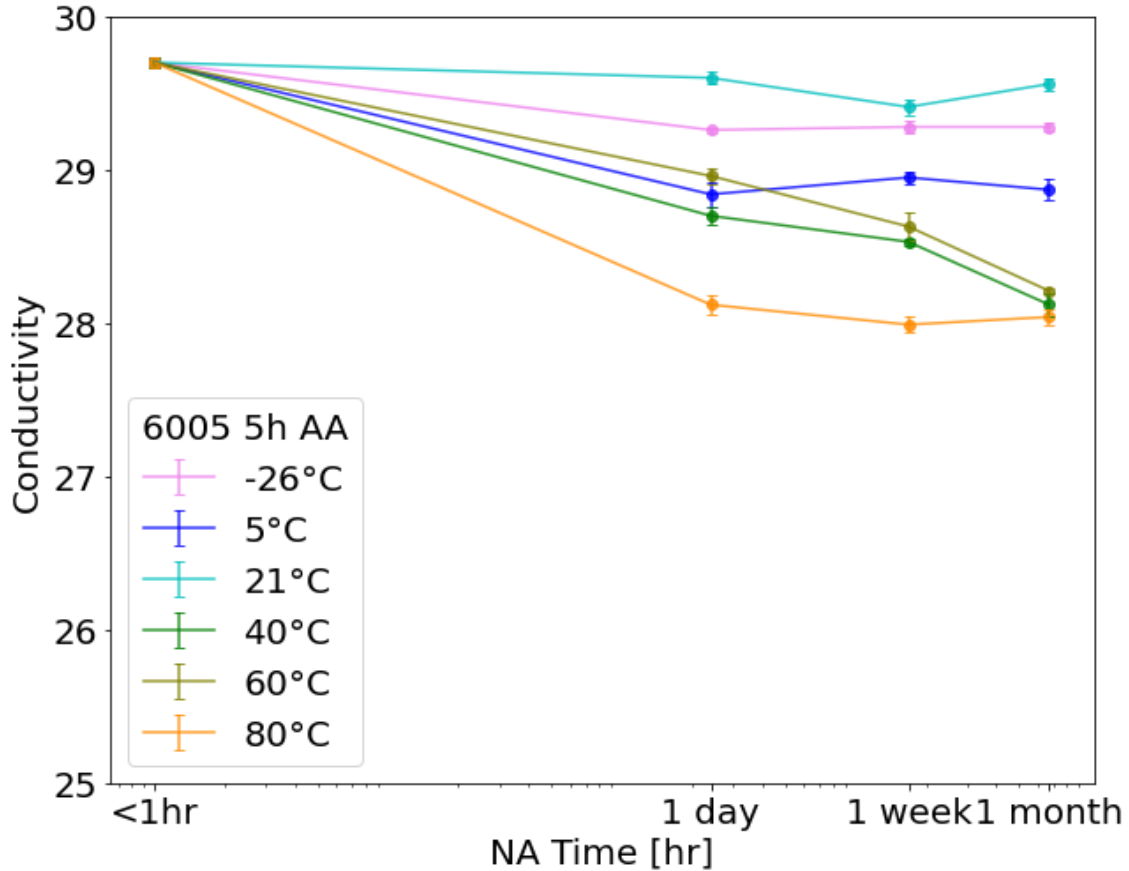
Figure 47: 6005 after AA conductivity curve.

B.1.2 6060

Table 16: 6060 after AA conductivity. The mean values are presented and the values in () are the standard deviation. 10 measurements are taken per condition. All values are in $\mathrm{MS\,m^{-1}}$. The direct age condition are presented in the top right corner.

After AA	Direct age: 31.93(0.09)		
NA temp.	1 day	1 week	1 month
-26°C	32.11(0.03)	32.31(0.03)	32.33(0.07)
5°C	30.97(0.11)	31.15(0.06)	30.79(0.06)
21°C	31.60(0.07)	31.70(0.08)	31.74(0.12)
40°C	31.64(0.03)	31.43(0.06)	30.51(0.03)
60°C	31.58(0.10)	31.53(0.10)	31.12(0.07)
80°C	31.75(0.10)	31.16(0.07)	30.93(0.04)
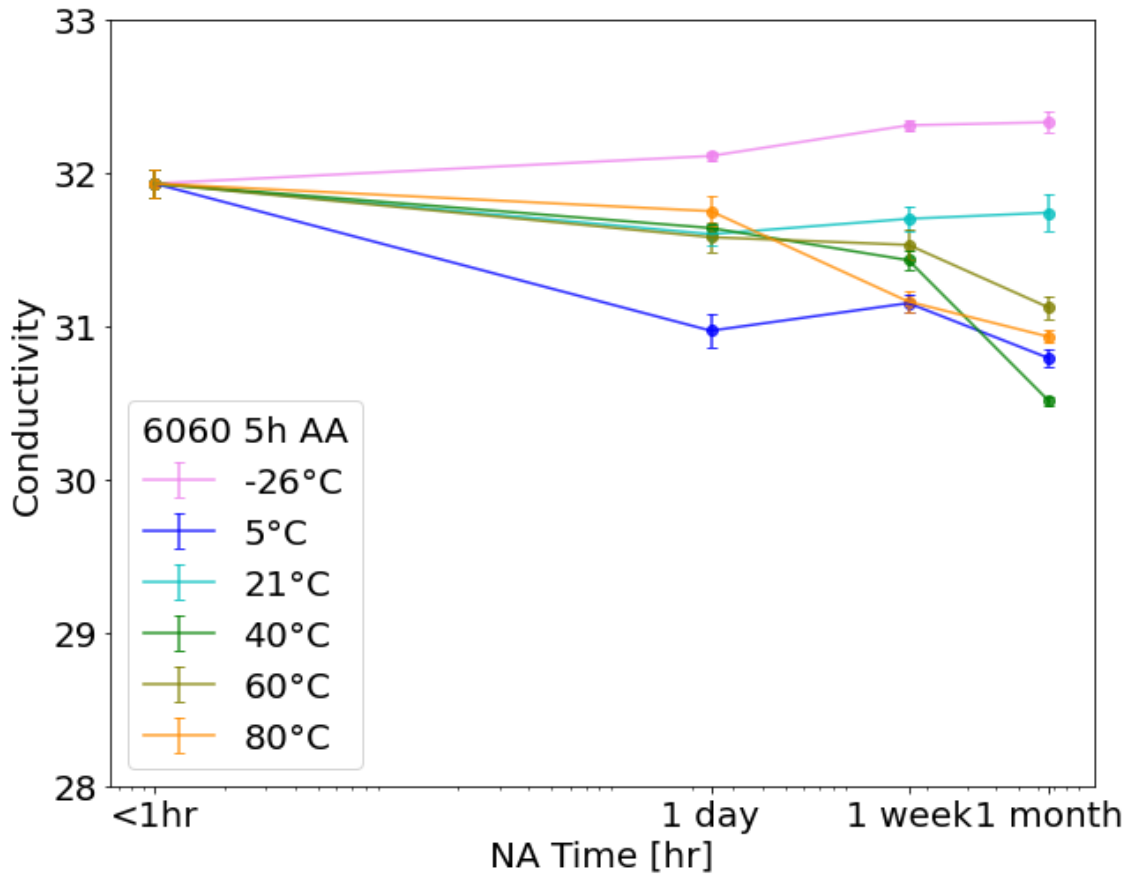
Figure 48: 6060 after AA conductivity curve.

B.1.3   6082

Table 17: 6082 after AA conductivity. The mean values are presented and the values in () are the standard deviation. 10 measurements are taken per condition. All values are in $MS\,m^{-1}$. The direct age condition are presented in the top right corner.

After AA	Direct age: 26.80(0.06)		
NA temp.	1 day	1 week	1 month
5°C	26.00(0.05)	26.19(0.08)	25.57(0.05)
21°C	26.93(0.05)	27.65(0.04)	27.67(0.06)
40°C	25.91(0.06)	25.69(0.10)	25.30(0.04)
60°C	26.13(0.06)	25.83(0.10)	25.41(0.05)
80°C	25.22(0.06)	25.19(0.03)	25.25(0.04)
100°C	25.60(0.04)	25.57(0.02)	25.35(0.05)
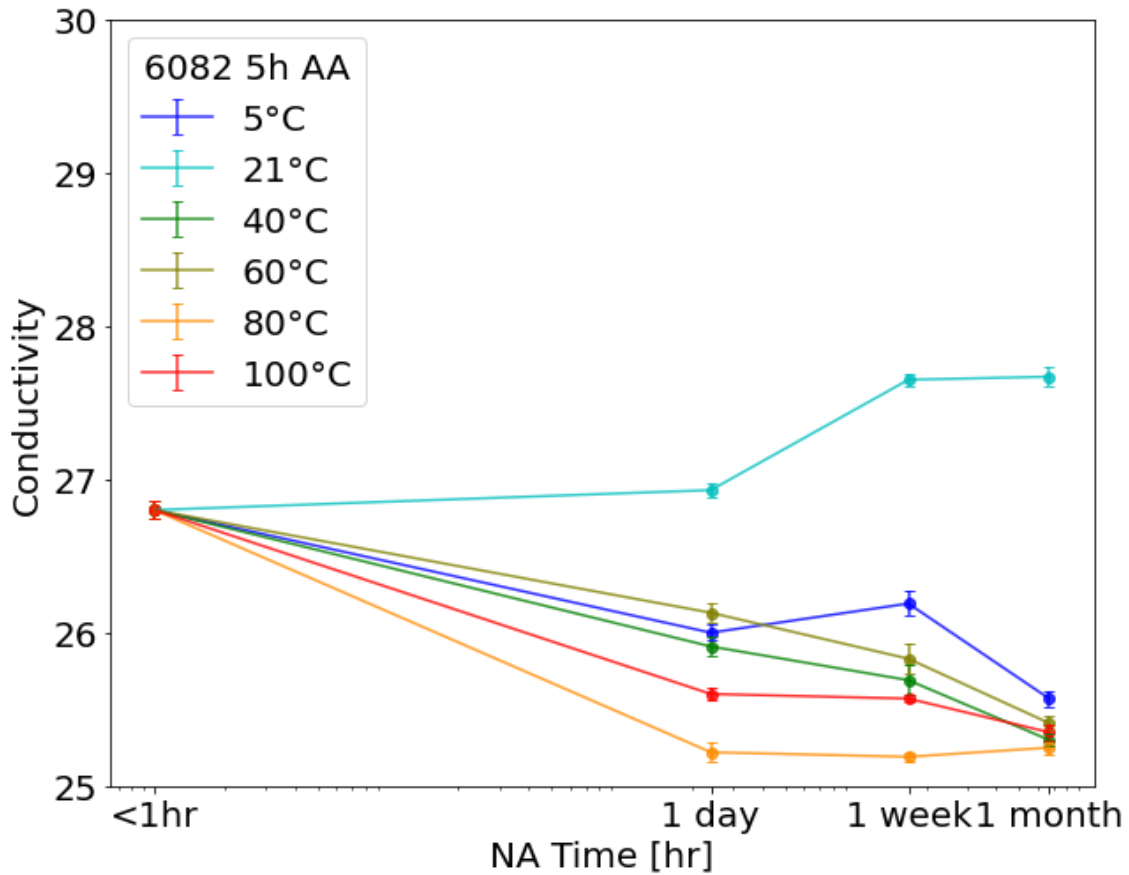
Figure 49: 6082 after AA conductivity curve.

B.1.4   6110

Table 18: 6110 after AA conductivity. The mean values are presented and the values in () are the standard deviation. 10 measurements are taken per condition. All values are in $\mathrm{MS\,m^{-1}}$. The direct age condition are presented in the top right corner.

After AA	Direct age: 26.16(0.05)		
NA temp.	1 day	1 week	1 month
5°C	25.03(0.05)	24.89(0.04)	25.07(0.10)
21°C	26.17(0.04)	26.06(0.04)	26.40(0.05)
40°C	25.08(0.03)	24.80(0.03)	24.52(0.05)
60°C	25.42(0.04)	25.10(0.10)	24.58(0.08)
80°C	24.22(0.05)	24.22(0.10)	23.99(0.03)
100°C	24.63(0.06)	24.48(0.02)	24.40(0.03)
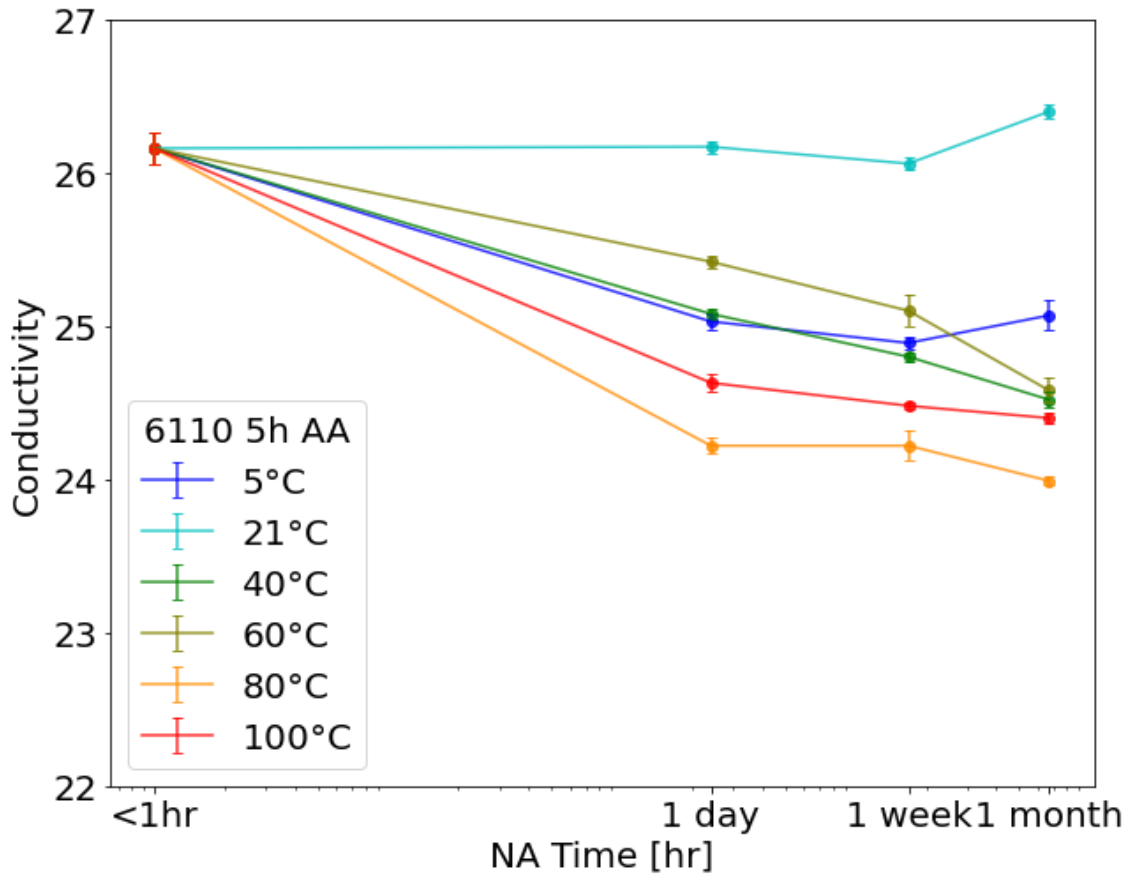
Figure 50: 6110 after AA conductivity curve.

B.2 Electrical Conductivity Data before AA

B.2.1 6005

Table 19: 6005 before AA conductivity data. The mean values are presented and the values in () are the standard deviation. 5-10 measurements are taken per condition. All values are in $\mathrm{MS\,m^{-1}}$. The direct measurement are presented in the top right corner. The direct measurement are here directly measured after SHT+quench.

Before AA	Direct: 27.73(0.07)		
NA temp.	1 day	1 week	1 month
-26°C	27.70(0.04)	27.80(0.03)	27.37(0.02)
5°C	26.74(0.01)	26.46(0.05)	26.50(0.03)
21°C	27.35(0.02)	27.27(0.02)	27.18(0.05)
40°C	27.21(0.03)	26.78(0.05)	26.48(0.06)
60°C	27.72(0.02)	27.33(0.05)	27.11(0.01)
80°C	27.12(0.07)	-	27.47(0.05)
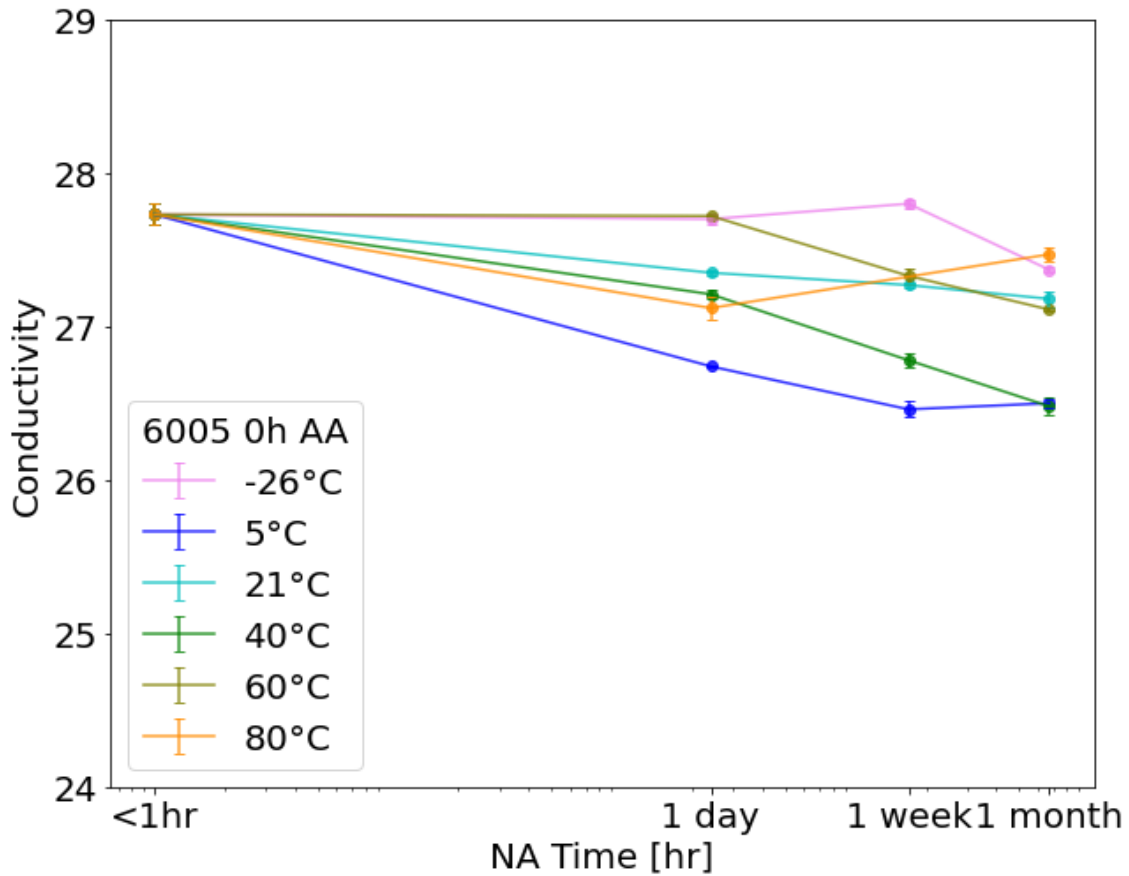
Figure 51: 6005 before AA conductivity curve.

B.2.2 6060

Table 20: 6060 before AA conductivity data. The mean values are presented and the values in () are the standard deviation. 5-10 measurements are taken per condition. All values are in $MS\,m^{-1}$. The direct measurement are presented in the top right corner. The direct measurement are here directly measured after SHT+quench.

Before AA	Direct: 30.46(0.06)		
NA temp.	1 day	1 week	1 month
-26°C	30.46(0.06)	30.63(0.05)	30.22(0.05)
5°C	29.57(0.06)	29.51(0.10)	29.28(0.04)
21°C	29.98(0.06)	29.82(0.06)	29.80(0.05)
40°C	29.93(0.03)	29.78(0.06)	29.41(0.04)
60°C	29.93(0.05)	29.89(0.09)	30.10(0.05)
80°C	29.99(0.02)	29.84(0.03)	30.27(0.02)
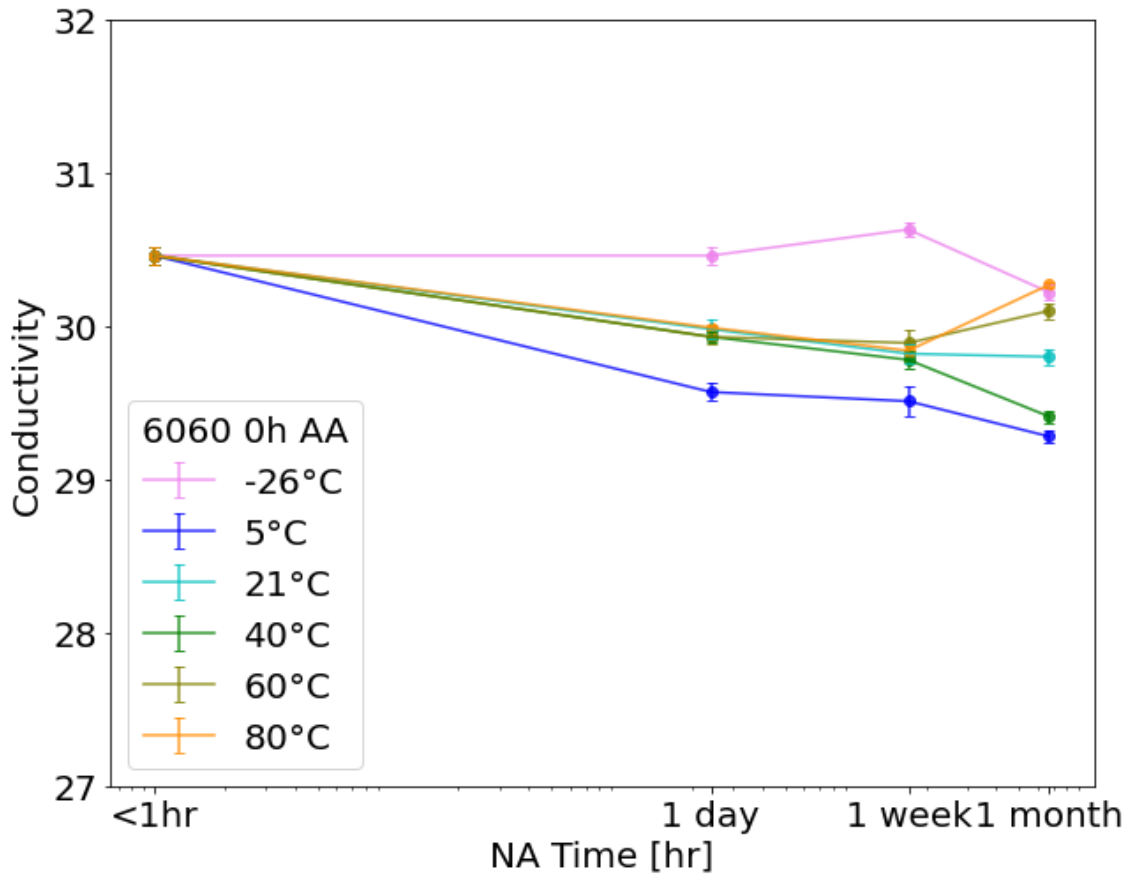
Figure 52: 6060 before AA conductivity curve.

B.2.3 6082

Table 21: 6082 before AA conductivity data. The mean values are presented and the values in ()
are the standard deviation. 5-10 measurements are taken per condition. All values are in $\mathrm{MS\,m^{-1}}$.
The direct measurement are presented in the top right corner. The direct measurement are here
directly measured after SHT+quench.

Before AA	Direct: 25.63(0.03)		
NA temp.	1 day	1 week	1 month
5°C	23.54(0.04)	23.22(0.04)	23.28(0.03)
21°C	24.08(0.02)	24.12(0.03)	24.15(0.03)
40°C	23.75(0.05)	23.52(0.03)	23.46(0.04)
60°C	24.10(0.04)	24.07(0.03)	24.07(0.04)
80°C	24.16(0.04)	23.88(0.04)	24.17(0.03)
100°C	24.49(0.04)	24.58(0.04)	24.69(0.04)
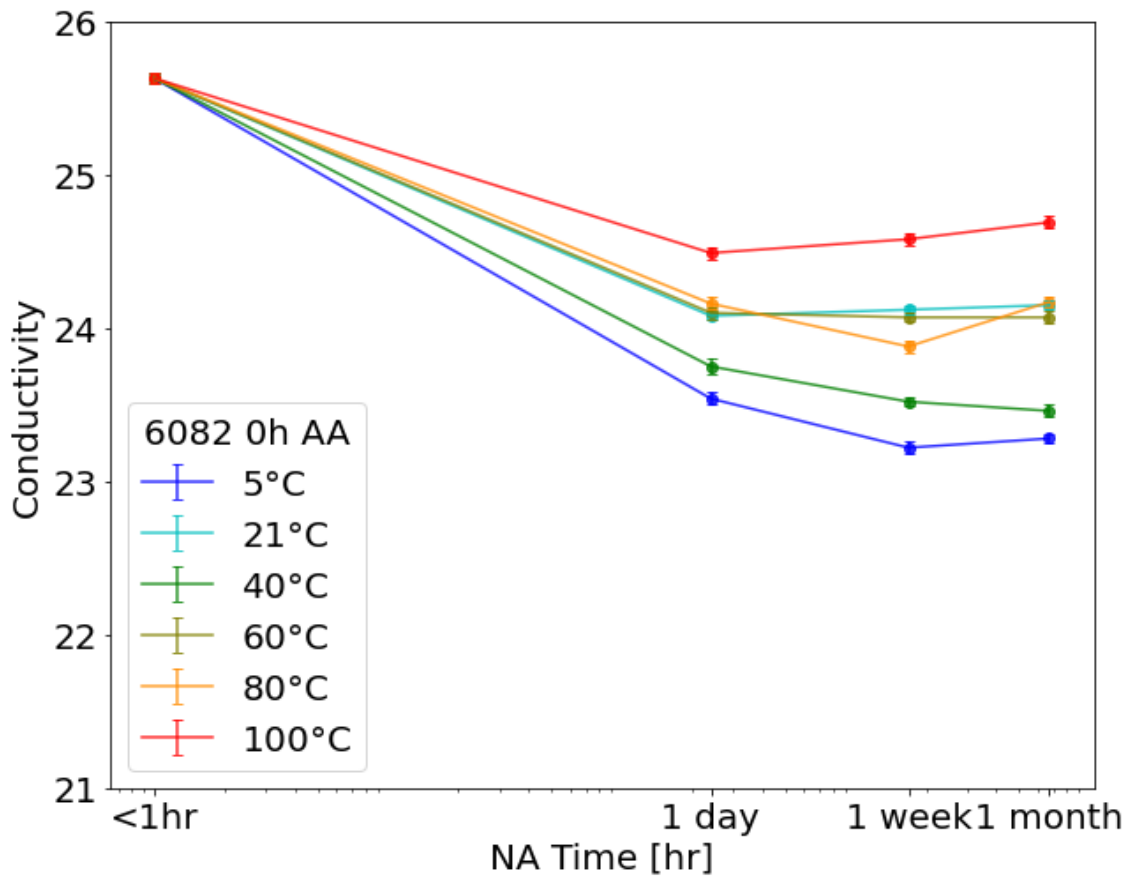
Figure 53: 6082 before AA conductivity curve.

B.2.4   6110

Table 22: 6110 before AA conductivity data. The mean values are presented and the values in () are the standard deviation. 5-10 measurements are taken per condition. All values are in $MS\,m^{-1}$. The direct measurement are presented in the top right corner. The direct measurement are here directly measured after SHT+quench.

Before AA	Direct: 24.36(0.04)		
NA temp.	1 day	1 week	1 month
5°C	22.85(0.03)	22.62(0.03)	22.56(0.03)
21°C	23.66(0.03)	23.57(0.04)	23.46(0.04)
40°C	23.15(0.06)	22.76(0.03)	22.60(0.02)
60°C	24.17(0.06)	23.46(0.04)	23.16(0.03)
80°C	23.29(0.03)	-	23.28(0.01)
100°C	23.55(0.05)	23.87(0.03)	23.85(0.05)
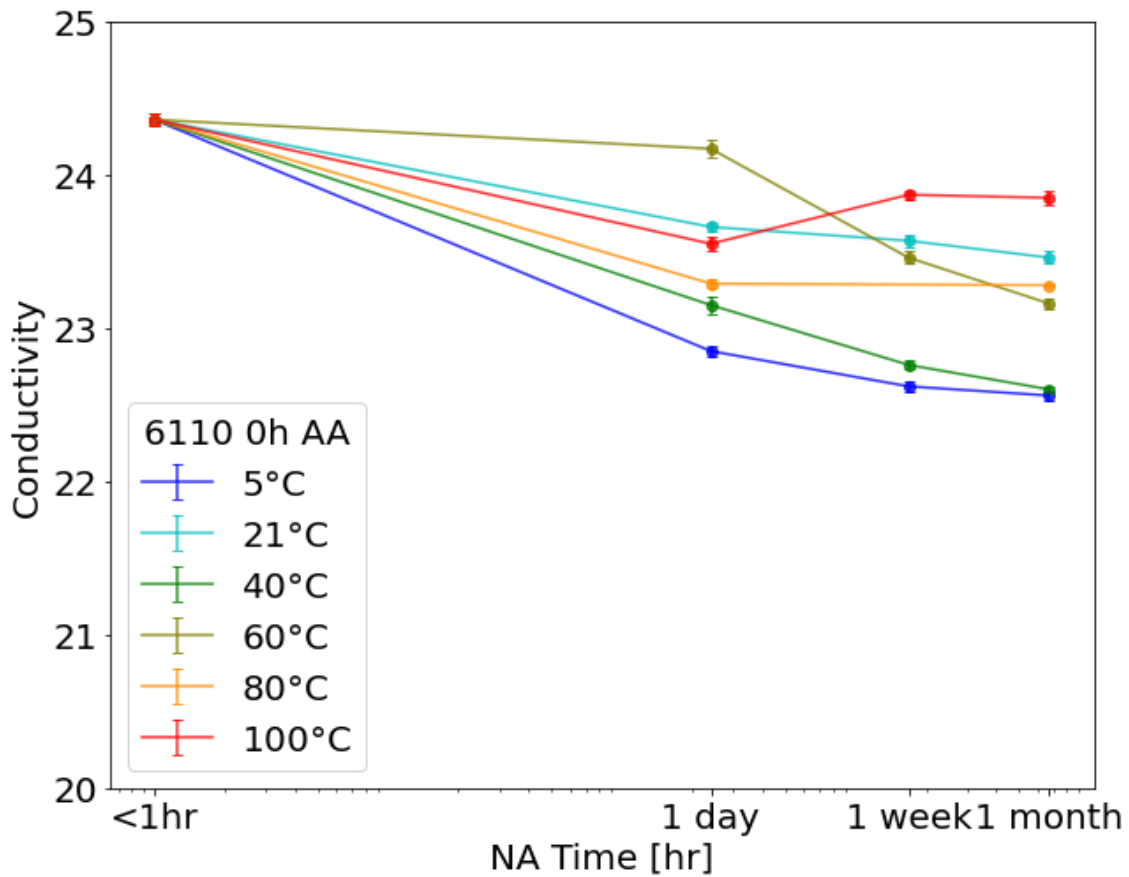
Figure 54: 6110 before AA conductivity curve.

C Appendix Extended Precipitate Statistics

C.1 Extended Tables

Extended tables of precipitate statistics are shown in table 23 for the 6060 conditions and table 24 for the 6082 conditions. The tables include several images per condition. A cell with the symbol $-\|-$ signifies it has the same value as the above cell. All information to calculate the precipitate statistics are included. The tables include the area A, the number of precipitates counted in the DF image N, the tilt (X, Y), the measured thickness t, the measured average precipitate length $< l >$, the precipitate number density ρ, the measured average cross-sectional area $< CS >$ and the calculated volume fraction of precipitates VF.

Table 23: Extended precipitate statistics from 6060 conditions. The direct aged, 5°C, 21°C and 80°C are included. Values in $< l >$ cells inside brackets () are the standard deviation.

A [nm^2]	N	$(X,Y)[°]$	t [nm]	$< l >$ [nm]	$\frac{\Delta <l>}{<l>}$	ρ [nm^{-3}]	$\frac{\Delta \rho}{\rho}$	$< CS >$ [nm^2]	VF [%]
6060									
Direct Aged									
500697.8	187	(-5.0,-5.6)	107.29	37.91 (22.77)	0.033	$7.72 \cdot 10^{-6}$	0.106	24.31 ±0.81	0.71
$-\|-$	123	(-7.5,-4.8)	64.75	35.20 (26.76)	0.060	$7.37 \cdot 10^{-6}$	0.110	$-\|-$	0.63
$-\|-$	244	(-7.1,-5.6)	105.61	31.88 (14.87)	0.034	$1.06 \cdot 10^{-5}$	0.105	$-\|-$	0.82
$-\|-$	118	(-5.5,-5.8)	81.57	40.51 (22.59)	0.049	$5.79 \cdot 10^{-6}$	0.109	$-\|-$	0.57
5°C									
500697.8	64	(-2.5,3.1)	38.6	30.07 (21.96)	0.038	$5.58 \cdot 10^{-6}$	0.113	17.62 ±1.92	0.30
$-\|-$	70	$-\|-$	31.4	$-\|-$	0.047	$6.82 \cdot 10^{-6}$	0.116	$-\|-$	0.36
$-\|-$	111	$-\|-$	58.9	$-\|-$	0.025	$7.48 \cdot 10^{-6}$	0.108	$-\|-$	0.40
21°C									
500697.8	290	(5.0,-1.0)	45.6	26.38 (15.03)	0.036	$2.43 \cdot 10^{-5}$	0.109	14.66 ±2.94	0.93
$-\|-$	368	$-\|-$	69.8	$-\|-$	0.024	$2.28 \cdot 10^{-5}$	0.106	$-\|-$	0.90
$-\|-$	283	$-\|-$	42.5	$-\|-$	0.038	$2.50 \cdot 10^{-5}$	0.110	$-\|-$	0.93
$-\|-$	346	$-\|-$	61.3	$-\|-$	0.026	$2.38 \cdot 10^{-5}$	0.107	$-\|-$	0.89
$-\|-$	311	$-\|-$	84.7	$-\|-$	0.020	$1.66 \cdot 10^{-5}$	0.105	$-\|-$	0.67
80°C									
500697.8	954	(-3.2,0.7)	64.03	13.25 (10.12)	0.008	$7.40 \cdot 10^{-5}$	0.104	7.11 ±0.26	0.70

Table 24: Extended precipitate statistics from 6082 conditions. The direct aged, 5°C and 21°C are included. Values in $< l >$ cells inside brackets () are the standard deviation.

A [nm^2]	N	$(X,Y)[°]$	t [nm]	$< l >$ [nm]	$\frac{\Delta <l>}{<l>}$	ρ [nm^{-3}]	$\frac{\Delta \rho}{\rho}$	$< CS >$ [nm^2]	VF [%]
6082									
Direct Aged									
116758.9	395	(-0.5,-9.5)	82.48	17.66 (12.65)	0.025	$1.01 \cdot 10^{-4}$	0.000	9.96 ±0.33	1.78
$-\|-$	392	(-1.3,-9.1)	78.53	16.35 (8.82)	0.024	$1.06 \cdot 10^{-4}$	0.000	$-\|-$	1.73
5°C									
500697.8	172	(0.7,-3.4)	46.02	48.09 (38.85)	0.045	$1.10 \cdot 10^{-5}$	0.117	23.08 ±1.81	1.22
$-\|-$	281	$-\|-$	41.04	$-\|-$	0.050	$1.89 \cdot 10^{-5}$	0.119	$-\|-$	2.10
$-\|-$	163	$-\|-$	51.84	$-\|-$	0.040	$9.77 \cdot 10^{-6}$	0.115	$-\|-$	1.08
21°C									
500697.8	443	(2.8,-0.2)	48.10	38.90 (22.92)	0.027	$3.12 \cdot 10^{-5}$	0.112	13.96 ±0.61	1.61
$-\|-$	491	$-\|-$	46.19	$-\|-$	0.037	$3.38 \cdot 10^{-5}$	0.114	$-\|-$	1.93

C.2 Histograms Precipitate Length and Cross-Section

Histograms are shown for precipitate length data and precipitate cross-section data for the investigated conditions. Figure 55, 56, 57 and 58 shows the precipitate length and cross-section distribution for the 6060 conditions. Figure 59, 60 and 61 shows the precipitate length and cross-section distribution for the 6082 conditions.
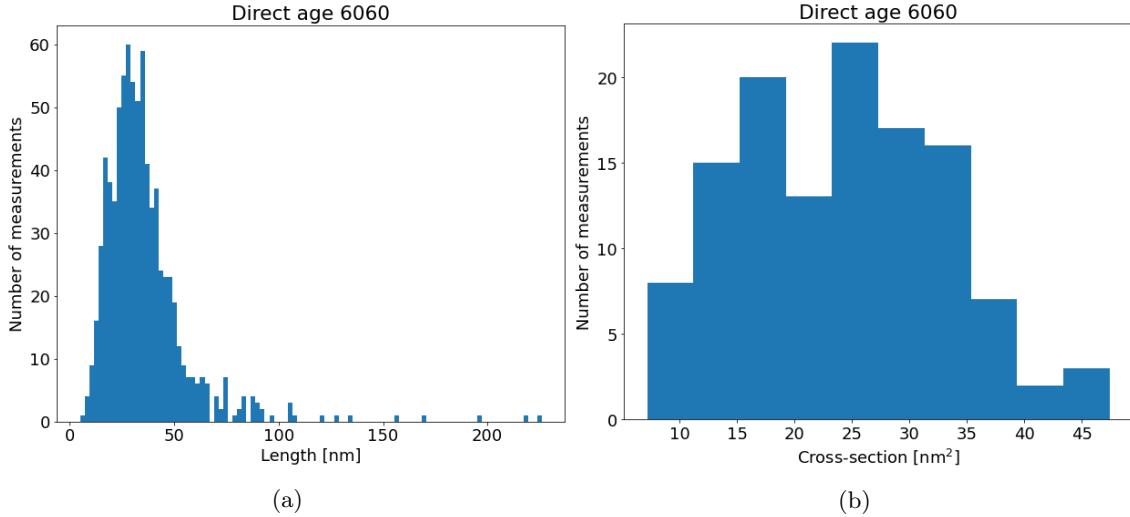
Figure 55: (a) Precipitate length distribution for the 6060 direct aged condition. Average length $< l >= 35.69$ nm with standard deviation $\sigma = 21.32$ nm. (b) Precipitate cross-section distribution for the 6060 direct aged condition. Average cross-section with standard error $< CS >= 24.31(81)$ nm^2.
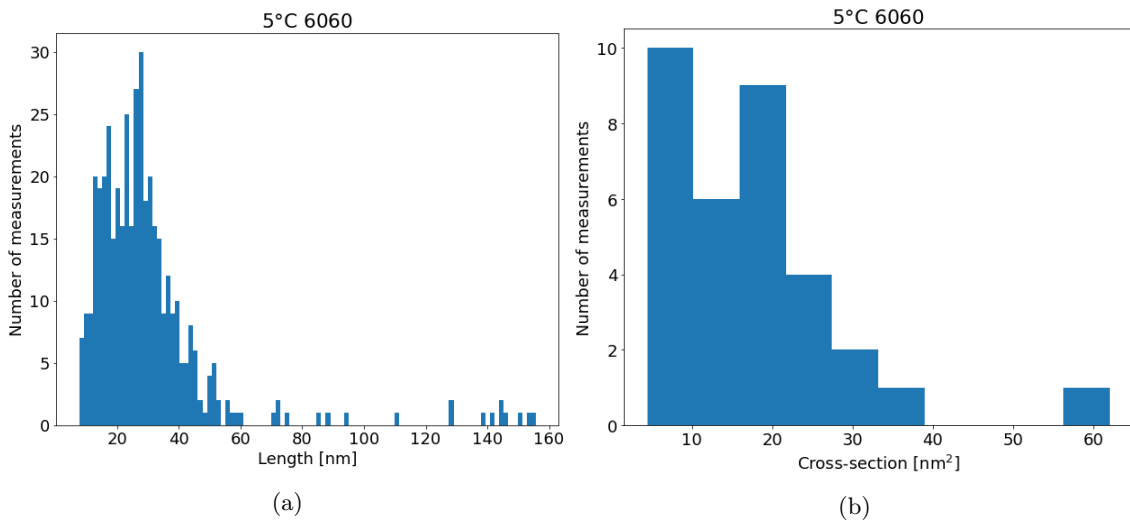
Figure 56: (a) Precipitate length distribution for the 6060 NA 5°C 1 month condition. Average length $< l >= 30.07$ nm with standard deviation $\sigma = 21.96$ nm. (b) Precipitate cross-section distribution for the 6060 NA 5°C 1 month condition. Average cross-section with standard error $< CS >= 17.62(192)$ nm^2
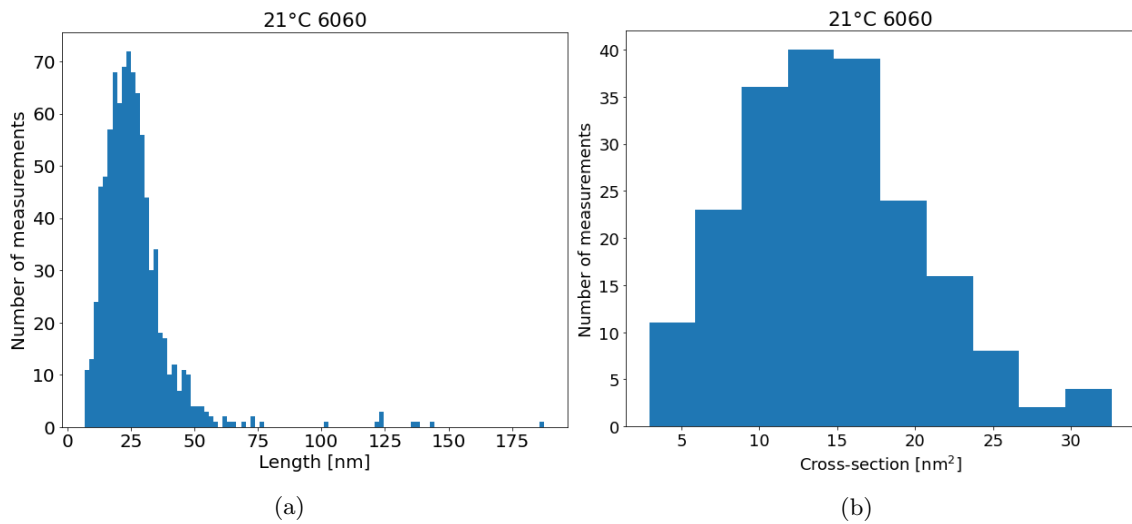
Figure 57: (a) Precipitate length distribution for the 6060 NA 21°C 1 month condition. Average length $< l > = 26.38$ nm with standard deviation $\sigma = 15.03$ nm. (b) Precipitate cross-section distribution for the 6060 NA 21°C 1 month condition. Average cross-section with standard error $< CS > = 14.66(294)$ nm^2
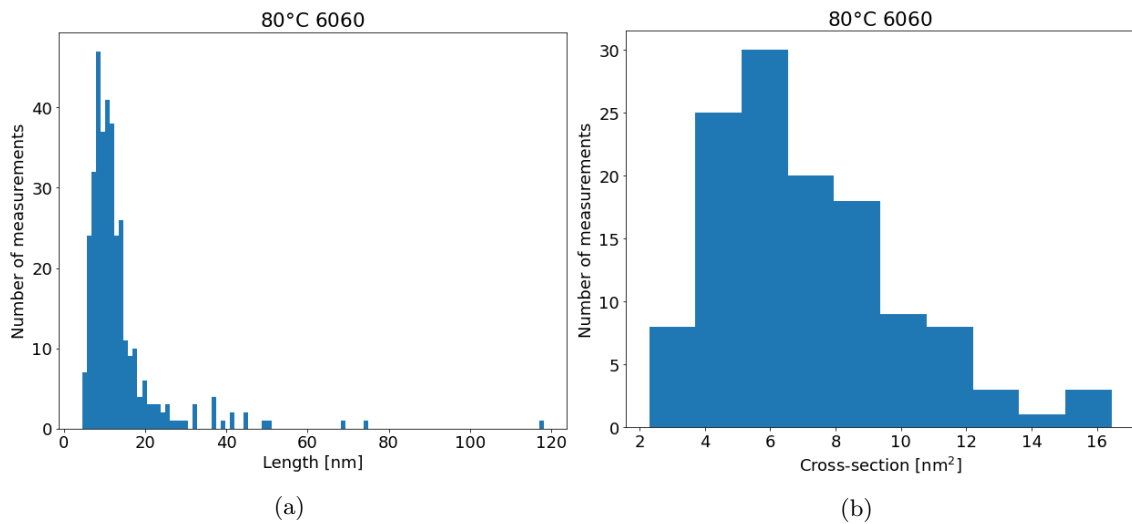
Figure 58: (a) Precipitate length distribution for the 6060 NA 80°C 1 month condition. Average length $< l > = 13.25$ nm with standard deviation $\sigma = 10.12$ nm. (b) Precipitate cross-section distribution for the 6060 NA 80°C 1 month condition. Average cross-section with standard error $< CS > = 7.11(26)$ nm^2
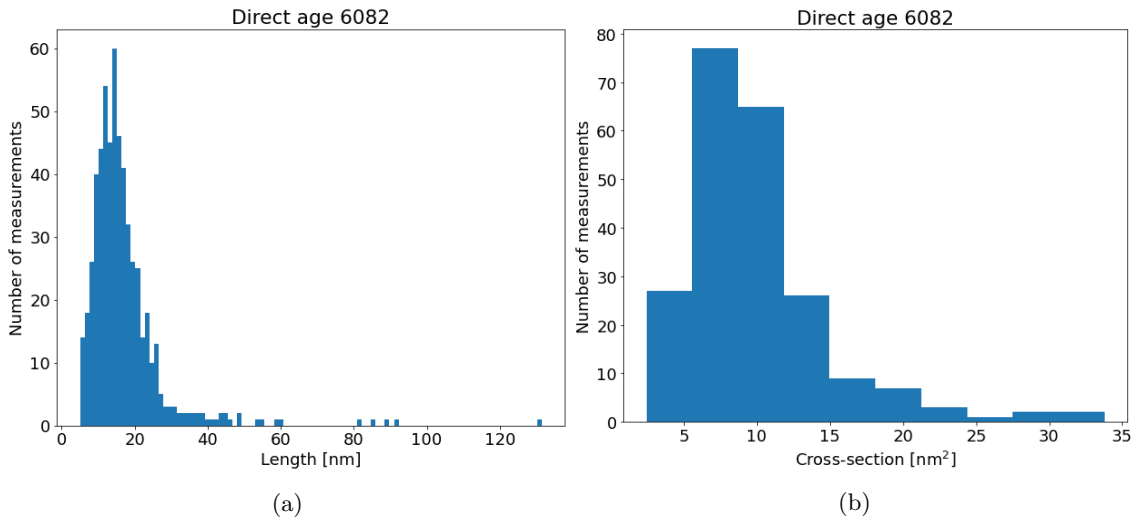
Figure 59: (a) Precipitate length distribution for the 6082 direct aged condition. Average length $< l > = 17.01$ nm with standard deviation $\sigma = 10.91$ nm. (b) Precipitate cross-section distribution for the 6082 direct aged condition. Average cross-section with standard error $< CS > = 9.96(33)$ nm^2
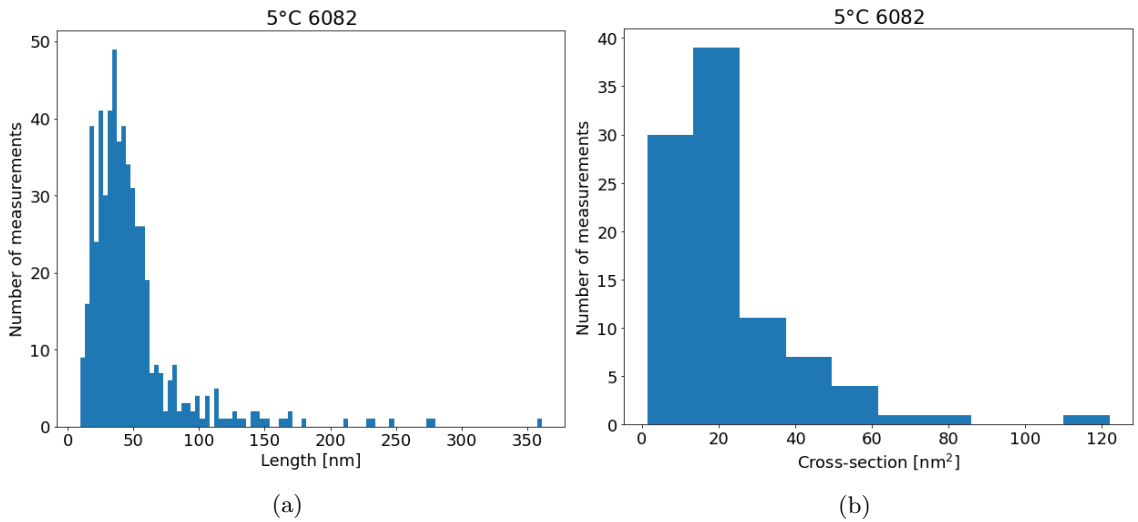
Figure 60: (a) Precipitate length distribution for the 6082 NA 5°C 1 month condition. Average length $< l > = 48.09$ nm with standard deviation $\sigma = 38.85$ nm. (b) Precipitate cross-section distribution for the 6082 NA 5°C 1 month condition. Average cross-section with standard error $< CS > = 23.08(181)$ nm^2
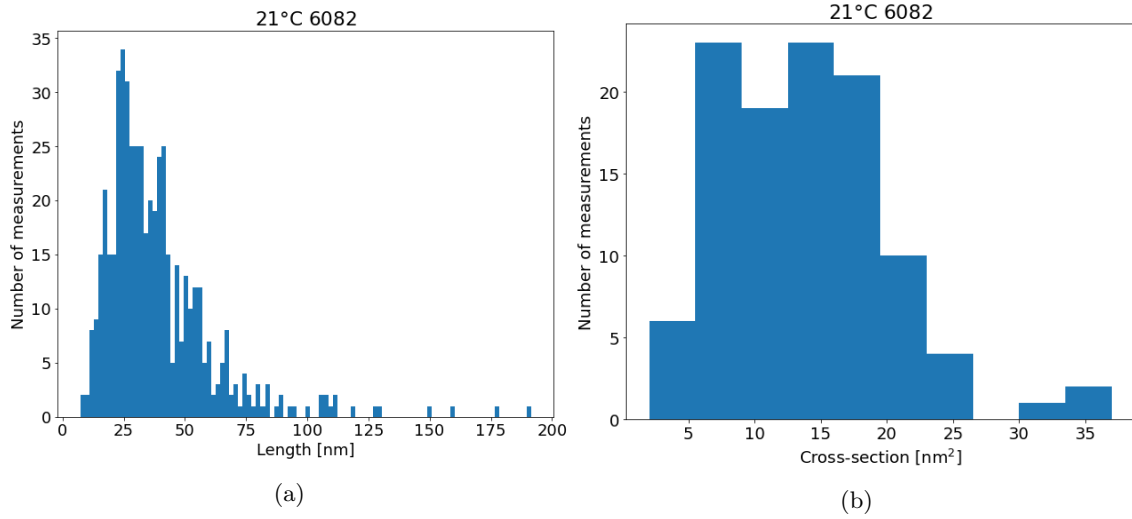
Figure 61: (a) Precipitate length distribution for the 6082 NA 21°C 1 month condition. Average length $< l >= 38.90$ nm with standard deviation $\sigma = 22.92$ nm. (b) Precipitate cross-section distribution for the 6082 NA 21°C 1 month condition. Average cross-section with standard error $< CS >= 13.96(61)$ nm^2

C.3 TEM Images

Here, a selection of TEM images are presented from each imaged condition. These images does not necessarily complete one image set. Firstly, images of the 6060 condition is presented starting with DA, then followed by 5°C, 21°C and 80°C. Images from the 6082 condition are presented afterwards in the same order, starting with DA, followed by 5°C and 21°c.

C.3.1 6060 DA

(a)   (b)
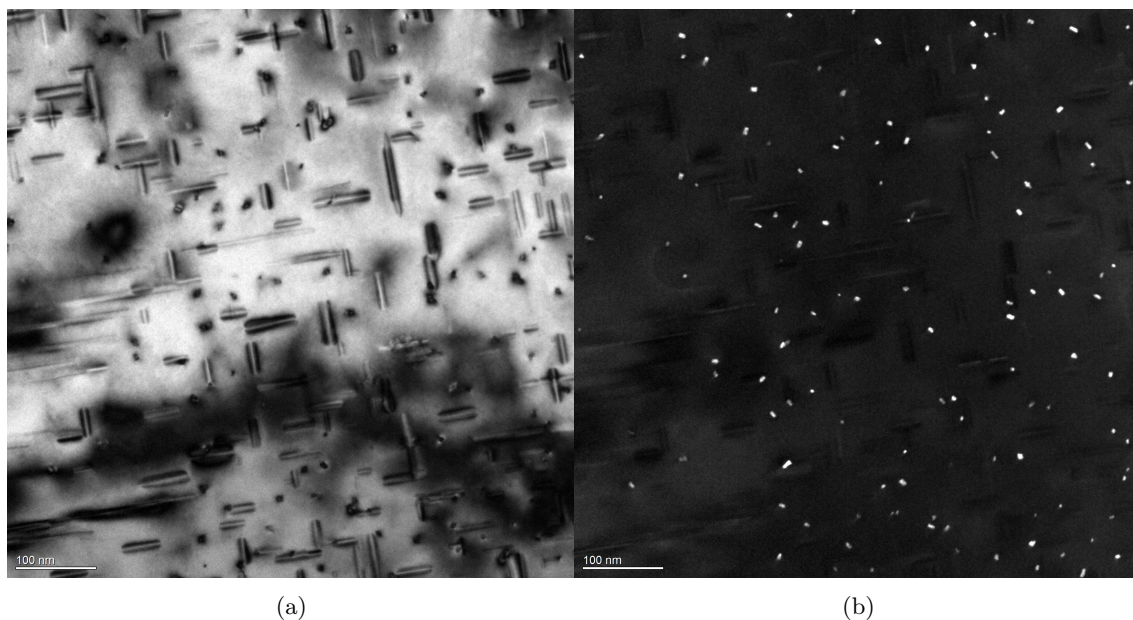
Figure 62: (a) BF taken at 120k magnification. (b) DF taken at 120k magnification.

(a)   (b)
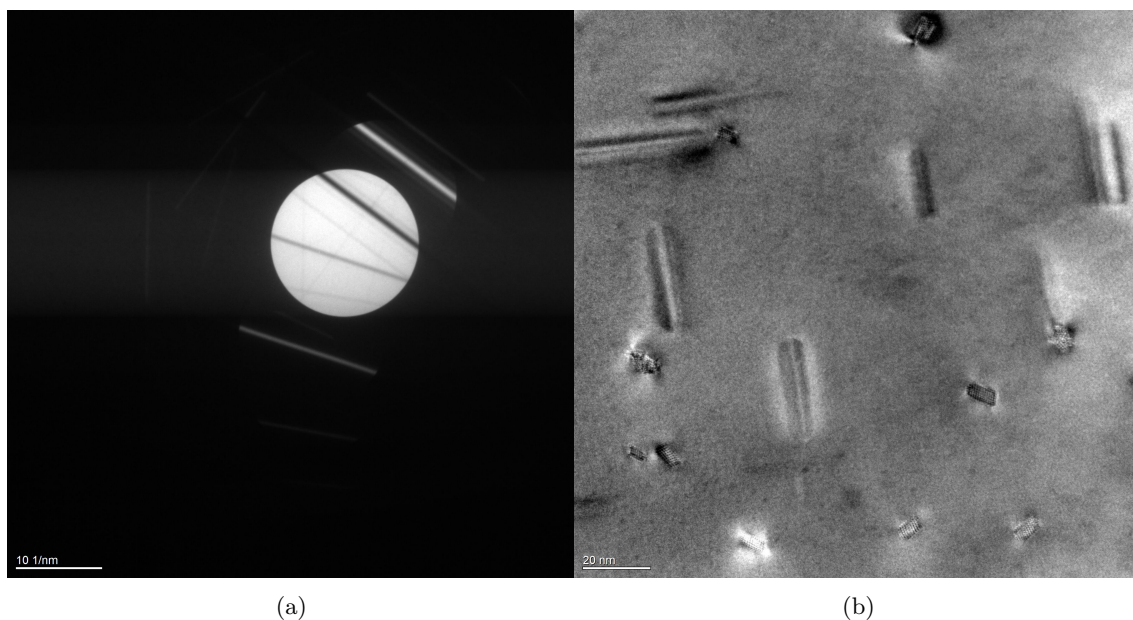
Figure 63: (a) CBED (b) HRTEM taken at 500k magnification.

C.3.2 6060 5°C
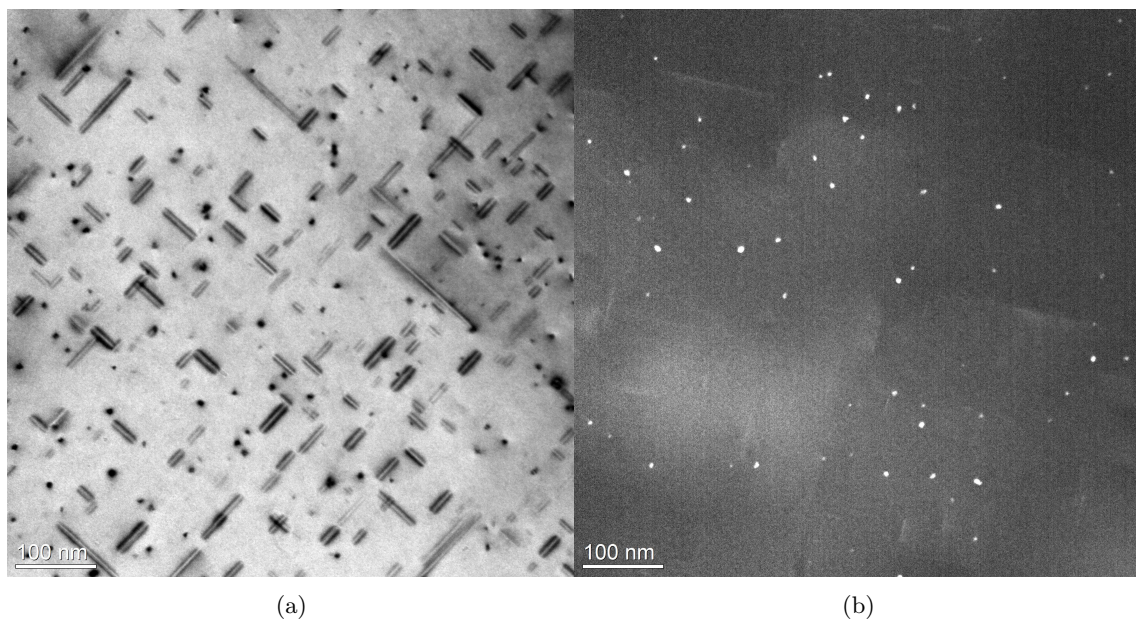
Figure 64: (a) BF taken at 120k magnification. (b) DF taken at 120k magnification.
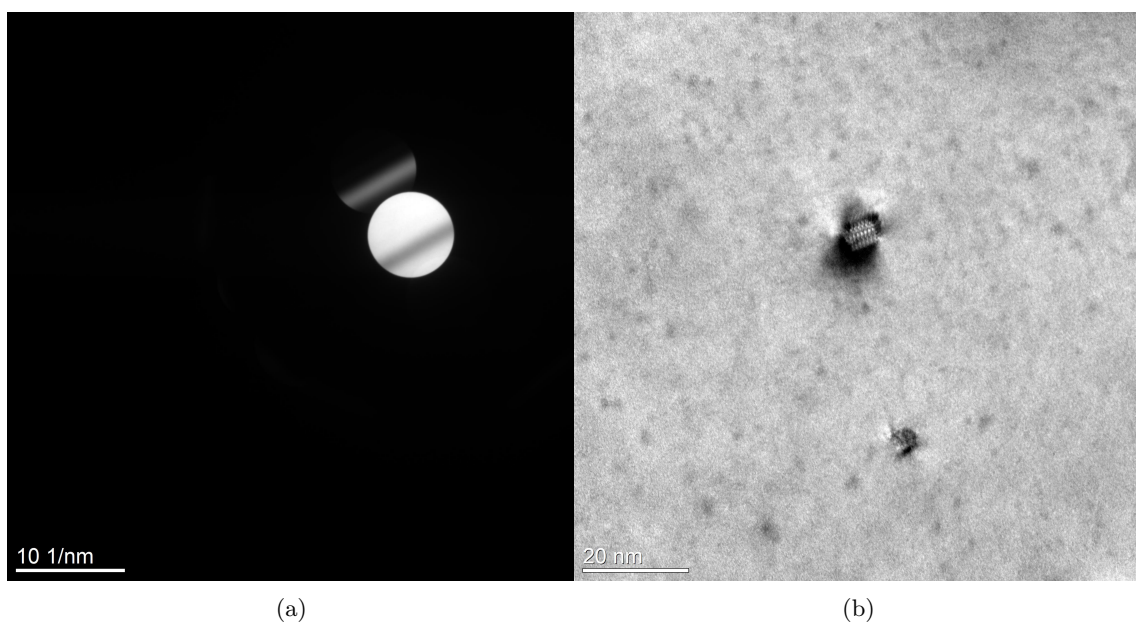
Figure 65: (a) CBED. (b) HRTEM taken at 800k magnification.

(a) \hspace{10cm} (b)
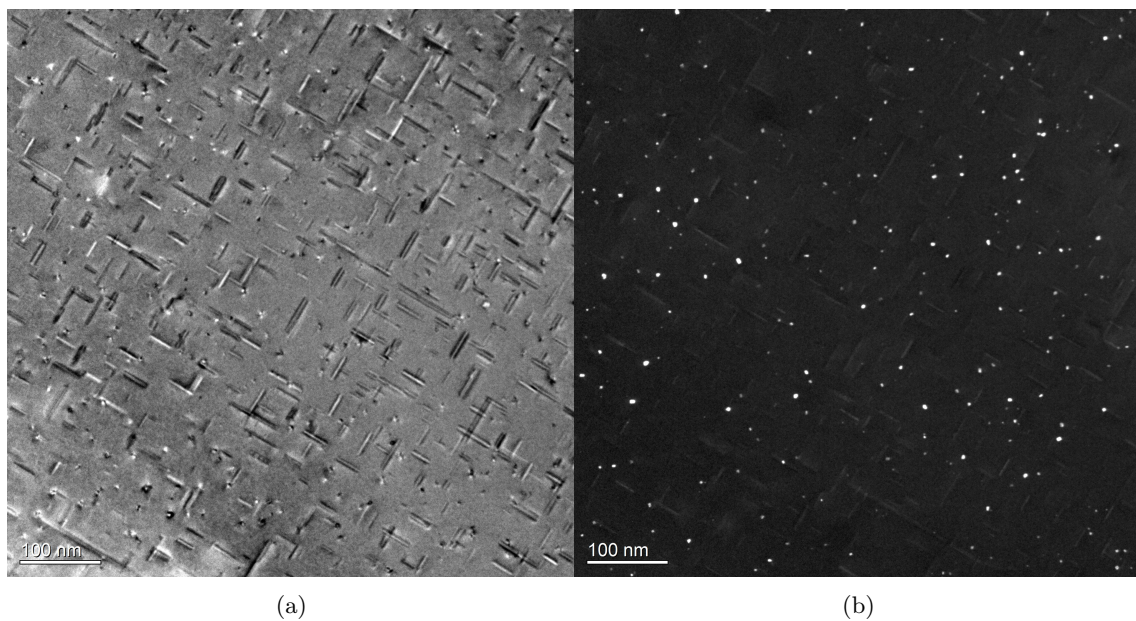
Figure 66: (a) BF taken at 120k magnification. (b) DF taken at 120k magnification.

(a) \hspace{10cm} (b)
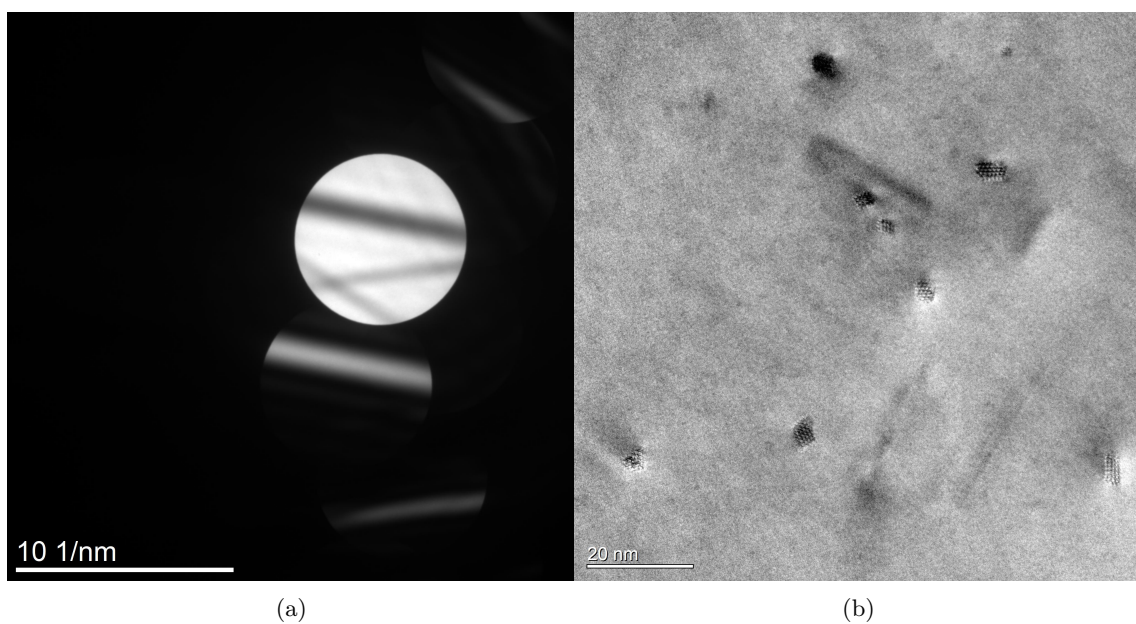
Figure 67: (a) CBED. (b) HRTEM taken at 800k magnification.

C.3.4   6060 80°C
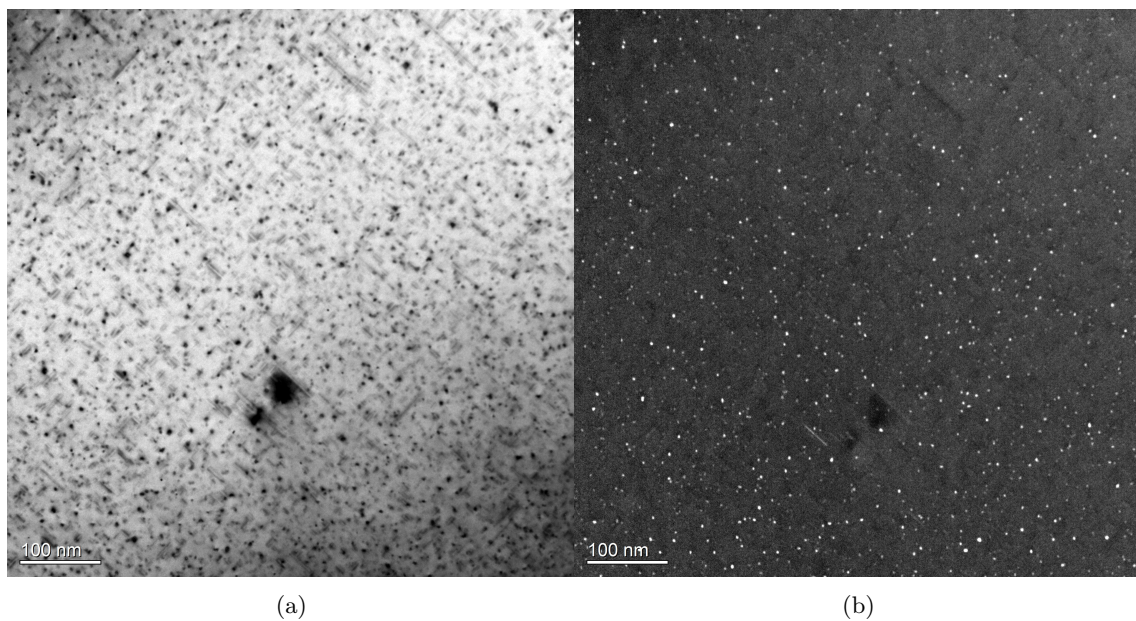
Figure 68: (a) BF taken at 120k magnification. (b) DF taken at 120k magnification.
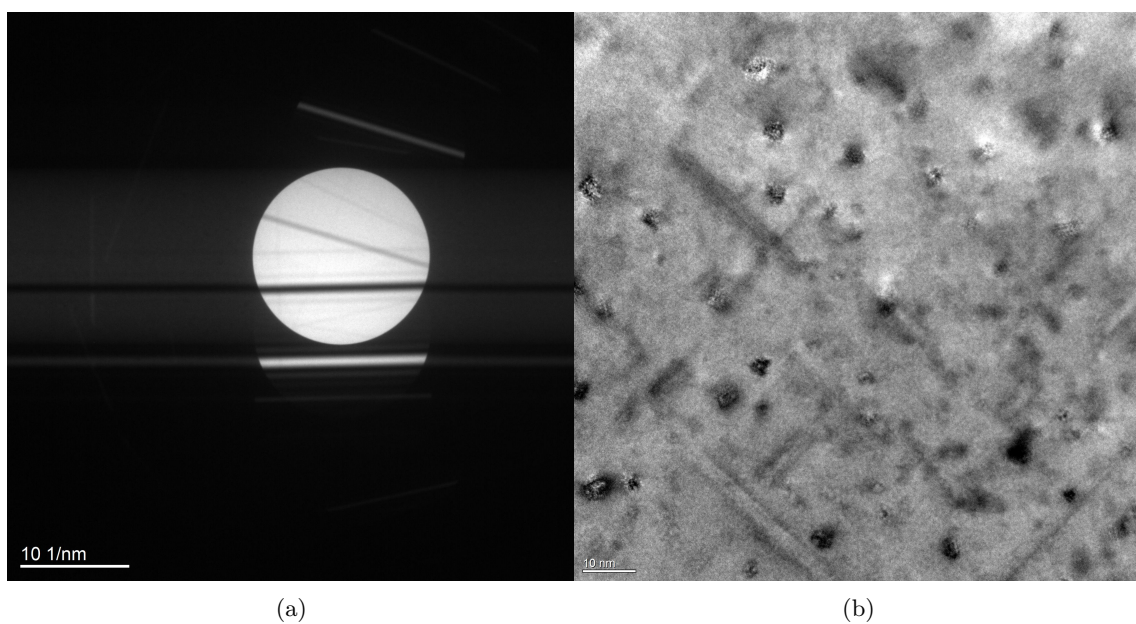
Figure 69: (a) CBED. (b) HRTEM taken at 800k magnification.

C.3.5   6082 DA

(a)   (b)
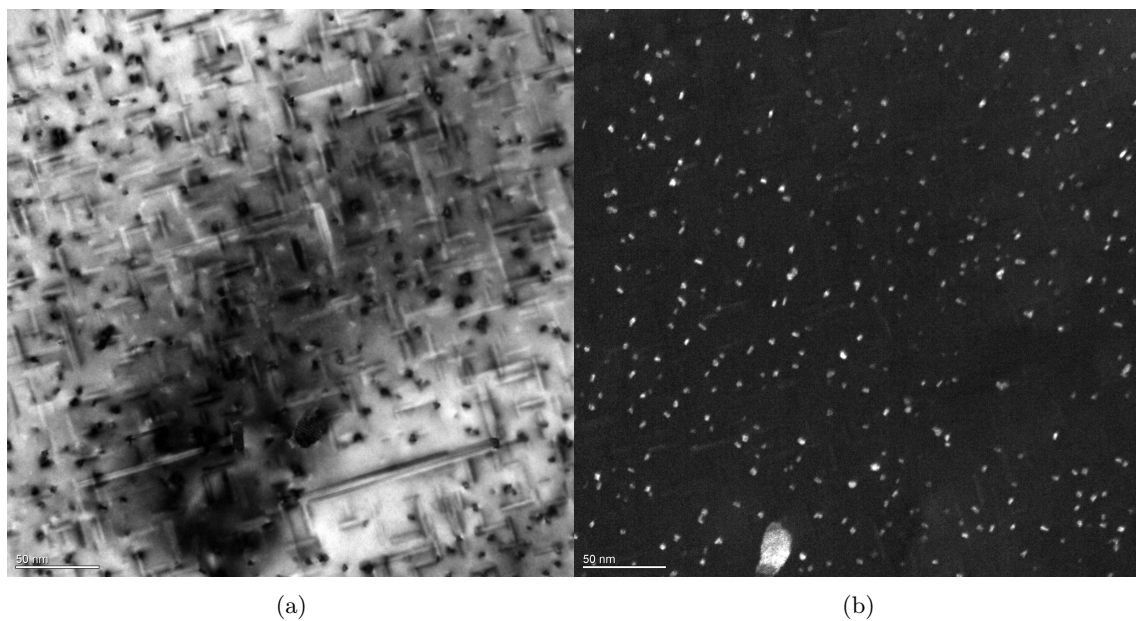
Figure 70: (a) BF taken at 250k magnification. (b) DF taken at 250k magnification.

(a)   (b)
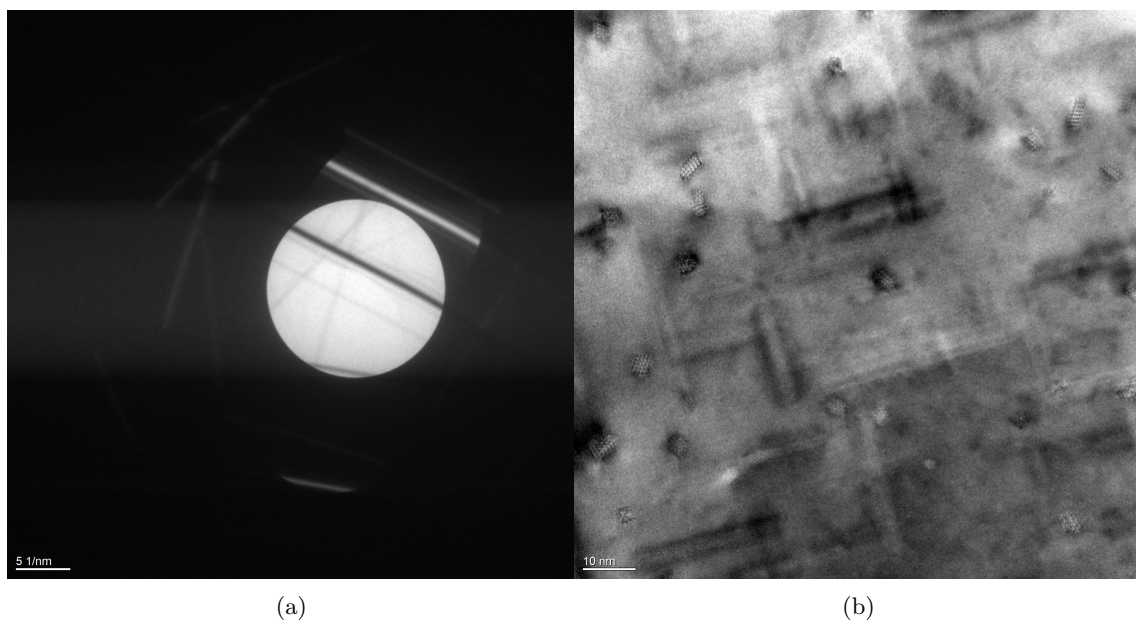
Figure 71: (a) CBED. (b) HRTEM taken at 800k magnification.

C.3.6 6082 5°C
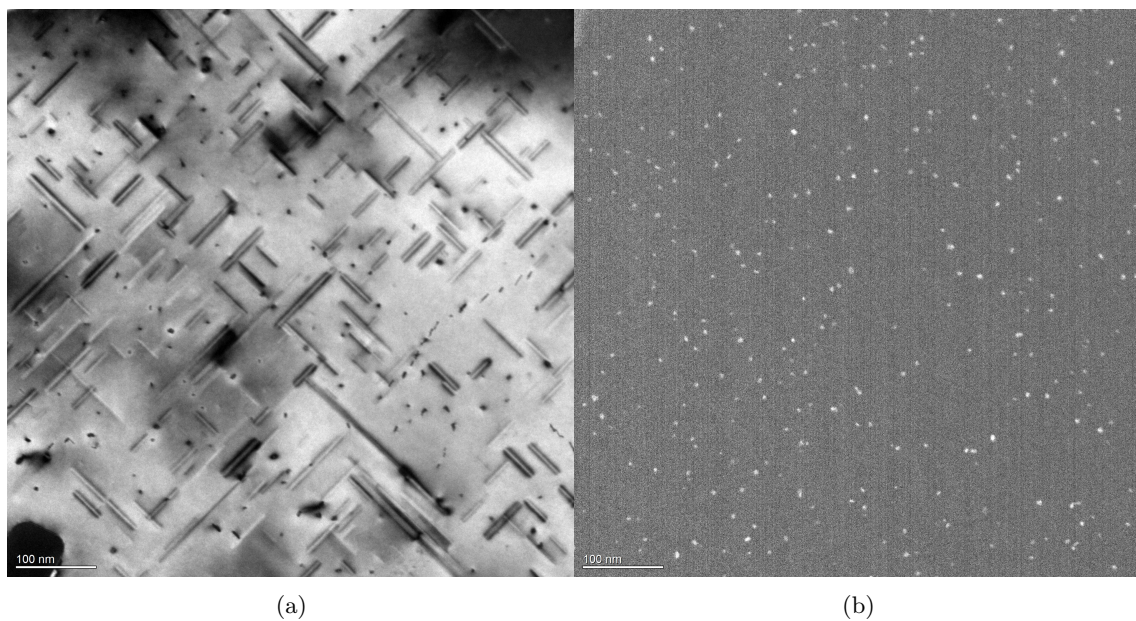
Figure 72: (a) BF taken at 120k magnification. (b) DF taken at 120k magnification.
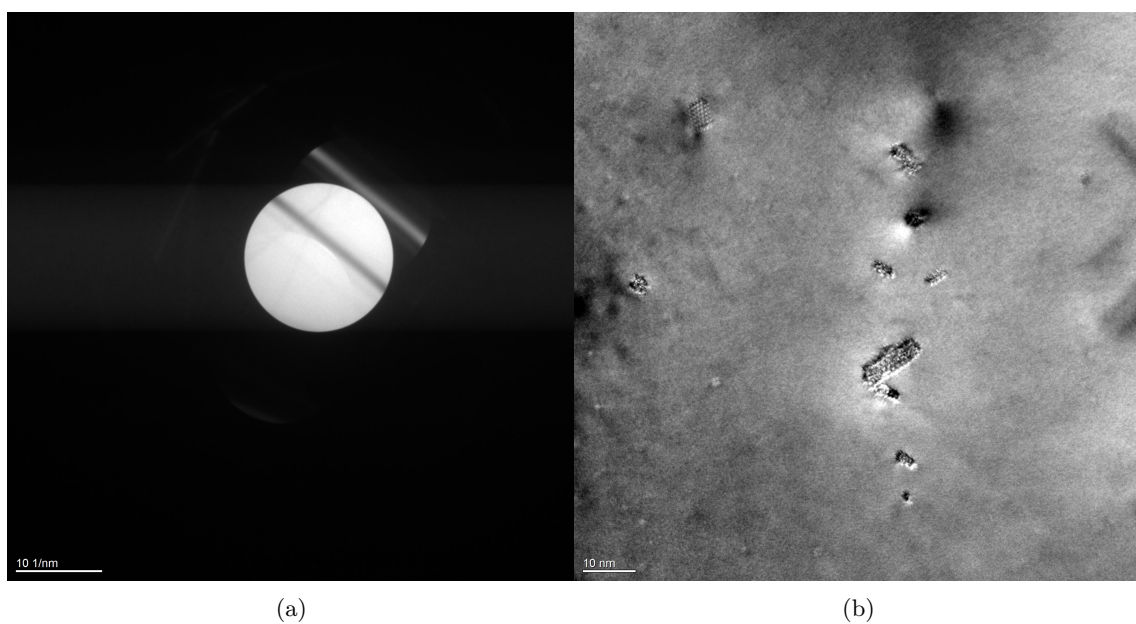
Figure 73: (a) CBED. (b) HRTEM taken at 800k magnification.

C.3.7   6082 21°C
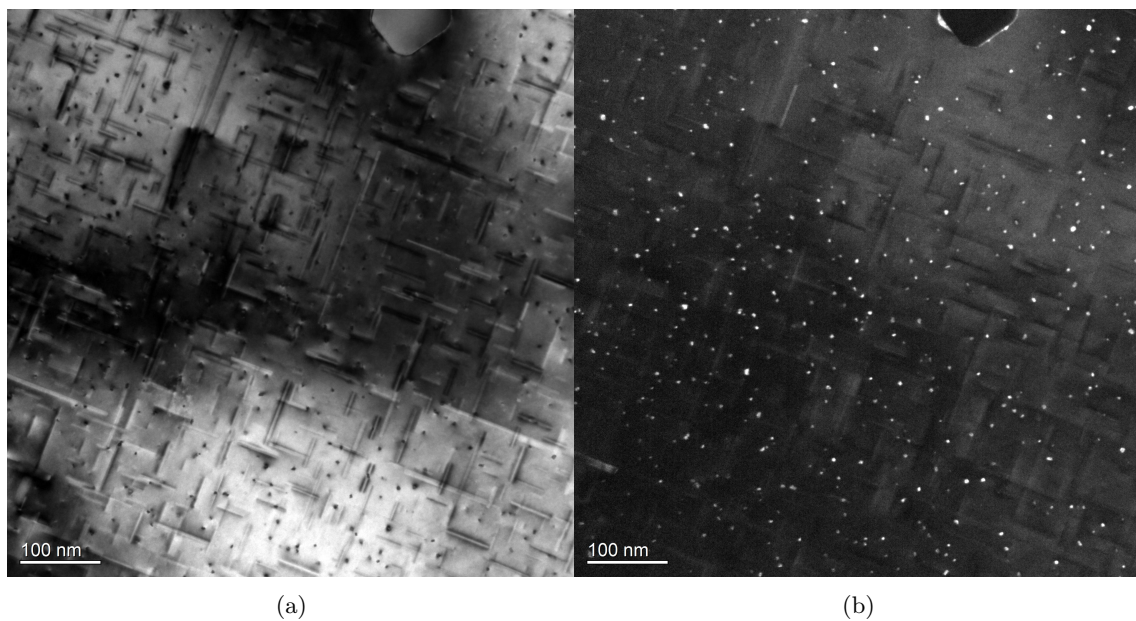
Figure 74: (a) BF taken at 120k magnification. (b) DF taken at 120k magnification.
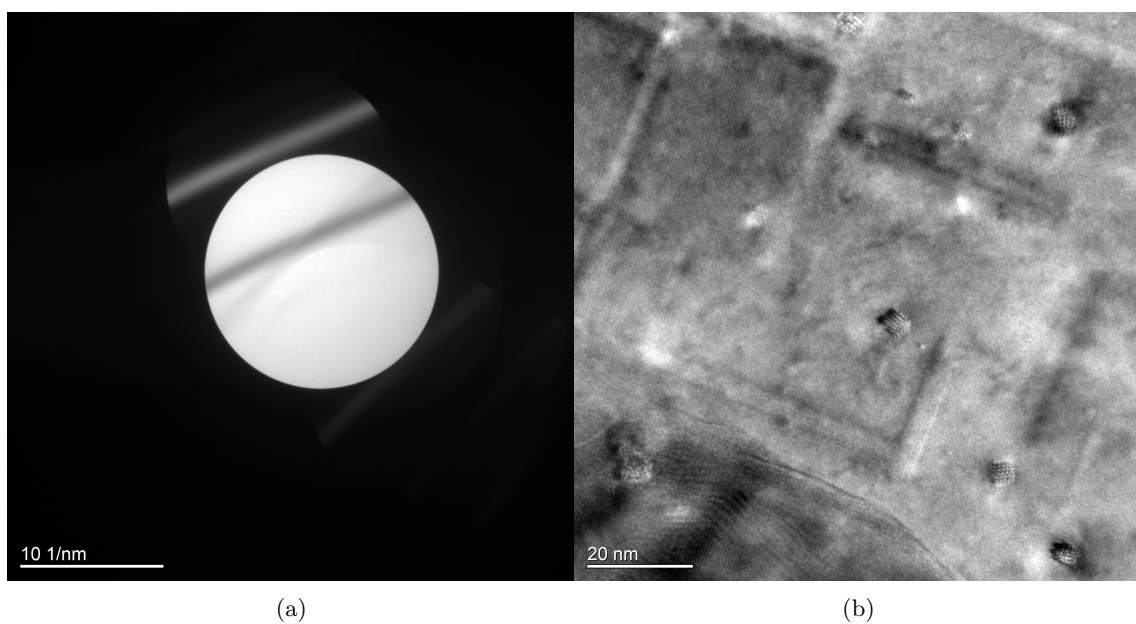
Figure 75: (a) CBED. (b) HRTEM taken at 800k magnification.

References

1. Røyset, J., Stene, T., Sæter, J. A. & Reiso, O. *The effect of intermediate storage temperature and time on the age hardening response of Al-Mg-Si alloys* in *Materials Science Forum* **519** (2006), 239–244.

2. Straumanis, M. & Woodward, C. Lattice parameters and thermal expansion coefficients of Al, Ag and Mo at low temperatures. Comparison with dilatometric data. *Acta Crystallographica Section A: Crystal Physics, Diffraction, Theoretical and General Crystallography* **27,** 549–551 (1971).

3. ESAB. *Understanding the Aluminum Alloy Designation System* https://www.esabna.com/us/en/education/blog/understanding-the-aluminum-alloy-designation-system.cfm (15th June 2022).

4. Dumitraschkewitz, P., Gerstl, S. S., Stephenson, L. T., Uggowitzer, P. J. & Pogatscher, S. Clustering in Age-Hardenable Aluminum Alloys. *Advanced Engineering Materials* **20,** 1800255 (2018).

5. Gottstein, G. *Physical foundations of materials science* (Springer Science & Business Media, 2013).

6. Saito, T. *et al.* Atomic structures of precipitates in Al–Mg–Si alloys with small additions of other elements. *Advanced Engineering Materials* **20,** 1800125 (2018).

7. Hell, C. *et al.* Influence of Natural Aging and Ramping Before Artificial Aging on the Microstructure of Two 6xxx Alloys.

8. JEOL. *JEM-2100 Electron Microscope Manual* https://www.aphys.kth.se/polopoly_fs/1.190438.1600689956!/Menu/general/column-content/attachment/TEM_manual_JEOL2100.pdf (16th June 2022).

9. Fultz, B. & Howe, J. M. *Transmission electron microscopy and diffractometry of materials* (Springer Science & Business Media, 2012).

10. Foerster. *SIGMATEST 2.069 Operating Manual* https://www.bergeng.com/mm5/downloads/foerster/Foerster-Sigmatest-2.069-Operating-Manual.pdf (9th June 2022).

11. Hell, C. M. *TEM-Gemini-Centre/ThicknessDeterminationTEM: CBED ThicknessDeterminationTEM* version V4. June 2022. https://doi.org/10.5281/zenodo.6602265.

12. Andersen, S. J. Quantification of the Mg2Si β and β phases in AlMgSi alloys by transmission electron microscopy. *Metallurgical and materials transactions A* **26,** 1931–1937 (1995).